

Dissertation  
Submitted to the  
Combined Faculties for the Natural Sciences and for Mathematics  
of the Ruperto-Carola University of Heidelberg, Germany  
for the Degree of  
Doctor of Natural Sciences

Presented by  
M.Sc. Jamie Frankish  
Born in Dublin, Ireland  
Oral-examination: 10.11.2017

# **Characterisation of the Regulation and Dynamics of the RIG-I signalling Network**

Referees

Prof. Dr. Ralf Bartenschlager

Prof. Dr. Ursula Klingmüller

The applicant, Jamie Ian Frankish, declares that he is the sole author of the submitted dissertation and no other sources or help from those specifically referred to have been used. Additionally, the applicant declares that he has not applied for permission to enter an examination procedure at any other institution and that this dissertation has not been presented to any other faculty and has not been used in its current or in any other form in another examination.

.....

Date

.....

Signature

## Acknowledgements

*This thesis is dedicated to my family and friends, old and new, whom without their support would have this a much more arduous task.*

I would like to especially thank Dr. Marco Binder, who has acted as an excellent group leader and mentor to me, guiding me, and allowing me to push my own limits and strive for great success.

To the members of AG Binder, AG Bartenschlager, and AG Galy, particularly Julia, Christopher, Sandra, I say thank you for working alongside me day by day and putting up with my *excellent* jokes and perfect imitations, I hope working together was as much fun for me as it was for you.

I would also like to extend my thanks to Joschka for proofreading my thesis, albeit not all of it, but also for acting as my lab partner for the past 4 years. Our discussions were always beneficial.

I would like to thank my family in particular, who have supported me through all my endeavours, despite moving so far away from them. Coming home was always something I looked forward to, and that is something I valued greatly. The Dr. Frankish title has always been an inspiration.

I would also like to thank Noemi, who has supported me so well during my Ph.D. studies and made my time in Heidelberg that much more special.

To all my dear friends, and I can't name you all, thank you for being there for me and making my life so much easier at home and abroad. I apologise for not naming you all but I think you all know who you are and how important you are to me and to the success of this Ph.D.

I would also like to extend my thanks to Darius and Lars, who have worked hard with us from the beginning to produce top quality mathematical modelling.

Last but not least, I would like to thank Prof. Dr. Ralf Bartenschlager and Prof. Dr. Ursula Klingmüller whom have always taken time out of their busy schedule to provide their excellent insight into my project. Additionally, I would also like thank them for acting as my referees during my research time.

Finally, I would to thank my examination commission, Prof. Dr. Ralf Bartenschlager, Prof. Dr. Ursula Klingmüller, Dr. Ingrid Hoffmann, and Dr. Richard Harbottle, for taking the time to consider my thesis.

## Summary

RIG-I is a pattern recognition receptor that is responsible for the initiation of an antiviral response to a variety of virus infections. Cytoplasmic nucleic acid derived from virus replication is detected by RIG-I resulting in the initiation of a signalling cascade that ultimately leads to the activation of transcription factors, namely IRF3 and NF $\kappa$ B. Activation of these transcription factors leads to the production and secretion of type I and III interferons (IFN), which act in an auto- and paracrine manner to induce the expression of a large array of IFN stimulated genes (ISGs). In concert, these ISGs promote an antiviral state of the cell, limiting viral replication and spread. Much is known about the individual steps and proteins involved in the RIG-I signalling pathway, however, much less is understood about its regulation and dynamics. Upon virus entry into a cell, the initial response phase is critical to the outcome and determines if the infection is cleared or established. Understanding the dynamics of these processes will be key to comprehend and possibly predict the outcome of a viral infection. The main goal of this thesis, therefore, was to identify novel regulators and to kinetically characterize the rapid induction of the cellular antiviral signalling cascade.

As for the identification of previously unrecognized regulators of the RIG-I pathway, we have performed an siRNA-based high-throughput screen of over 600 known and putative E3 ubiquitin ligase genes. Post-translational ubiquitination has been shown to constitute a major regulatory process in innate immune signalling. From our screening approach, we were able to identify several genes that significantly impacted IRF3 activation upon silencing during viral infection.

The main part of this thesis deals with the temporal characterisation of RIG-I-initiated antiviral signalling. For that purpose, we developed an approach which permitted the completely synchronous stimulation of cells with virus-like double-stranded RNA. In contrast to authentic infections or classical liposome-based transfections, this method allows for a very high degree of time-resolution in measuring the flow of the signal along the cascade. Quantitative, time-resolved activation measurements of critical proteins in the RIG-I pathway showed that RIG-I signalling is rapid and, in contrary to previous reports, strictly deterministic with very little variability from cell to cell. Furthermore, we extensively characterized the transcriptional program triggered by RIG-I in a time-resolved manner by full-genomic transcriptional profiling. We found that the panel of genes upregulated directly by the primary IRF3 response is surprisingly large and congruent with the ISGs classically known to be induced only by IFN signalling, with only very few genes exhibiting a strict dependence on IFN/JAK/STAT signalling.

This work represents the first detailed molecular characterization of the kinetics of host cellular processes triggered in the first few minutes after virus infection. The comprehensive quantitative and time-resolved data generated can serve as a solid basis for a mathematical model that combines viral replication dynamics and host antiviral responses. Such a model will be an unprecedented and powerful tool to study the principles governing the outcome of viral infection and to help understanding how certain viruses manage to overcome host immunity and cause fulminant disease or even establish life-long persistence.

## Zusammenfassung

RIG-I ist ein *pattern recognition receptor* (dt. etwa Mustererkennungsrezeptor) der für die Initiierung eines antiviralen Zustandes in der Zelle nach Virus-Infektion verantwortlich ist. Er erkennt und bindet bei der Virus-Replikation entstehende Nukleinsäuren im Cytoplasma, wird aktiviert und stößt eine Signalkaskade an, die letztendlich zur Aktivierung der Transkriptionsfaktoren IRF3 und NF $\kappa$ B führt. Dies wiederum resultiert in der Produktion und Sekretion von Typ I und III-Interferonen (IFN), die dann auto- und parakrin wirken und die Expression eines breiten Panels an IFN-stimulierten Genen (ISGs) hervorrufen. Zusammen schaffen diese ISGs einen stark antiviralen Zustand in der Zelle und limitieren somit die Virus-Replikation und die Ausbreitung der Infektion. Obwohl die einzelnen Schritte und involvierten Proteine des RIG-I-Signalweges bereits gut erforscht sind, fehlen noch wichtige Erkenntnisse über deren Regulation und Dynamiken. Die initiale Phase einer Infektion ist ausschlaggebend für deren weiteren Verlauf und entscheidet ob sich der Virus vermehren kann oder ob er ausgelöscht wird. Eine Auflösung dieser sehr frühen Dynamiken ist somit unerlässlich für ein besseres Verständnis von Virus-Infektionen und kann die Vorhersage des Verlaufs einer solchen Infektion ermöglichen. Das Hauptziel dieser Arbeit war es folglich bisher unbekannte Regulatoren dieser antiviralen Signalkaskade zu identifizieren und ihre rapide Aktivierung in hoher Zeitauflösung zu dokumentieren. Zur Identifizierung neuer Regulatoren des RIG-I-Signalweges führten wir einen siRNA-basierten Hochdurchsatz-Screen mit mehr als 600 bekannten und vermuteten E3-Ubiquitin-Ligasen durch, da post-translationale Ubiquitinierung als weit verbreitetes Mittel zur Regulierung der Immunantwort gilt. Auf diese Weise konnten wir mehrere Gene identifizieren die einen entscheidenden Einfluss auf die Aktivierung von IRF3 bei Virus-Infektion haben.

Der Hauptteil dieser Arbeit beschäftigt sich allerdings mit der zeitlich hoch-aufgelösten Charakterisierung der RIG-I-initiierten antiviralen Immunantwort. Hierzu haben wir eine Methode entwickelt die es uns ermöglicht eine Vielzahl von Zellen gleichzeitig mit Virus-ähnlicher Doppelstrang-RNA zu aktivieren. Im Gegensatz zur *in vitro*-Infektion oder klassischen Liposomen-basierten Transfektion erreichen wir hiermit eine hohe zeitliche Präzision zur exakten Messung der Signal-Weiterleitung. Die Quantifizierung dieser Messungen hat zum einen die enorme Geschwindigkeit der Aktivierung und Signal-Weiterleitung innerhalb des RIG-I-Signalweges gezeigt. Zum anderen konnten wir im Gegensatz zu bisherigen Publikationen zeigen, dass die Aktivierung des RIG-I-Signalweges sehr deterministisch ist und kaum Variationen von Zelle zu Zelle aufweist.

Weiterhin haben wir eine Zeit-aufgelöste Genexpressions-Analyse nach Aktivierung des RIG-I-Signalweges durchgeführt. Diese hat eine überraschend große Gruppe an Genen gezeigt deren Expression direkt durch die initiale IRF3-Aktivierung induziert wird und mit den bekannten klassischen ISGs nach IFN-Stimulation übereinstimmt. Nur weniger dieser Gene waren strikt von der Aktivität des IFN/JAK/STAT-Signalweges abhängig.

Diese Arbeit zeigt als erste eine detaillierte Charakterisierung der Dynamiken der Signalaktivierung und -weiterleitung auf molekularer Ebene in der Zelle nach Virus-Infektion. Die gewonnenen Daten können aufgrund ihrer hohen Zeitauflösung und der genauen Quantifizierung als Basis zur Entwicklung eines mathematischen Modells dienen, welches die Dynamiken der Virus-Replikation mit denen der antiviralen Signalwege vernetzt. Solch ein Modell kann helfen den Verlauf und das Ergebnis von Virus-Infektionen vorherzusagen

# Table of Contents

<b>Acknowledgements</b> .....	<b>iv</b>
<b>Summary</b> .....	<b>v</b>
<b>Zusammenfassung</b> .....	<b>vi</b>
<b>Table of Contents</b> .....	<b>1</b>
<b>Table of Figures</b> .....	<b>5</b>
<b>Table of Tables</b> .....	<b>7</b>
<b>1.0 Introduction</b> .....	<b>7</b>
<b>1.1 The immune system</b> .....	<b>8</b>
<b>1.2 cells of the immune system</b> .....	<b>9</b>
<b>1.2.1 Immune cells and their functions</b> .....	<b>10</b>
1.2.1.1 Myeloid cells .....	10
1.2.1.2 Antigen presentation .....	10
1.2.1.3 Lymphoid cells .....	11
1.2.1.4 The adaptive immune response .....	12
<b>1.3 The innate immune response to viruses</b> .....	<b>15</b>
<b>1.3.1 RIG-I signalling</b> .....	<b>17</b>
1.3.1.1 Structure and function of RIG-I.....	17
1.3.1.2 LGP2 and MDA5.....	18
1.3.1.3 RIG-I signalling overview.....	20
1.3.1.4 RIG-I activation of MAVS .....	22
1.3.1.5 MAVS mediated signal transduction .....	23
1.3.1.6 IRF3/7 activation.....	23
1.3.1.7 NFκB .....	26
<b>1.4 IFN signalling</b> .....	<b>29</b>
<b>1.5 Signalling dynamics and modelling</b> .....	<b>30</b>
<b>1.6 Ubiquitination</b> .....	<b>31</b>
<b>2.0 Materials</b> .....	<b>34</b>
<b>2.1 Cell Culture</b> .....	<b>34</b>

<b>2.2 DNA and RNA</b> .....	<b>35</b>
<b>2.3 Plasmids</b> .....	<b>36</b>
<b>2.4 Protein Biochemistry</b> .....	<b>37</b>
<b>2.5 Primary Antibodies</b> .....	<b>37</b>
<b>2.6 Secondary Antibodies</b> .....	<b>38</b>
<b>2.7 Molecular probes and dyes</b> .....	<b>39</b>
<b>2.8 Luciferase Assay Buffers and Reagents</b> .....	<b>39</b>
<b>2.9 Primer sequences</b> .....	<b>39</b>
<b>2.10 Viruses</b> .....	<b>41</b>
<b>2.11 Bacteria and Bacterial cultures</b> .....	<b>41</b>
<b>2.12 Software</b> .....	<b>42</b>
<b>2.13 Equipment</b> .....	<b>42</b>
<b>2.14 Consumable materials</b> .....	<b>43</b>
<b>3.0 Methods</b> .....	<b>45</b>
<b>3.1 Cloning and bacterial culturing</b> .....	<b>45</b>
3.1.1 Transformation of competent bacteria .....	45
3.1.2 Plasmid amplification and purification .....	45
3.1.3 Small scale plasmid purification .....	45
Large scale plasmid purification .....	45
3.1.4 Polymerase chain reaction .....	46
3.1.5 Overlap-extension PCR .....	47
3.1.6 Gateway™ cloning.....	47
3.1.6.1 Generation of entry clones (BP reaction).....	48
3.1.6.2 Generation of expression clones (LR reaction) .....	49
3.1.7 Sequencing analysis of plasmid DNA .....	49
<b>3.2 Cell Culture</b> .....	<b>49</b>
3.2.1 Cell culturing.....	49
3.2.2 Cryopreservation of mammalian cells .....	50
3.2.3 Determining cell numbers in solution .....	50
3.2.4 Transfection of recombinant DNA .....	51
3.2.4.1 Lipofectamine 2000 ®.....	51
3.2.4.2 jetPEI ® .....	51
3.2.5 Transduction of recombinant DNA .....	52
3.2.5.1 Lentiviral mediated stable integration of recombinant DNA.....	52



3.2.6 In vitro transcription .....	53
3.2.7 Generating Double Stranded RNA .....	53
<b>3.3 Biochemical and Molecular Biological Assays.....</b>	<b>54</b>
3.3.1 Protein Complementation Assay .....	54
3.3.1.1 PCA Constructs.....	54
3.3.1.2 Assay procedure.....	55
3.3.2 Luciferase Assay.....	56
3.3.3 Western Blot.....	57
3.3.3.1 Sodium Dodecyl Sulphate Polyacrylamide Gel Electrophoresis.....	57
3.3.3.2 Western Blot Electrophoresis .....	58
3.3.3.3 Western Blot staining.....	58
3.3.3.4 Western Blot Quantification .....	59
3.3.4 Synchronised Dynamics Analysis .....	59
3.3.4.1 Synchronised Dynamics Sample Acquisition .....	59
3.3.5 Live Synchronised Cell Imaging.....	60
3.3.6 ELISA .....	61
3.3.7 RNA and quantitative PCR .....	61
3.3.7.1 RNA isolation.....	61
3.3.7.2 Quantitative Real-Time PCR.....	62
3.3.8 Illumina HumanHT-12 Chip expression profiling .....	63
3.3.9 Proteome analysis .....	63
<b>4.0 Results.....</b>	<b>64</b>
<b>4.1 Identifying novel regulators of the RIG-I signalling network.....</b>	<b>64</b>
<b>4.2 RIG-I Signalling – From Tools to Dynamics Data .....</b>	<b>75</b>
<b>4.3 RIG-I Signalling Dynamics.....</b>	<b>87</b>
<b>5.0 Discussion.....</b>	<b>117</b>
<b>5.1 siRNA screen for E3 Ligases regulating RIG-I signalling .....</b>	<b>117</b>
<b>5.2 Measuring PPIs.....</b>	<b>119</b>
5.2.1 PCA .....	119
5.2.2 PCA suitability .....	120
<b>5.3 RIG-I signalling.....</b>	<b>122</b>
5.3.1 Quantitatively measuring RIG-I signalling.....	122
5.3.2 A question of stochasticity .....	122
5.3.3 Characterisation of RIG-I signalling dynamics – progress and limitations .....	124

5.3.3.1 Progress .....	124
5.3.3.2 Limitations .....	127
5.3.4 Analysing downstream signalling dynamics .....	129
5.3.5 Interferon signalling.....	131
<b>5.4 Modelling .....</b>	<b>134</b>
<b>6.0 References.....</b>	<b>136</b>
<b>7.0 Presentations and Publications .....</b>	<b>149</b>
7.1 Poster/oral presentations.....	149
7.2 Publications.....	149
<b>8.0 Appendix .....</b>	<b>150</b>

# Table of Figures

Figure 1.1 Cells of the immune system.....	8
Figure 1.2 Immune stem cells .....	9
Figure 1.3 Immune response to a virus.....	14
Figure 1.4 Time dependent responses of the immune system.....	14
Figure 1.5 Domain structure of RIG-I.....	17
Figure 1.6 RLR structure homology .....	19
Figure 1.7 RIG-I ligands .....	21
Figure 1.8 Overview of RIG-I signalling.....	28
Figure 4.1.1 RIG-I induction construct .....	65
Figure 4.1.2 RIG-I <sup>2CARD</sup> induction .....	67
Figure 4.1.3 FACS sorting dual fluorescent cells.....	69
Figure 4.1.4 siRNA screening.....	72
Figure 4.2.1 IRF3 translocation tracking .....	75
Figure 4.2.2 PCA overview .....	78
Figure 4.2.3 PCA preliminary results.....	79
Figure 4.2.4 PCA controls.....	81
Figure 4.2.5 PCA based luciferase activity over time .....	83
Figure 4.2.6 Cell electroporation overview .....	85
Figure 4.3.1 Liposome- vs electro-dsRNA transfection.....	88
Figure 4.3.2 IRF3 nuclear translocation quantification.....	89
Figure 4.3.3 Canonical RIG-I signalling protein dynamics analysis .....	91
Figure 4.3.4 Canonical RIG-I signalling protein dynamics quantification.....	93
Figure 4.3.5 Mathematical modelling.....	96
Figure 4.3.6 Parameter fitting.....	98
Figure 4.3.7 ISG mRNA analysis .....	100
Figure 4.3.8 IFIT1 protein expression .....	101
Figure 4.3.9 IFN $\beta$ analysis.....	102
Figure 4.3.10 STAT1 analysis.....	105

<b>Figure 4.3.11 Electro-transfection controls .....</b>	<b>106</b>
<b>Figure 4.3.12 RIG-I dynamics overview .....</b>	<b>107</b>
<b>Figure 4.3.13 ISG expression after 6 hours .....</b>	<b>109</b>
<b>Figure 4.3.14 Different phases of ISG induction.....</b>	<b>111</b>
<b>Figure 4.3.15 Type I/III IFN expression .....</b>	<b>112</b>
<b>Figure 4.3.16 ISG expression .....</b>	<b>113</b>
<b>Figure 4.3.17 IFN dependent ISGs .....</b>	<b>114</b>
<b>Figure 4.3.18 IFN regulated ISG expression .....</b>	<b>115</b>
<b>Figure 4.3.19 Transcriptome of siRNA screen based hits.....</b>	<b>116</b>
<b>Figure 8.1 NFkB signalling gene expression comparison .....</b>	<b>152</b>
<b>Figure 8.2 Partial tryptic digestion of RIG-I.....</b>	<b>153</b>
<b>Figure 8.3 Cross-linking of RIG-I and MAVS.....</b>	<b>153</b>

# Table of Tables

<b>Table 1 Cell culture reagents .....</b>	<b>34</b>
<b>Table 2 Mammalian cells .....</b>	<b>34</b>
<b>Table 3 DNA and RNA .....</b>	<b>35</b>
<b>Table 4 Plasmids .....</b>	<b>36</b>
<b>Table 5 Protein biochemistry .....</b>	<b>37</b>
<b>Table 6 Primary antibodies.....</b>	<b>37</b>
<b>Table 7 secondary antibodies .....</b>	<b>38</b>
<b>Table 8 probes and dyes .....</b>	<b>39</b>
<b>Table 9 luciferase assay .....</b>	<b>39</b>
<b>Table 10 primer sequences .....</b>	<b>39</b>
<b>Table 11 viruses .....</b>	<b>41</b>
<b>Table 12 Bacteria.....</b>	<b>41</b>
<b>Table 13 software .....</b>	<b>42</b>
<b>Table 14 Equipment.....</b>	<b>42</b>
<b>Table 15 Consumables .....</b>	<b>43</b>
<b>Table 16 PCR reaction mix .....</b>	<b>46</b>
<b>Table 17 PCR program.....</b>	<b>46</b>
<b>Table 18 GW primers.....</b>	<b>48</b>
<b>Table 19 GW reaction.....</b>	<b>48</b>
<b>Table 20 GW shuttling.....</b>	<b>49</b>
<b>Table 21 in vitro transcription of RNA.....</b>	<b>53</b>
<b>Table 22 dsRNA primers.....</b>	<b>54</b>
<b>Table 23 luciferase assay protocol.....</b>	<b>56</b>
<b>Table 24 A and B cDNA synthesis protocol.....</b>	<b>62</b>
<b>Table 25 A and B qPCR protocol .....</b>	<b>62</b>
<b>Table 26 siRNA screen candidates .....</b>	<b>74</b>

# 1.0 Introduction

## 1.1 The immune system

The immune system of the vertebrate has come a long way in its evolution in order to establish defences from invading intracellular or extracellular pathogenic microorganisms, which would seek to exploit their hosts rich abundance of nutrients. The immune system is one of the fundamental pillars of survival, without an immune response, hosts are unable to protect themselves from a myriad of dangerous and life-threatening microorganisms. The immune *system* itself is a collection of defences and responses that work in unison together to mount an effective reaction to sterilise the host environment and maintain homeostasis. In humans, in order to achieve this, there are specialised subsets of cells that play specific rolls in mounting a protective response against invading microorganisms [Figure 1.1]. As shown, these cells release soluble mediators that confer a specific protective response, be it cell type-cell type communication/activation or a direct and/or indirect response against the invading pathogen.

**Figure 1.1 Cells of the immune system**

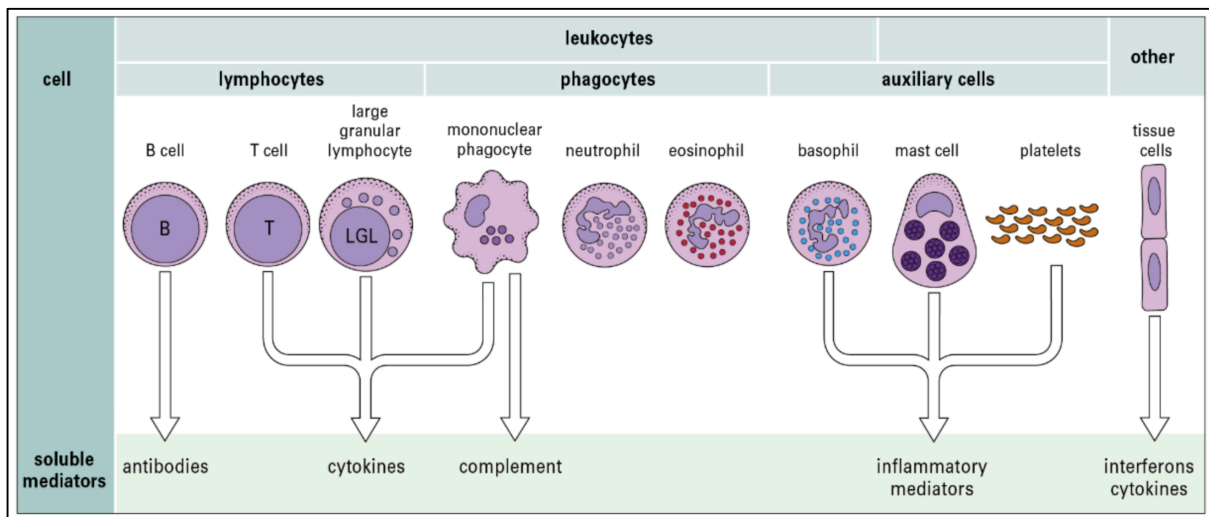


Figure 1.1. Male et al. Immunology 8<sup>th</sup> edition, Elsevier Saunders. Cells of the immune system.

Commonly referred to as white blood cells, leukocytes, or lymphocytes, these cells originate from hematopoietic stem cells and circulate via the lymphatic system of the human body. Each lymphocyte subtype has a specific role to play in the systemic immune response, producing soluble mediators that directly effect the type of immune response. These responses can be subdivided into two categories; the innate immune response, and the adaptive immune response.

## 1.2 cells of the immune system

Figure 1.2 Immune stem cells

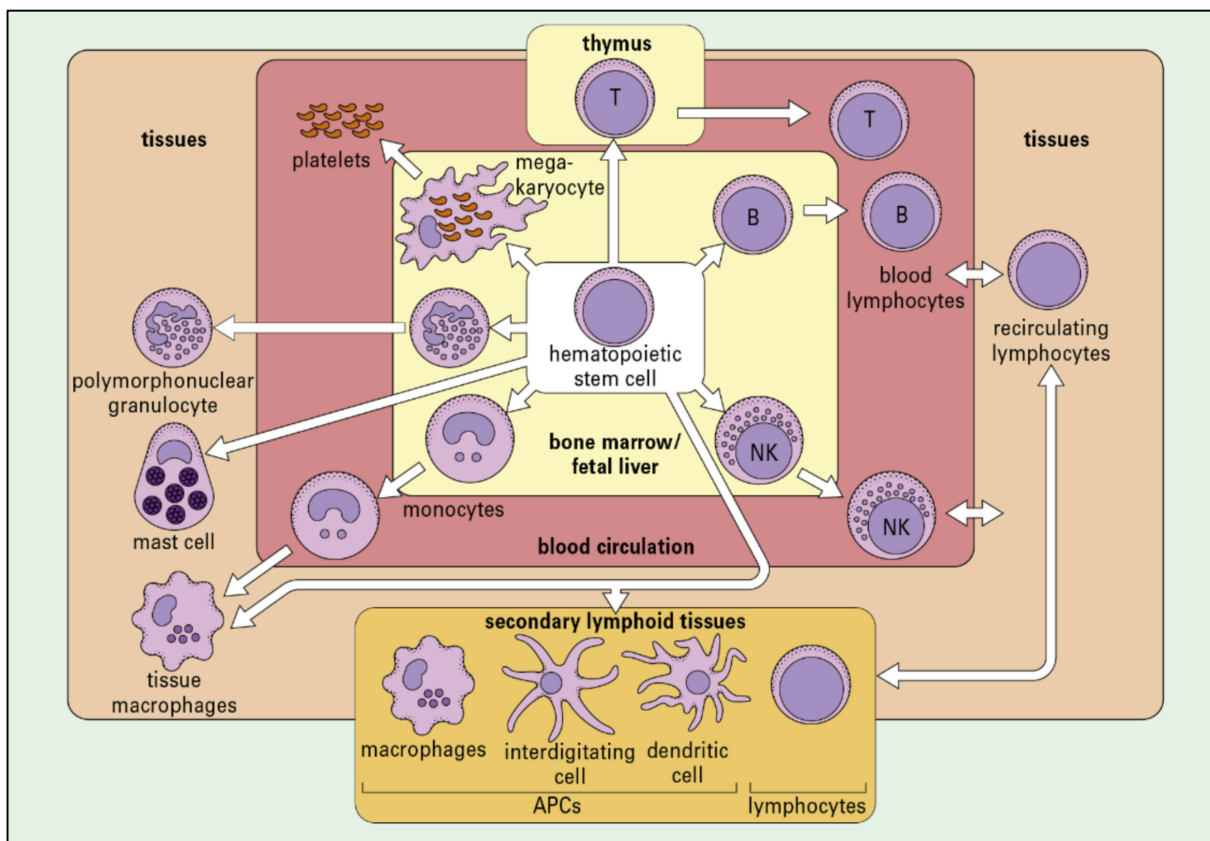


Figure 1.2 Male et al. Immunology 8<sup>th</sup> edition, Elsevier Saunders. Origin of cells of the immune system.

As described previously, leukocytes originate from hematopoietic stem cells that are largely located in the bone marrow, but also found in fetal liver tissue. Furthermore,

the two axes of immune system (adaptive/innate) contain specific cell lineage subsets. For example, the innate axis of the immune system comprises of the myeloid cell lineage (meaning bone marrow derived); monocytes/macrophages, polymorphonuclear granulocytes, mast cells, and platelets. The adaptive axis of immune system comprises of lymphoid cells such as thymus matured lymphoid cells (T cells) and bone marrow matured lymphoid cells (B cells), and in addition, natural killer cells (NK cells), which are lymphoid in origin despite being primarily associated with the innate axis of immunity.

## **1.2.1 Immune cells and their functions**

### *1.2.1.1 Myeloid cells*

Myeloid cells are defined as cells originating from the bone marrow, where they supply the peripheral blood system with leukocytes. These include monocytes and granulocytes. Monocytes can be matured into a range of cells, depending on the tissue in which they reside. For example, monocytes can be terminally matured into macrophages, which are present as kupffer cells in the liver, alveolar macrophages in the lungs, osteoclasts in the bone, and mesangial macrophages in the kidneys. Monocytes may also differentiate into specific dendritic cells (DCs). These are present in lymphoid organs (DCs) and in the skin (Langerhans cells)[1].

### *1.2.1.2 Antigen presentation*

DCs are considered “professional” antigen presenting cells (APCs). Their specific function is to present peptides for inspection by the adaptive immune cells (T cells and B cells) in order to differentiate non-host derived peptides from host derived peptides, such that an immune response can be mounted [2]. A common cellular function of these DCs is the regular turnover of proteins within the cell. Special receptors known as Major histocompatibility complexes (MHCs type I and II), are expressed in DCs and post translationally processed. During this processing, the MHC molecules are sent to



the ER and, in a random fashion, bind cellular peptides that are generated during *cis* degradation mechanisms. Thus, by regularly binding peptides that are produced from constitutively active proteosomal degradation, any protein derived from a foreign microorganism that is degraded in addition to host proteins, will be bound by MHC molecules and presented on the surface of the APC for recognition by T/B cells [3]. DCs, and indeed monocytes and macrophages, are particularly important for the immune response because they can not only express MHC molecules that present endogenously derived peptides, but due to phagocytosis, also possess the ability to express MHC molecules that present *exogenously* derived peptides. MHC class I expressing cells (Non B cells) are present in every major tissue investigated, with the exception of the brain parenchyma, however, whereas MHC class II is exclusively expressed on specific myeloid cells (DCs, monocytes, macrophages) [4].

The primary goal of the immune system is to first determine what is “self” and what is “non-self”. The hypothesis that differentiation of self and non-self was due to a clonal selection mechanism of genetically distinct mother/daughter/sister T and B cells during development was first postulated in 1957 by Burnet [5]. Extensive research has shown that Burnet’s initial modification of the theory was correct. Indeed, genetically unique T and B cells are only clonally selected if they do not respond to host derived peptides during development and maturation. This critical determination of “self” versus “non-self” is carried out by specific receptors of cells within the body. In the case of T cells and B cells, DCs provide a mechanism by which these adaptive immune cells can investigate the human body for invading pathogens by presenting molecular structures derived from potentially pathogenic microorganisms on their surface via MHC molecules [6, 7].

### *1.2.1.3 Lymphoid cells*

As with myeloid cells, lymphoid cells originate from hematopoietic stem cells and confer the adaptive axis of the immune system [8-11]. T and B cells are the primary lymphoid cells, however it is known that NK cells are in addition defined as lymphoid cells, despite the fact they are not classically defined as adaptive immune cells [12]. T and B cells are responsible for the adaptive axis of the immune system, and rely on

the foundations of the innate axis of the immune system to confer their effector function. T and B cell activation requires the antigen presentation system of the innate immune system, once activated, the adaptive immune system can begin on coordinating its immune response.

#### *1.2.1.4 The adaptive immune response*

T cells are subdivided into several types that are transformed from a pluripotent stem cell using epigenetic mechanisms and transcriptional control [13-15]. These transformation mechanisms, in addition to T cell receptor (TCR) rearrangements, commit T cell progenitor cells to specific subtypes of T cells, which are defined by their TCR and transcriptional control [14]. The different effector T cells consist of Helper T cells which are marked as being CD4<sup>+</sup> T cells (T<sub>H</sub>1, T<sub>H</sub>2, T<sub>H</sub>17, T<sub>H</sub>9, and T<sub>H</sub> cells) [16], and Cytotoxic T cells or Cytotoxic lymphocytes (CTLs) (CTLs, T<sub>C</sub>2, T<sub>C</sub>17, and T<sub>C</sub>9 cells) which are marked as being CD8<sup>+</sup> T cell [17]. The main role for APCs, in the context of lymphoid cells, is to activate the lymphoid effector function. APCs will engulf extracellular pathogens, or be infected by intracellular pathogens and present peptides derived from these foreign microorganisms, if the correct signalling conditions are in place, the APC will activate a specific clone of a T cell [17]. CD4<sup>+</sup> and CD8<sup>+</sup> T cells, although sharing similar T cell receptor gene identity, require different MHC class molecules in order to be activated. CD4<sup>+</sup> T cells and their TCR require a co-stimulation by its cognate peptide sequence displayed by MHC class II molecules, while CD8<sup>+</sup> T cells and their TCR require co-stimulation by MHC class I molecules. Despite recognition of a non-host molecular pattern displayed by MHCs, further stimulation is necessary. TCR activation requires a non-host molecular pattern accompanied by the inflammatory cytokine IL-12, and the co-expression of CD80/86 on the APC that is cross-presenting the antigen. Only with the trifecta of co-stimulatory signals will a T cell become activated [18].

This is an excellent example of the coordinated machinery involved in regulating the immune response. These necessary “permission” steps define the coordination of the systemic nature of the immune system. If this highly regulated system was to become unregulated, then the host can suffer from auto-immune

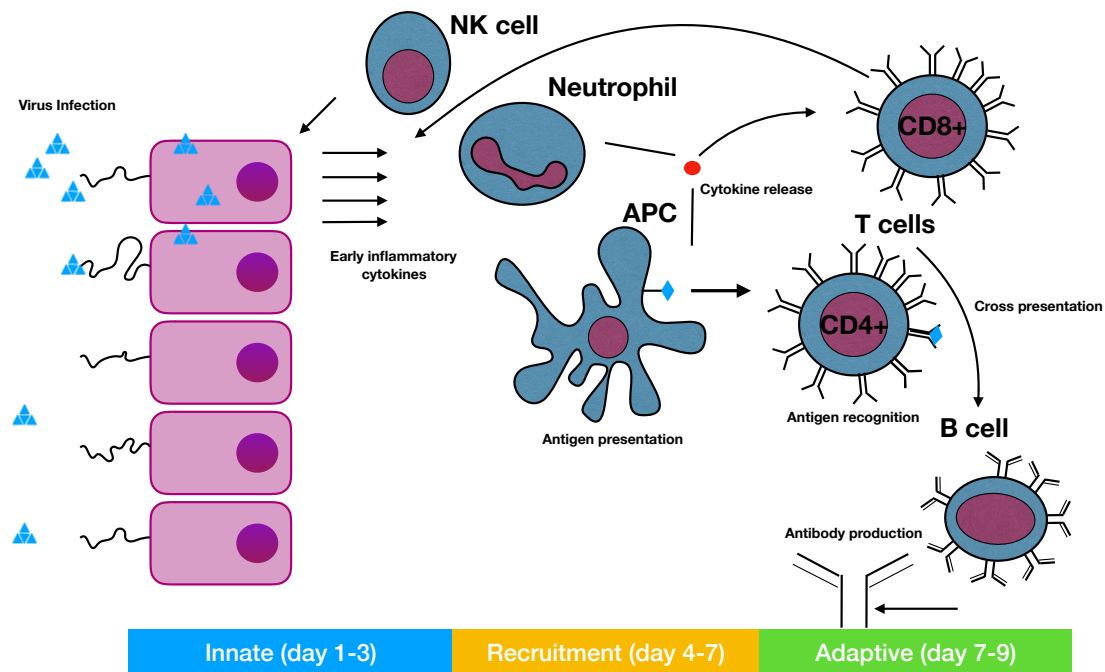
related diseases such as diabetes mellitus type 1, multiple sclerosis, inflammatory bowel disease, rheumatoid arthritis, or systemic lupus erythematosus.

Activated T cells then coordinate with B cells via the B cell receptor (BCR) and TCR in order to activate the production of antigen specific antibodies through clonal expansion and antibody maturation [19]. The B cell receptor is a complex multimeric receptor that undergoes a considerable amount of regulation during its activation initiation signal [19-22]. B cells can become activated in a similar fashion to T cells (APC depending activation), but can also be directly activated by T cells that have already recognised and been activated by a foreign molecular pattern [19, 23]. Once activated, the antigen specific BCR expressing B cell will proliferate (clonal expansion) and produce and excrete the antigen specific antibody in vast numbers in order to clear the infection.

Thus, activation is dependent on the intricate organisation of a considerable range of molecules, requiring the coordination of not only both intracellular signalling pathways and intercellular communication, but additionally the coordination of immune cell subtypes (figure 1.3). As previously introduced, the cell-cell coordination and regulation is of the utmost importance for a regularly functioning immune system. This is another example of the intricate regulation involved in the immune response, but on the intracellular level of a single cell.

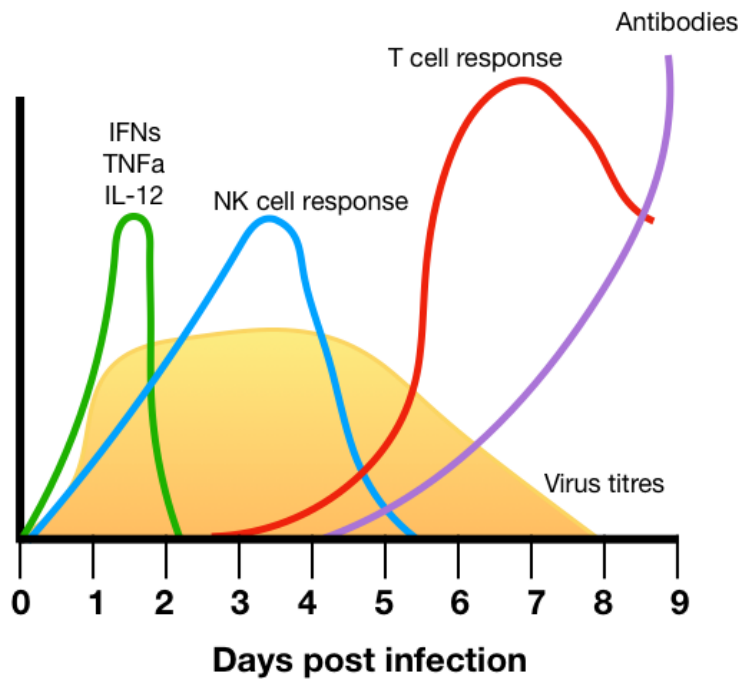
The innate axis of the immune system provides a rapid, and relatively nonspecific, initial response to pathogens that is necessary to recruit and activate the adaptive axis of the immune system (figure 1.4). Together, the immune *system* confers four classic features of a protective response, namely; specificity, memory, diversity, and self/non-self discrimination. In the case of virus infections, the innate immune system, as with any other infection, will coordinate with the adaptive immune system in order to fully clear the virus and protect the host.

**Figure 1.3 Immune response to a virus**



**Figure 1.3:** schematic overview of the general response of the immune system as a coordinated system, in response to a virus infection.

**Figure 1.4 Time dependent responses of the immune system**



**Figure 1.4:** schematic representation of the general responses over time to a virus infection: The rapid response of the innate immune system (factors include IFNs,  $TNF\alpha$ , and interleukins such as IL12) is followed cell specific activation dynamics which ultimately results the activation of B cells and the production of antigen specific antibodies.

As described in the chapter thus far, and shown in figure 1.3 and 1.4, the immune system as a whole relies on various cell types and responses in order for a successful coordinated systemic immune response to occur. What is also clear is that the innate system provides a pillar on which the immune system stands in order to effectively respond to invading pathogens. Without the early detection and alarm systems, the adaptive immune system cannot effectively exert its response of 'clearing' the specific pathogen due to the lack of activation by the innate immune system. The primary focus of this thesis is the innate immune response to a virus infection.

### **1.3 The innate immune response to viruses**

Viruses are the most abundant pathogens that the human immune system is challenged with. They are the most diverse and rapidly evolving class of pathogens to date, and therefore represent a significant threat to health. As introduced previously, the innate immune axis provides an essential role for the immune system. Without a fully functional innate immune system, many serious diseases may arise. An example of this is  $IKK\gamma$  (NEMO) deficiency syndrome, which presents itself as a severe form of hypohidrotic ectodermal dysplasia, which is characterised by severe abnormalities in skin, nail, hair, and sweat gland development [24, 25]. Additionally, for TLR3, which is receptor associate with the recognition of viruses, there are studies suggesting it is redundant, however it is specifically necessary in protecting the CNS from HSV-1 infection. TLR3 deficiency syndrome results in a clinical manifestation of HSV-1 induced encephalitis [25-27]. Other immunodeficiency related diseases regarding the innate immune system include MyD88 deficiency (caused by an inherited mutation in the gene *MYD88* and results in early-life invasive bacterial infections that can be life threatening), IRAK4 deficiency (another inherited disorder resulting in bacterial

infections), WHIM syndrome, Epidermodysplasia verruciformis (a rare skin disorder with a high risk for cancer development), and Chronic mucocutaneous candidiasis (a T cell disorder resulting in chronic infection by candida fungi) [25].

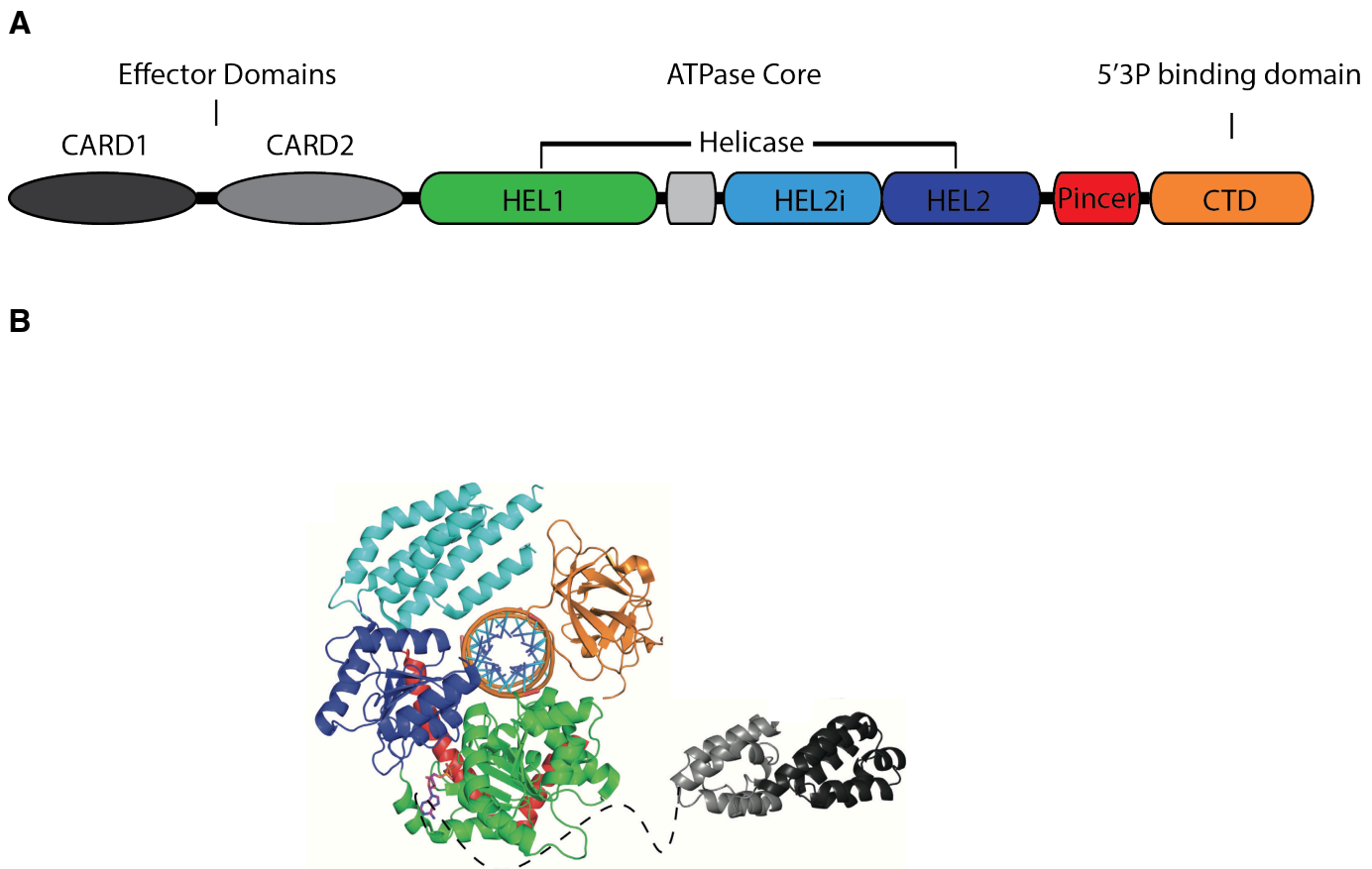
Viruses must be rapidly detected in order to protect the host. The innate immune system provides the first line of defence against virus infections. In the early 2000's, almost nothing was known about the cellular machinery or mechanisms by which viruses were detected, resulting in the subsequent production of IFN and inflammatory cytokines. It is now well understood how receptors, known as pattern recognition receptors (PRRs), which are ubiquitously expressed in different tissues of the human body and specifically detect molecular patterns of viral origin (pathogen associated molecular patterns (PAMPs)). A significant body of research has led to a monumental shift in the understanding of the host defence against viruses compared to 20 years ago [28-31].

There are two subfamilies of PRRs that responsible for detecting and responding to viruses. The first family is the toll-like receptor (TLR) family that, in humans, is made up of TLR1-10, while TLR3, TLR7, TLR8, and TLR9 are specific antiviral innate immunity [32]. There are however cases where classically bacterial associated TLRs play a role in antiviral immunity, for example, TLR4 specifically binding a viral protein from respiratory syncytial virus to initiate innate immune signalling [33]. The second family of PRRs is the RIG-I-like receptor (RLR) family of PRRs, which encompasses RIG-I (*DDX58*) MDA5 (*IFIH1*), and LGP2 (*DHX58*). Viral nucleic acids (both RNA and DNA ss/ds) provide the all-important pathogen associated molecular pattern (PAMP) that is recognised and bound by the PRRs, discriminating self from non-self. This thesis will specifically focus on RIG-I mediated detection of dsRNA and signal transduction.

## 1.3.1 RIG-I signalling

### 1.3.1.1 Structure and function of RIG-I

**Figure 1.5 Domain structure of RIG-I**



**Figure 1.5: (A)** Colour coordinated schematic overview of the domain structure of RIG-I. **(B)** Colour coordinated crystal structure of RIG-I in its open conformation, Rawling *et al.*, 2014 [34].

As shown in figure 1.5, RIG-I is divided into different domains which each serve a role for RIG-I functionality. There is a tandem CARD domain (caspase activation and recruitment domain) on the N-terminus and a regulatory domain on the C-terminus (CTD), linked to a pincer domain. These domains surround the ATPase core of RIG-I, which is made up of a SF2 RNA helicase domain. RIG-I helicase domain is

separated into three subdomains, HEL1, HEL2, and HEL2i, however only HEL1 and HEL2 interact with functional groups of the RNA [35, 36]. All RLR's are formed around this ATPase core with the homologous SF2 RNA helicase motif 'DExD/H box'. For these RLRs the RNA helicase structure has a relatively unique set of modifications. For example, two of the three alpha-helices within the helicase domain are orientated very differently. Normally in SF2 RNA helicases, the alpha-helices are found parallel to the beta sheet. In RIG-I they protrude out towards the pincer domain, this functions to allow the RLRs to bind RNA in a duplex formation. Around the helicase core of RIG-I, there are two tandem caspase activation and recruitment domains (CARD) on its N-terminus which are found as an inactive form of the protein in a "closed" conformation [37]. The C terminal domain (CTD, or regulatory domain (RD)) of RIG-I is responsible for the binding of 5'triphosphorylated (5'3P) dsRNA, a non-self molecular pattern [37-41]. Unlike other helicase enzymes, RIG-I does not unwind the duplex, but rather translocates to the 5'3P of the dsRNA for binding. This results in a conformational change of the tandem CARD domains to an "open" position, where they are exposed for post translational modifications, which is required for the activation of downstream effector molecules [36, 39, 42, 43]. Furthermore, it has been shown that RIG-I binds in an oligomeric fashion, resulting in filament formations of RIG-I along the length of the dsRNA, which is suggested to be a prerequisite for functional downstream signalling to occur [44-46]. The process of oligomerisation of RIG-I along dsRNA has been demonstrated to require binding of unanchored K63-link polyubiquitin chains [47, 48]. Downstream of the helicase domain and upstream of the CTD/RD lies a pincer domain, which has been demonstrated to be required for the facilitation of dsRNA binding, via a 'nano mechanical' bridging mechanism, and is essential for efficient IFN production [34, 49, 50].

#### *1.3.1.2 LGP2 and MDA5*

LGP2, otherwise known as DHX58, lacks the essential CARD domains necessary for the interaction with MAVS, a mitochondrial associated adaptor protein (which will be discussed in detail in 1.3.1.4). Its role in RLR mediated signal transduction has been inconsistently reported, with several groups offering evidence of a positive role for

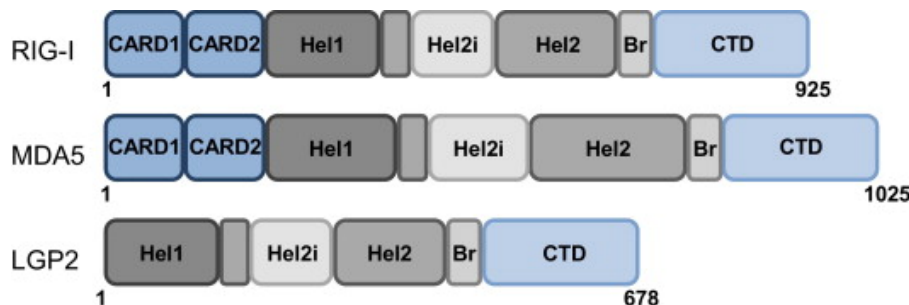


signal transduction, while other groups offer evidence for a negative role [51-53]. More recently however, the role LGP2 plays in terms of positively regulating MDA5, has been made unambiguous [54, 55]. LGP2 cooperates with MDA5 in order to enhance signalling by binding dsRNA via its C-terminus and initiating nucleation of MDA5 [56].

MDA5's PAMP has been relatively unknown, however it has been suggested that the primary PAMP is long dsRNA molecules, and that MDA5 oligomerises along the dsRNA molecule in order to initiate signal transduction, with the help of LGP2 [44, 56]. The regulation of its activation is yet to be fully elucidated, although binding of unanchored ubiquitin chains and/or SUMOylation are post translational modifications which may play an important role [48, 57].

A comparison between the structural domains of each RLR can be seen in figure 1.6. Given that RIG-I and MDA5 are structurally quite similar, and the fact that LGP2 lacks the tandem CARD domains, there may be strict post translational regulatory steps involved in the divergence of the modes of activation between RIG-I and MDA, and to a certain extent, LGP2.

**Figure 1.6 RLR structure homology**



**Figure 1.6:** Schematic overview of the RLRs' structures; RIG-I, MDA5, and LGP2, modified from Chiang *et al.*, 2014 [58]

### *1.3.1.3 RIG-I signalling overview*








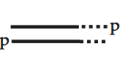




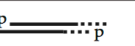
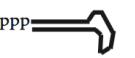
Due to the potential for pro-inflammatory cytokine production of the innate antiviral immune response, an uncontrolled, overzealous, or disproportionate response can be detrimental to the host, therefore the entire signalling system is tightly controlled. Conversely, upon viral infection, the response by RIG-I and IFN must be rapid in order to protect the host. As such, several positive and negative regulators exist for controlling the RIG-I signalling cascade [32].

The primary ligand required for RIG-I activation is 5'3P duplex RNA or dsRNA, but it has been demonstrated that the dependence on the 5'3P group decreases as the length of the RNA molecules increases [28, 38, 40, 42, 45, 59-62]. Despite being specific to a certain type of PAMP, RIG-I has been reported to recognise and respond to various forms of dsRNA, which can be reviewed in figure 1.7, in addition to DNA viruses. Furthermore, literature suggests that sequence motifs of dsRNA also play a role in the amplitude of RIG-I mediated IFN responses, and that RIG-I can not only respond to 5'3P but also 5'2P dsRNA [63, 64]. Additionally, there is a report suggesting that RIG-I is responsible for directing the antiviral response against CCHFV, which is harbours 5'1P dsRNA PAMP [65].

The canonical steps following RIG-I recognition of viral RNA/DNA, which will be discussed in detail in sections 1.3.1.4-7, include the interaction with an adaptor protein known as MAVS (mitochondrial antiviral stimulator) via the tandem CARD domain of RIG-I, causing MAVS aggregates to form (MAVS nucleation) [66]. Activated MAVS complexes then recruit a variety of adaptor proteins which have been described to mediate the signal transduction via formation of a large signalling complex. At this point, RIG-I signalling diverges into two canonical signalling pathways, leading to IRF3/7 activation and NF $\kappa$ B activation [67]. However, RIG-I signalling is primarily an antiviral associated signalling pathway and thus IRF3/7 activation is more predominant than NF $\kappa$ B activation. Once MAVS has recruited its adaptor proteins, specific kinase enzymes are phosphorylated in order to mediate transcription factor activation. For the IRF3/7 canonical signalling, the essential kinases that are required are TBK1 and I $\kappa$ K $\epsilon$ , which directly phosphorylate IRF3/7 [68]. For NF $\kappa$ B canonical signalling, the kinases that are responsible for mediating activation include I $\kappa$ K $\alpha$ / $\beta$ / $\gamma$ . Together they

cause the disassociation of NF $\kappa$ B from its inhibitor I $\kappa$ B $\alpha$ . I $\kappa$ B $\alpha$  becomes phosphorylated by I $\kappa$ K $\alpha$ / $\beta$  and then dissociates from NF $\kappa$ B where it is then targeted for degradation [69]. These steps and the proteins involved have been defined as the canonical steps in RIG-I signalling, leading the production of interferon, interferon stimulated genes, and pro-inflammatory cytokines and ultimately generating an antiviral state.

**Figure 1.7 RIG-I ligands**

Name	Length (nt)	Structure (source)	5'	3'	Test system	
GFP2	24	ds and ss 3pRNA (phage polymerase IVT)		3p	OH	IFN- $\alpha$ / $\beta$ ELISA in human cell lines (HEK293, HeLa, K562, etc.)
Lamin A/C	50–1,000	ds 3pRNA, 5' and 3' blunt end (phage polymerase IVT)		3p	OH	IFN- $\alpha$ / $\beta$ ELISA in murine cDCs, MEFs
VSV	11,000	ss 3pRNA (VSV genomic RNA)		3p	OH	
Tri-GFPs	24	ss 3pRNA (phage polymerase IVT)		3p	OH	IFN- $\alpha$ / $\beta$ ELISA in human monocytes, murine cDCs, MEFs
SAD $\Delta$ PLp	11,900	ss 3pRNA (Rabies genomic RNA)		3p	OH	IFN- $\beta$ reporter assay in human cell lines (Vero and HEK293)
Tri-G-AC-U	31	ss 3pRNA (phage polymerase IVT)		3p	OH	Interaction of RIG-I protein with tri-G-AC-U by pull-down assay
Flu vRNA	890–2,341	ss 3pRNA (Influenza A genomic RNA, 8 segments)		3p	OH	IFN- $\alpha$ ELISA in murine DCs, IFN- $\beta$ reporter assay in human cell line (HEK293), interaction of vRNA with RIG-I-protein (gel shift assay)
RNaseL fragments	<200	ss and dsRNA, 5'- or 3'-overhangs (digestion of cellular RNA with RNaseL)		OH	1p	Induction of IFN- $\beta$ in murine MEFs
pppRVL	58	ss 3pRNA (phage polymerase IVT)		3p	OH	RIG-I protein by fluorescence anisotropy, RIG-I dimerization by chromatography
pppVSVL	60	ss 3pRNA (phage polymerase IVT)		3p	OH	IFN- $\beta$ reporter assay in human cell line (HEK293), pull down assay with RIG-I protein
ppp-shRNA-luc3	22+24 loop	sh 3pRNA, 2-nt 3'-overhang (phage polymerase IVT)		3p	OH	IFN- $\beta$ ELISA in human cell line (HeLa)
PU/UC	105	ss 3pRNA (phage polymerase IVT)		3p	OH	IFN- $\beta$ reporter assay in human cell line (Huh7) and MEFs, IFN- $\beta$ RT-PCR in MEFs, IRF-3 dimerization in Huh7, binding to RIG-I (gel shift), IFN- $\beta$ ELISA of mouse serum
Short poly I:C	300	ds 1pRNA, 2-nt 3'-overhang (digestion of poly I:C with RNase III)		1p	OH	IFN- $\beta$ ELISA in MEFs, ATPase assay with RIG-I protein, interaction with RIG-I protein by atomic force microscopy
PolyAU	(20–?)	ds 3pRNA, generated <i>in vivo</i> by transcription of transfected DNA poly(dAdT) by cellular RNA polymerase III		3p	OH	Induction of IFN- $\beta$ promoter reporter assay in HEK293 cells and of IFN- $\alpha$ in human monocytes and IFN- $\beta$ in murine MEFs

**Figure 1.7:** Overview of putative RIG-I ligands that may initiate signal transduction, reviewed by Schlee and Hartmann, 2010 [70].

#### *1.3.1.4 RIG-I activation of MAVS*

Once RIG-I has bound to its cognate PAMP and initiates its conformational changes previously described, the CARD domains of RIG-I become ubiquitinated (K63-linked ubiquitination) by E3 ligase enzymes TRIM25 and RNF135 (RIplet) [71-74], a process which requires initial dephosphorylation of RIG-I. This is mediated by PP1 $\alpha/\gamma$ , which target S8 and T160 of RIG-I in order facilitate ubiquitination [75, 76]. More recently, T667 has also been shown to be an important phospho-site for RIG-I [77]. RIG-I CARD domains, which are exposed and ubiquitinated upon recognition of dsRNA, interact with the CARD domains of an adaptor protein known as MAVS, which is found primarily on mitochondrial membranes [36, 78, 79]. Overexpression of MAVS leads to an enhanced IFN $\beta$  response, and contrastingly, depletion of MAVS in mice leads to impairment of the antiviral responses [80, 81], and additionally, virally induced dissociation of MAVS from the mitochondrial membrane also perturbs the antiviral responses [82]. Thus, MAVS has been revealed to be an important protein in antiviral signalling.

MAVS undergoes its own strict post translational modifications. Most importantly, activated MAVS forms prion-like aggregates on the surface of the mitochondrial membrane, these aggregates act as a robust signalling platform for downstream molecules to continue signal transduction [46, 83]. RIG-I CARD domains transiently interact with the CARD domain of MAVS, which requires a tetrameric formation of RIG-I molecules (hence the prerequisite for oligomerised RIG-I for induction of signalling). RIG-I interaction with MAVS results in the nucleation of MAVS molecules, and the transient nature of the interaction allows MAVS to recruit inactive MAVS, ultimately forming an aggregate of activated MAVS on the surface of the mitochondrial membrane [46]. It is here, at the surface of the mitochondrial membrane, where signal transduction is rapidly induced using two canonical signalling pathways that activate specific transcription factors involved in the expression of ISGs,

inflammatory cytokines, and most importantly, type I/III IFNs. These transcription factors are IRF3/7 and NF $\kappa$ B.

#### *1.3.1.5 MAVS mediated signal transduction*

Several proteins are recruited to the signalling platform formed by MAVS aggregates upon RIG-I activation in a spatio-temporal specific manner. A family of proteins recruited to MAVS is the tumour necrosis factor (TNF) receptor-associated factor proteins (TRAF) [84]. TRAF proteins are required for downstream signalling to occur, and this is mediated by the TRAF-interaction motif found on MAVS. One such member of the TRAF family is TRAF3, which has been shown to be required for the activation of IRF3 (but not NF $\kappa$ B) and production of IFN $\beta$ , and more recently than that, TRAF5 has been implicated in IRF3 activation [85-88]. Consequently, it was discovered that recruitment of E3 ligases to activated MAVS was an essential process in the transmission of the signal to transcription factors IRF3/NF $\kappa$ B. TRAF2, TRAF3, TRAF6, and LUBAC, are all E3 ligases that are recruited to MAVS during antiviral signalling [84, 89]. Recruitment of these E3 ligases is mediated by the interaction with death domain (DD) containing proteins; Fas-associated death domain (FADD) protein, TNF receptor-associated death domain (TRADD), and RIP1 [90-93]. While FADD and RIP1 have been demonstrated to be specific for the NF $\kappa$ B (both TNF $\alpha$ R and RIG-I mediated), literature points out that TRADD, FADD, and RIP1 form a complex at the MAVS signalling platform, and that it is from this complex that the canonical signalling pathways (IRF3/ NF $\kappa$ B) are separated from one another.

#### *1.3.1.6 IRF3/7 activation*

TRAF3, a crucial E3-ligase enzyme involved in IRF3 activation, is first ubiquitinated by E3 ligases cIAP1/2 (K63-linked ubiquitination) [94]. Polyubiquitinated TRAF3 then interacts with specific kinases that were found to be essential for the activation of IRF3 via phosphorylation. These kinases are 'TRAF family member associated NF $\kappa$ B activator TANK-binding kinase 1', or more commonly referred to as TBK1, and the

inducible I $\kappa$ B $\alpha$  kinase known as I $\kappa$ K-i or I $\kappa$ K $\epsilon$  (henceforth referred to as I $\kappa$ K $\epsilon$ ) [68, 95-97].

TBK1 and I $\kappa$ K $\epsilon$  are pivotal regulators of the IFN response, in fact, loss of both of these kinases impairs IFN $\beta$  production in response to virus infection [96, 98, 99]. A study carried out by Hemmi *et al.*, 2004., suggested that there is a certain level of redundancy regarding both kinases, although they are essential for IRF3 activation, the exact differences between their roles (if any) is yet to be fully elucidated. These two kinases, once activated by the multimeric complex at MAVS described previously, interact with TANK, NAP1, and SINTBAD, which have all been shown to be necessary for type I IFN production [96, 98, 100-103].

Functional studies by Goncalves *et al.*, 2011., demonstrate that there is a requirement for the interaction with aforementioned proteins, which act as adaptor/recruitment proteins, such that if TBK1, defective in binding these proteins, is expressed in mice lacking wild-type TBK1, then the mice have an impaired ability to induce IFN $\beta$  [103]. Despite this, there is a study that was carried out that describes mice with no apparent impairment of type I IFN production when lacking TANK [104]. It has also been described that DDX3, another DEAD box helicase, is activated by active TBK1, and that this process is necessary for the production of IFN $\beta$ , however the mechanism behind these findings are yet to be fully determined, although it is suggested that DDX3 couples I $\kappa$ K $\epsilon$  to IRF3, potentially via a direct interaction with TRAF3 and/or I $\kappa$ K $\epsilon$  [105-107]. More studies on DDX3 are required to fully clarify its role on IRF3 activation.

TBK1 and I $\kappa$ K $\epsilon$  are attributed with a ubiquitin-like domain (ULD) within their kinase domain (KD), in addition to a scaffolding/dimerisation domain (SDD), which is shared among all I $\kappa$ K related kinases. Like other I $\kappa$ K related kinases, TBK1 and I $\kappa$ K $\epsilon$  require a scaffold in order to become phosphorylated, and thus carry out their effector function. Both TBK1 and I $\kappa$ K $\epsilon$  require phosphorylation at Ser172 in order to become active [108-111]. Preceding phosphorylation is K63-linked ubiquitination at the ULD, which is mediated by MIB1/2 [112]. Phosphorylation at the Ser172 site is described to be mediated by a trans-autophosphorylation mechanism, which is facilitated by the scaffolding complex [69]. The scaffolding complex is formed from the adaptor proteins described previously that are recruited to the MAVS complex via TRAF3 [110, 113,

114]. As described, TRAF3 ubiquitination provides the means for this scaffolding complex to form, and this allows the autophosphorylation event of TBK1 to occur. It has been suggested by Clark *et al*, 2011, that TBK1/I $\kappa$ K $\epsilon$  Ser172 autophosphorylation event is mediated by an interaction with I $\kappa$ K $\beta$ , as specific inhibitors of resulted I $\kappa$ K $\beta$  resulted in diminished phosphorylation of TBK1/I $\kappa$ K $\epsilon$  [113]. Despite more work being required to fully define the mode of phosphorylation of these kinases, it has been shown that I $\kappa$ K $\beta$  get in close proximity with TBK1/I $\kappa$ K $\epsilon$ , mediated by a bridge formed by NEMO (also known as I $\kappa$ K $\gamma$ ) from the canonical NF $\kappa$ B pathway [69, 113-115]. It has been described that NEMO bridges I $\kappa$ K $\beta$  to TBK1 by binding to the K63-linked polyubiquitin chains formed on TBK1 by MIB1/2 [114].

Despite the unclear mechanism of phosphorylation of TBK1/I $\kappa$ K $\epsilon$ , when activated (defined by their Ser172 phospho-site), they work to phosphorylate the transcription factor IRF3, and once expressed, IRF7 in addition. This has been defined as a canonical step in IRF3/7 activation, which can only be achieved through MAVS nucleation upon RIG-I stimulation.

IRF3 and IRF7 activation occurs in the cytoplasm through their C-terminal domain [68]. In IRF3, there are 7 phospho-sites (Ser/Thr) on the C-terminus, between Ser385-Ser405. Only one phosphorylated residue between Ser396-Ser405 is necessary to mediate the interaction with CREB binding protein (CBP), a protein that mediates the activation of transcription, while Ser385 and Ser386 [116] mediate dimerisation and translocation from the cytoplasm to the nucleus [97, 117-120]. While IRF3 is constitutively expressed in most cells that have been examined, IRF7 is only expressed in lymphocytes and myeloid cells, or upon treatment of cells with IFN $\alpha$  [121]. IRF7 is activated much in the same way that IRF3 is activated, and upon phosphorylation, can form homodimers or heterodimers with IRF3/5 in order to translocate to the nucleus for transcription [122]. The IRF family of transcription factors all contain a DNA binding domains (DBDs) where they bind interferon stimulated response elements (ISREs) and mediate the transcription of ISGs and type I/III IFNs [123-126].

### 1.3.1.7 NF $\kappa$ B

Similar to IRF3 activation, with regards to RIG-I mediated signal transduction, NF $\kappa$ B requires MAVS aggregation on the surface of the mitochondrial membrane, but via a separated signalling pathway (canonical I $\kappa$ K dependent signalling). TRAF2 and TRAF6 interact with MAVS to mediate the recruitment of the adaptor proteins necessary for the scaffold that activates the canonical kinases involved in NF $\kappa$ B activation, although it has been shown there is a strong level of redundancy regarding the E3 ligases recruited to MAVS in this respect [79, 84].

NF $\kappa$ B is encoded for by five polypeptides that assemble in various combinations of subunits to form the NF $\kappa$ B transcription factors. The stability and affinity of the subunit interactions is mediated specific amino acid residues, however the most stable and commonly found NF $\kappa$ B transcription factor is made from RelA and p50 [127]. Each subunit contains the Rel homology region (RHR) at its N-terminus, followed by the dimerisation domain (DD). The two domains are linked via flexible linker sequence, and at the C-terminus the nuclear localisation signal (NLS) can be found. Three of the five sequences encoded for NF $\kappa$ B (RelA, c-Rel, and RelB) contain the transcription activation domain (TAD), which is necessary for the NF $\kappa$ B specific gene expression. The DD mediates the formation of hetero and homo dimers between the 5 different subunits of NF $\kappa$ B, for a possible total of 15 unique dimers, and of these, 12 have been described *in vivo* [127, 128].

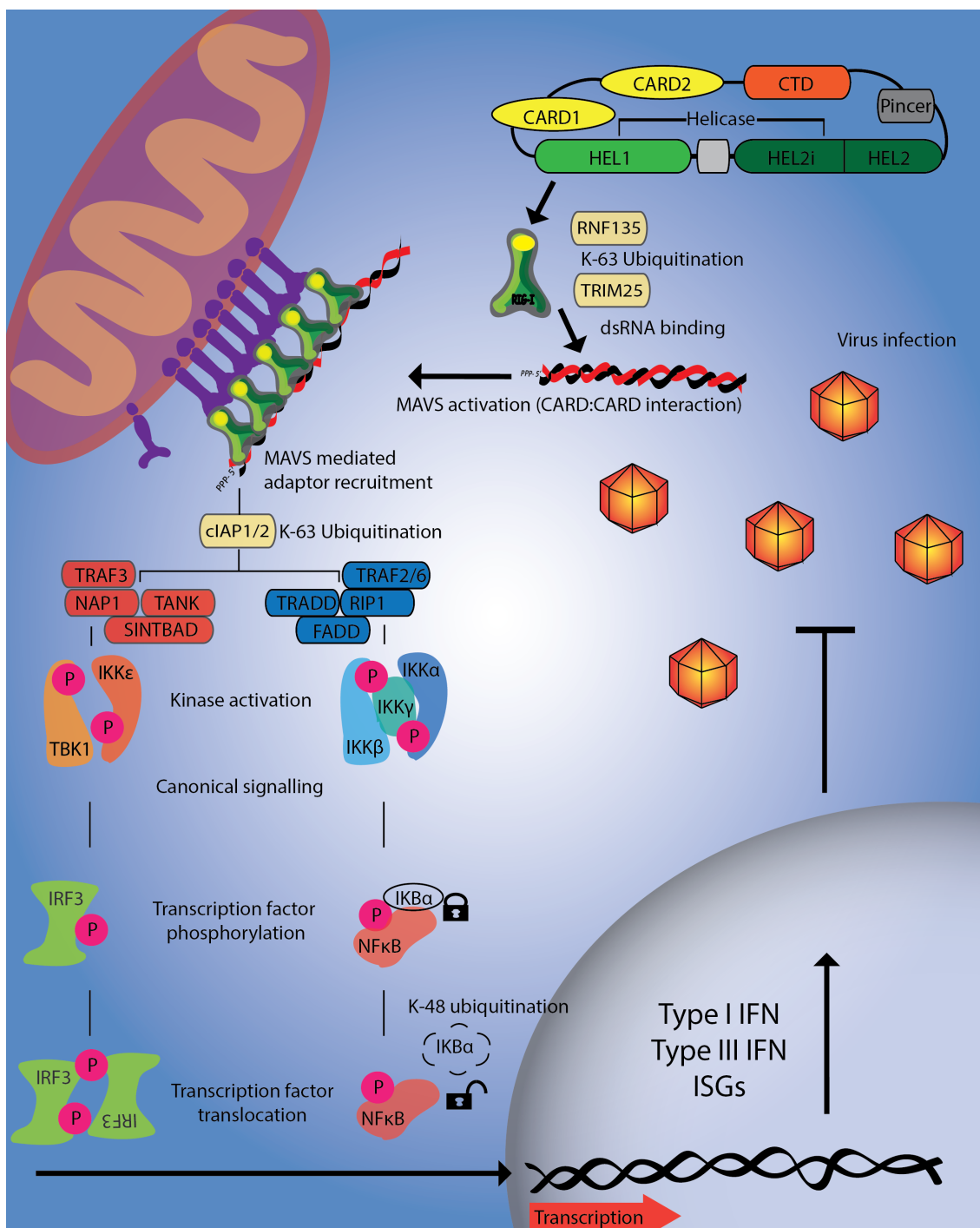
NF $\kappa$ B is constitutively inactive within the cytoplasm of cells due to its interaction with a family of inhibitory proteins, such as I $\kappa$ B $\alpha$ ,  $\beta$ , and  $\epsilon$ , which are classically found in the cytoplasm, however I $\kappa$ B $\alpha$  is by far the most predominant and prevalent inhibitor. There are, in addition, nuclear I $\kappa$ B proteins (Bcl-3, I $\kappa$ B $\zeta$ , and I $\kappa$ BNS), [27, 127, 129-131]. Nuclear I $\kappa$ B's are themselves products of NF $\kappa$ B transcription, and unlike classical I $\kappa$ B's specifically bind homodimers of p50 [132]. Nuclear I $\kappa$ B relevance must not be underestimated however, despite being non-classical, a study carried out in 2004 by Yamamoto *et al.*, described the loss of the ability of mice lacking I $\kappa$ B $\zeta$  to produce IL-6, a central pro-inflammatory cytokine [133].



Of the former mentioned cytoplasmic inhibitors ( $I\kappa B\alpha/\beta/\epsilon$ ), each contain six central Ankyrin repeats (~33 Amino acids), which mediate the interaction with  $NF\kappa B$ . Domains also found on  $I\kappa B$ 's include the phosphorylation site necessary for activation of  $NF\kappa B$  (S32 and S36), and the functional nuclear export signal NES. Despite the NES, the  $I\kappa B$  interaction with  $NF\kappa B$  functions to mask the NLS sequence on  $NF\kappa B$  [134].  $NF\kappa B:I\kappa B$  classical complexes ( $I\kappa B\alpha/\beta$  mediated) reside stably in the cytoplasm, whereas  $I\kappa B\epsilon$  acts as a negative feedback inhibitor [127, 135].

Following MAVS activation, while TRAF3 mediates the recruitment of adaptor proteins necessary for IRF3 activation, TRAF2/6 mediate the recruitment of adaptor proteins (TRADD, FADD, RIP1) for  $NF\kappa B$  [84, 88, 94, 136]. These adaptor proteins form a scaffold by which the canonical kinases required for  $NF\kappa B$  activation,  $I\kappa K\alpha/\beta$ , are recruited for their phosphorylation and subsequent activation [137-139]. Ubiquitination of  $I\kappa K\alpha/\beta$  allows NEMO to bridge  $I\kappa K\alpha/\beta$ , forming a kinase complex that facilitates autophosphorylation [139-143]. The active form of  $I\kappa K\alpha/\beta$ , formed with NEMO, is responsible for the phosphorylation of  $I\kappa B\alpha/\beta/\epsilon$ , which, in the case of  $I\kappa B\alpha$ , results in the direct K48-linked ubiquitination by the  $Ubc5/E3RS^{I\kappa B}$  E3 ligase pair [139, 144, 145] ultimately leading to its degradation, and thus releasing  $NF\kappa B$  from being localised to the cytoplasm, where it is phosphorylated in addition to  $I\kappa B\alpha/\beta$ . RelA is the target for phosphorylation at S536, and once phosphorylated and free of  $I\kappa B\alpha$ ,  $NF\kappa B$  translocates to the nucleus to mediate transcription of pro-inflammatory cytokines [27, 113, 139, 144, 146, 147]. Figure 1.8 provides an overview of RIG-I mediated signal transduction.

**Figure 1.8 Overview of RIG-I signalling**



**Figure 1.8:** Overview of RIG-I mediated activation of IRF3 and NFκB in response to dsRNA.

## 1.4 IFN signalling

There are 3 types of classical IFNs, deemed type I, II, and III IFNs. Type I/III IFNs are mostly related to antiviral induced signalling while type II (IFN $\gamma$ ) is specifically produced by “professional” immune cells such as NK cells and T cells. Type I and III IFNs are a family of cytokines that are related by structure, regulation, and function. All the type I IFN genes across mammalian species share clear homology sequences and chromosome location, suggesting a divergence from a single ancestral protein. Type I IFNs include IFN $\beta$ , IFN $\kappa$ , IFN $\omega$ , and IFN $\alpha$ , of which there are 13 known sub-types [148]. In contrast to type I IFNs, type III IFNs (IFN $\lambda$ 1 (IL29), IFN $\lambda$ 2 (IL28A), IFN $\lambda$ 3 (IL28B)) are more closely related in structure and chromosome location to IL10, an immune response inhibitory cytokine [149]. Once type I/III IFNs are produced, they are excreted and bind to specific receptors. There is little known about the exact mechanism of the secretory pathway for type I/III IFNs, although for IFN $\gamma$  it has been described that it is stored in granules in close proximity to the membrane surface ready for release, which is a similar secretory method for other cytokines such as IL4 and TNF $\alpha$  [150, 151]. For type I/III IFNs, it likely they exploit the same basic mechanism of secretion as most other cytokines, which is via site-specific (signal peptide) glycosylation [151]. Indeed, for IFN $\beta$ , it is glycosylated at N80, suggesting classic secretion mechanism, although the regulation of secretion of IFNs requires further research. IFN $\alpha/\beta$  bind to the ubiquitously expressed IFN $\alpha$ R made up of the IFNAR1 and IFNAR2 chains [152]. However, literature suggests the affinity and site binding on the IFNAR may vary depending on which IFN is binding it [153].

IFN $\lambda$ , binds to an unrelated receptor composed of the IL10 receptor and IFN $\lambda$  receptor (IL10R2 chain and IFNLR1 chain, respectively), which is mainly expressed on epithelial cells and DCs [154]. The importance IFN signalling must not be underestimated; of the very few cases of individuals born with defective IFN receptors, none have survived infancy [155].

The IFN receptors are formed from the Janus tyrosine-kinase receptor family chains (specifically Jak1 and Tyk2), which form stable dimers and autophosphorylate each other in order to mediate signal transduction. This results in the recruitment and phosphorylation of STAT proteins, namely STAT1 and STAT2, and in addition, with

regard to IFN $\lambda$ , STAT3. STAT1/2 forms heterotrimers with IRF9 (forming a complex known as ISGF3) or, additionally, STAT1 forms homodimers, and these complexes act as the primary downstream transcription factors which express ISGs [112, 120, 156-163]. The ISGs production and kinetics induced by IFN signalling vary depending on the type of IFN signalling induced, for example, type I IFN signalling results in a short but rapid burst in ISG expression, while type III IFN signalling yields a weaker, but a longer sustained expression of ISGs [164]. There are even reported differences in the level of gene expression for type I IFNs, for example, the gene Beta-R1 is expressed due to IFN $\beta$ , but not IFN $\alpha$ , despite binding to the same receptor [153].

Type I IFNs are primarily related to ISGF3 activation, while IFN $\gamma$  signalling is related to STAT1 homodimer activation. The phosphorylation of STAT1 and STAT2 (at Y701 and Y690 respectively) is a necessary post translational modification required for transcription factor activation and ISG expression [165].

## **1.5 Signalling dynamics and modelling**

As discussed thus far, the development of our understanding of the molecular biology of antiviral signalling is extensive. Identifying proteins involved in the molecular machinery of the cell is a major step forward with regard to research and medicine, but identifying a protein and understanding its regulation and interaction dynamics on a quantitative level, is another thing entirely. If one can understand the exact nature of the dynamics of the activation at the molecular level, one can gain insight into its regulation, potentially leading an understanding of the progression of disease states, in addition to the prevention of disease progression. This requires a multidiscipline approach, encompassing a wide range of skills. Mathematical modelling describes those observations by mathematical equations (ordinary differential equations – ODE's) and are based on the molecular biology behind those processes, which can be measured using various biochemical or molecular biological techniques. Mathematical modelling can provide a deeper insight into the regulation of changes within a biological process, as one could use the model to examine conditions not so easily observed from a molecular biology point of view. An excellent example of applying a model to further elucidate the nature of signalling dynamics and regulation

is a study published in 2002 by Alexander Hoffmann, where he and colleagues demonstrated a bimodal signal processing characteristic with respect to NF $\kappa$ B stimulus duration, and its regulation by I $\kappa$ B $\alpha/\beta/\epsilon$ , which had not been characterised before [166].

This study quantitatively analyses the molecular events that regulate RIG-I signal transduction from the level of detecting viral RNA to the level of transcription factor activation. This is achieved by resolving the time dependent activation states of canonical signalling proteins within the RIG-I signalling cascade that lead to both IRF3 activation and NF $\kappa$ B activation. By monitoring the phosphorylation levels and other activation states of specific proteins in the signalling cascade, namely TBK1, I $\kappa$ K $\epsilon$ , I $\kappa$ K $\beta$ , I $\kappa$ B $\alpha$ , IRF3, and RelA of NF $\kappa$ B, quantitative data can be used to formulate a mathematical model that describes these changes. Furthermore, ISG production, and indeed IFN signal transduction, is also examined in terms of the time dependent expression/activation rates of genes and proteins of interest. By applying the basic knowledge of the kinetics of regulatory steps during signal transduction to mathematical modelling, the temporal dynamics of the RIG-I signalling cascade will be elucidated and further our understanding of how the cell responds to a virus under certain conditions, how the virus succeeds in establishing an infection, or how it fails to establish an infection.

## 1.6 Ubiquitination

Ubiquitin is one of the most versatile post-translational modifications that occur in human cells, and is without a doubt indispensable for cellular homeostasis and fully functioning intracellular networks. The prevalence and importance of ubiquitination emerged in the 1970s, where the discovery of ubiquitin was just the tip of the iceberg of a complex and pivotal regulatory system [167-170]. Ubiquitins, named so because they are *ubiquitously* expressed in all cells, are processed into peptides of 76 amino acids. The key features of ubiquitins are the 7 lysine residues (K6, K11, K27, K29, K33, K48, and K63, in addition to Methionine 1) [171, 172], all of which can be modified with further ubiquitins, giving rise to isopeptide-linked ubiquitin chains which are the basis for ubiquitination as a post-translational modification. Many proteins contain a

ubiquitin binding domain (UBD) and are post translationally modified with either mono- or poly-ubiquitin chains to modify their function. This process is a multistage process involving three families of enzymes, named E1, E2, and E3 [172, 173]. Ubiquitin is first activated by E1 enzymes (activating enzyme) which produce a high-energy thioester bond involving the use of ATP [174, 175]. Ubiquitin is then transferred to E2 enzymes (conjugation enzyme) [176], and with the help of E3 enzymes (ligase enzymes), substrate specificity is determined, where ubiquitin is then conjugated to the  $\epsilon$ -amino group of the lysine residue specified by the E3 ligase on the target protein [174, 177, 178]. Ubiquitinated proteins are recognised by specific receptors or adaptor proteins that contain a ubiquitin binding domain homology (UBD), which have many roles in cells resulting in multitude of different signals [172]. Further, these ubiquitinated proteins are deactivated through interactions with deubiquitination enzymes (DUBs) [179]. During the process of ubiquitination, each of the 7 lysine residues can be utilised for the formation of ubiquitin polypeptides, and each ubiquitin chain takes on a distinct tertiary structure which results in recognition by specific E3 ligase enzyme [180]. The type of ubiquitination is determined by the lysine residue targeted for ubiquitination, for example, K48-linked ubiquitination is renowned for its targeting of protein for proteosomal degradation, an essential process in terms of cellular homeostasis [181]. K63-linked ubiquitination on the other hand is associated with a non-degradative/activatory modification [182]

While there only a handful of E1 and E2 enzymes, there are over 600 E3 enzymes encoded by the human genome which control various aspects of the complex cellular networks within human cells. The RIG-I signalling network is no exception to this fact, and in truth, ubiquitination is one of the most important features of the regulation of the antiviral system and has been intensively studied [84, 183-190], many of which have already been described in section 1.3.1. The emerging role of ubiquitination, and indeed deubiquitination in RIG-I mediated signalling has been gaining increased attention, and has been reviewed by Maelfait and Beyaert in 2012 [191]. Considering this, it is evident that research on the ubiquitination on antiviral signalling in general will continue to play an important role in defining our understanding on innate antiviral immunity and the pathogenesis of viruses. Taking this into account, we decided to investigate E3 ligases in more detail to expedite the

research in this regard. A comprehensive siRNA screening approach was devised in order to determine the extent of the missing links regarding E3 ligase regulation of RIG-I signalling. In 2008, a group published an extensive genome-wide and functional annotation of putative E3-ligases based on UBDs [192], and this became the basis for our approach to determine novel E3 ligases regulating RIG-I signal transduction (described in section 4.3).

# 2.0 Materials

## 2.1 Cell Culture

Table 1 Cell culture reagents

Table of Cell Culture Reagents	
Reagent	Components
<b>Cryo solution</b>	90% FCS, 10% DMSO
<b>DMEM - - -</b>	Gibco® Dulbecco's Modified Eagle Medium 1X +4.5g L-Glutamine - Pyruvate
<b>DMEM + - -</b>	DMEM FCS free and antibiotic free + MEM (1x)
<b>DMEM + - +</b>	DMEM Antibiotic free + MEM (1x) + 10% v/v Fetal calf serum (Gibco®)
<b>DMEM + + +</b>	DMEM complete + MEM (1x) + 100U/mL Penicillin and Streptomycin (Gibco®) + 10% v/v Fetal calf serum (Gibco®)
<b>Microscope Media</b>	DMEM complete without phenol red + MEM (1x) + 100U/mL Penicillin and Streptomycin (Gibco®) + 10% v/v Fetal calf serum (Gibco®)
<b>jetPEI®</b>	Polyplus jetPEI® transfection reagent
<b>Lipofectamine 2000®</b>	Invitrogen Lipofectamine 2000® transfection reagent 1mg/mL
<b>MEM</b>	Gibco® Minimal Essential Amino Acids 100X
<b>Opti-MEM</b>	Chemically defined medium with low serum requirement (Gibco®)
<b>PBS</b>	1X Phosphate buffered saline solution
<b>Trypsin</b>	0.05% trypsin + 0.02% EDTA in PBS
<b>Cytomix</b>	120 mM KCl, 0.15 mM CaCl <sub>2</sub> , 10 mM KPO <sub>4</sub> (pH 7.6), 25 mM Hepes, 2 mM EGTA, 5 mM MgCl <sub>2</sub> adjusted to pH 7.6 with KOH, supplemented with 2 mM ATP and 5 mM Glutathione

Table 2 Mammalian cells

Mammalian Cells	
Name	Expression and Resistance
<b>A549</b>	N/A
<b>A549 eGFP-IRF3</b>	eGFP-IRF3 Puromycin
<b>A549 eGFP-IRF3 mCherry-RelA</b>	eGFP-IRF3 Puromycin mCherry-RelA Neomycin
<b>A549 Tet-on</b>	Tet repressor (trans-activator) Blastidicin
<b>A549 Tet-on NLS-mCherry-2A-RIG-I<sup>2CARD</sup></b>	Tet repressor (trans-activator) Blastidicin NLS-mCherry-2A-RIG-I <sup>2CARD</sup> Hygromycin
<b>HEK293T</b>	N/A
<b>HEK293T RIG-I</b>	RIG-I Blastidicin



Huh 7 LucUbiNeo-ET	HCV RNA replicon with stable production of Firefly luciferase <i>Neomycin</i>
Huh 7.5 RIG-I	RIG-I <i>Blasticidin</i>
Huh 7.5 RIG-I eGFP-IRF3	RIG-I <i>Blasticidin</i> eGFP-IRF3 <i>Puromycin</i>

## 2.2 DNA and RNA

Table 3 DNA and RNA

Table of DNA and RNA Reagents and Kits	
Reagent/Kit	Company/Components
Annealing buffer	150 mM NaCl, 5 mM Tris
10mM dNTPs	PeqLab
25mM rNTPs	Roche
5X RRL buffer	(400mM Hepes pH 7.0, 60mM MgCl <sub>2</sub> , 10mM spermidin, 200mM DTT)
Midori Green ®	Nippon Genetics
50X TAE Buffer	2 M Tris, 2 M Acetic Acid, 50 mM EDTA, pH 8.3
6X DNA loading dye	45mL 50% glycerol, 1mL TAE 50X, 0.5 mL 100 mM EDTA pH 8.0, 0.13g orange, ddH <sub>2</sub> O to 50 mL
Accuprime ® high fidelity polymerase	Thermo Fisher
Fidelitaq ® polymerase	Affymetrix
Gateway ® LR/BP clonase ® enzyme cloning kit	Invitrogen
High capacity cDNA Reverse transcriptase ® kit	Applied Biosystems
NEB Assorted Restriction Enzymes	New England Biolabs
NEB buffer 1.1	New England Biolabs
NEB buffer 2.1	New England Biolabs
NEB buffer 3.1	New England Biolabs
NEB buffer CutSmart ®	New England Biolabs
NEB T4 DNA ligase	New England Biolabs
Nucleospin ® Gel and PCR clean up kit	Machery-Nagel
Nucleospin ® Plasmid extraction kit	Machery-Nagel
Nucleospin ® RNA plus kit	Machery-Nagel
Q5 ® high fidelity polymerase	New England Biolabs
RNAse ® inhibitor	Promega
RQ1 RNAse Free DNase ®	Promega
T4 DNA ligase buffer	50 mM Tris-HCl (pH 7.5), 10 mM MgCl <sub>2</sub> 1mM ATP, 10mM DTT
T7 RNA polymerase	

## 2.3 Plasmids

Table 4 Plasmids

Table of Plasmids				
Recombinant DNA	Promoter	Tag	Vector	Resistance
Firefly Luciferase	ISG56	-	pGL3B	-
Fos	CMV	Guassia Fragment (N2)	pcDNA3.1	-
IRAK2	CMV	Guassia Fragment (N1)	pcDNA3.1	-
IRF3	EF1- $\alpha$	LifeAct-mTurquoise	pWPI	Puromycin
IRF3	EF1- $\alpha$	eGFP	pWPI	Puromycin
IRF3	EF1- $\alpha$	mCherry	pWPI	Puromycin
Jun	CMV	Guassia Fragment (N1)	pcDNA3.1	-
LGP2	CMV	Guassia Fragment (N2)	pcDNA3.1	-
MAVS	ROSA26	N/A	pWPI	Blasticidin
MAVS	CMV	Guassia Fragment (N1)	pcDNA3.1	-
MAVS	CMV	Guassia Fragment (N2)	pcDNA3.1	-
mVenus	ISG56	N/A	pWPI	Blasticidin
NLS-Mcherry-2A-RIG-I <sup>2CARD</sup>	EF1- $\alpha$	N/A	pWPI	Blasticidin
NLS-Mcherry-2A-RIG-I <sup>2CARD</sup>	P-tight	P pgk	pWPI	Blasticidin
NLS-Mcherry-2A-RIG-I <sup>2CARD</sup>	P-tight	P pgk	pWPI	Hygromycin
NS3/4A (Con1)	EF1- $\alpha$	GFP-GUN	pWPI	Neomycin
NS5A	EF1- $\alpha$	HA	pWPI	Puromycin
RelA	EF1- $\alpha$	BFP	pWPI	Neomycin
RelA	EF1- $\alpha$	BFP	pWPI	Hygromycin
RelA	EF1- $\alpha$	mCherry	pWPI	Neomycin
Renilla Luciferase	SV40	-	pGL3B	-
RIG-I	EF1- $\alpha$	CFP	pWPI	Puromycin
STAT1	CMV	Guassia Fragment (N1)	pcDNA3.1	-
STAT2	CMV	Guassia Fragment (N2)	pcDNA3.1	-
Tet operator	TRE	PGK promoter	pLVX	Puromycin
Tet operator	TRE	PGK promoter	pLVX	Blasticidin
TRAF2	CMV	Guassia Fragment (N1)	pcDNA3.1	-
TRAF2	CMV	Guassia Fragment (N2)	pcDNA3.1	-
TRAF3	CMV	Guassia Fragment (N2)	pcDNA3.1	-
TRAF6	CMV	Guassia Fragment (N2)	pcDNA3.1	-
TRIM25	CMV	Guassia Fragment (N1)	pcDNA3.1	-

## 2.4 Protein Biochemistry

Table 5 Protein biochemistry

Table of Protein Biochemistry Related Buffers/Kits	
Name	Company/Components
10X PBS	80 mM $\text{Na}_2\text{HPO}_4$ , 1.4 M NaCl, 2.7 mM KCl, 1.76mM $\text{KH}_2\text{PO}_4$
TBS (10x), pH 7.5	20 mM Tris-Hcl, 150 mM NaCl, adjust pH to 7.5 with NaOH
10X TGS	150 mM Tris, 1.92 M Glycine, 1% w/v SDS
Cross-linking buffer	1% PFA in 1X PBS
Cross-linking quenching buffer	1.25M Glycine in 1X PBS
Laemmli Protein extraction Buffer	9.75 mL 0.5 M Tris (pH 6.8), 15 mL glycerol, 10 mL 10% SDS, 3.75 mL $\beta$ -mercaptoethanol, 3mg Bromophenol Blue, 6.5 mL ddH <sub>2</sub> O
Lumikine® human IFN $\beta$ ELISA kit	InvivoGen
Resolving Gel Buffer	1.5 M Tris, 0.8% w/v SDS (pH 8.8)
RIPA Protein extraction buffer	50 mM Tris HCl, pH 8.0; 150 mM NaCl, 1% (v/v) NP-40, 0.5% (w/v) sodium deoxycholate, 0.1% (w/v) SDS
Stacking Gel buffer	1 M Tris, 0.8% w/v SDS (pH 6.8)
Western Blot BSA Blocking Buffer	1X TBS, 5% w/v BSA 0.2% v/v Tween-20
Western Blot Milk Blocking Buffer	1X PBS, 5% w/v Protease Free Milk powder 0.2% v/v Tween-20
Western Blot Wash Buffer	1X PBS/TBS 0.2% (v/v) Tween-20

## 2.5 Primary Antibodies

Table 6 Primary antibodies

Table of Primary Antibodies				
Antibody	Origin	Specificity	Company	Reference
Calnexin	rabbit	poly	Enzo Life science	ADI-SPA-865-F
GAPDH	mouse	mono	Santa Cruz	sc-47724
IFIT1	rabbit	mono	Abnova	H00003434-DO1
I $\kappa$ B-alpha	rabbit	mono	Cell Signaling	9242
IKK beta	Rabbit	mono	Cell Signaling	D3OC6
IKK epsilon	Rabbit	Poly	Abcam	ab7891

<b>IRF1</b>	Rabbit	mono	Cell Signaling	D5E4
<b>IRF3 (FL-425)</b>	rabbit	poly	Santa Cruz	sc-9082
<b>IRF7 (pSer477)</b>	Rabbit	mono	Cell Signaling	D7E1W
<b>IRF9</b>	Rabbit	Poly	Abcam	ab126940
<b>MAVS</b>	rabbit	poly	Enzo Life science	AT107
<b>NF-Kappa-B p65</b>	Mouse	mono	Cell Signaling	L8F6
<b>P-IKK-alpha (S176) / IKK-beta (S177) (C84E11)</b>	Rabbit	mono	Cell Signaling	2078
<b>P-IRF3 (S396) (4D4G)</b>	rabbit	mono	Cell Signaling	4947
<b>pDDX58 (RIG-I) (pS8)</b>	rabbit	poly	Abnova	PAB15905
<b>pIKK-epsilon (pSer172)</b>	rabbit	poly	Millipore	06-1340
<b>pNF-kappa-B p65 (S536)</b>	rabbit	mono	Cell Signaling	3033
<b>pSTAT1 (pY701)</b>	mouse	mono	BD	612232
<b>pStat2 (pY690)</b>	Rabbit	mono	Cell Signaling	D3P2P
<b>pTBK1 (pS172)</b>	rabbit	mono	abcam	ab109272
<b>RIG-I</b>	rabbit	poly	Enzo Life science	ALX-210-932-C100
<b>STAT1</b>	mouse	mono	BD	610115
<b>TBK1</b>	rabbit	mono	Cell Signaling	3504
<b>β-Actin</b>	mouse	mono	Sigma-Aldrich	A5441

## 2.6 Secondary Antibodies

Table 7 secondary antibodies

<b>Table of Primary Antibodies</b>				
<b>Antibody</b>	<b>Origin</b>	<b>Specificity</b>	<b>Company</b>	<b>Reference</b>
<b>Mouse-HRP</b>	Goat	poly	Sigma-Aldrich	AP130P
<b>Rabbit-HRP</b>	Goat	poly	Sigma-Aldrich	AP186P
<b>Goat-HRP</b>	Donkey	poly	Santa Cruz	Sc-2020

## 2.7 Molecular probes and dyes

Table 8 probes and dyes

Table of probes and dyes		
Name	Company	Application
<b>DAPI</b> (4',6-diamidino-2-phenylindole dihydrochloride)	Invitrogen	Fluorescence (fixed)
<b>Hoechst 33258</b> (2'-(4-hydroxyphenyl)-5-(4-methyl-1-piperazinyl)-2,5'-bi-1H-benzimidazole trihydrochloride hydrate)	Sigma-Aldrich	Fluorescence (live)
<b>Aminoallyl-UTP - ATTO-647N</b> (C12H20N3O15P3 - ATTO 647N)	Jena Bioscience	Fluorescence (dye)

## 2.8 Luciferase Assay Buffers and Reagents

Table 9 luciferase assay

Table of luciferase assay buffers and reagents	
Name	Components
<b>0.1 M KPO<sub>4</sub></b>	17ml KH <sub>2</sub> PO <sub>4</sub> + 183ml K <sub>2</sub> HPO <sub>4</sub> 200ml H <sub>2</sub> O
<b>0.2 M EGTA</b>	15.2g EGTA (380.35 g/mol) in 200 mL ddH <sub>2</sub> O, adjust to pH 7.8 (does not dissolve until pH is adjusted)
<b>0.2 M K<sub>2</sub>HPO<sub>4</sub></b>	34.83g (174,18g/mol) in ddH <sub>2</sub> O
<b>0.2 M KH<sub>2</sub>PO<sub>4</sub></b>	27.21g KH <sub>2</sub> PO <sub>4</sub> (136,09 g/mol) in ddH <sub>2</sub> O
<b>0.5 M Glycylglycine</b>	Glycylglycine in ddH <sub>2</sub> O
<b>1 M MgSO<sub>4</sub></b>	15.2g EGTA (380.35 g/mol) in 200ml H <sub>2</sub> O, adjust pH to 7.8 using KOH.
<b>Coelenterazine</b>	5 mg coelenterazine (PJK) in 11.8 mL Methanol
<b>D-Luciferin</b>	84.1 mg D-luciferin (PJK) in 300 mL, 25 mM Glycylglycine
<b>Luciferase Assay Buffer</b>	200 mL: 10 mL Glycylglycine (0.5 M pH 7.8), 30 mL KPO <sub>4</sub> (0.1 M pH 7.8), 3 mL MgSO <sub>4</sub> (1 M), 4 mL EGTA (0.2 M pH 7.8), 153 mL ddH <sub>2</sub> O
<b>Luciferase Lysis Buffer</b>	500 mL: 5 mL Triton-X100, 25 mL Glycylglycine (0.5 M pH 7.8), 7.5 mL MgSO <sub>4</sub> (1 M), 10 mL EGTA (0.2 M pH 7.8), 50 mL glycerol, 402.5 ddH <sub>2</sub> O
<b>PCA Assay Buffer</b>	1X PBS 10 μM Coelenterazine

## 2.9 Primer sequences

Table 10 primer sequences

Table of primer sequences		
Name	Sequence (5'-3')	Application
<b>2A RIG-I Rv</b>	CTTTTGTTCATAGACGCCATGGGCCCGGATTTTCCTCCA C	PCR
<b>2A RIG-I-CA overlap Fw</b>	GTGGAGGAAAAATCCCGGGCCCATGGCGTCTATGGAACAAAA G	PCR
<b>Asc1 mCherry Fw</b>	ATCTATGGCGCGCCGATGGTGAGCAAGGG	PCR
<b>attB NLS Fw</b>	GGGGACAAGTTTGTACAAAAAAGCAGGCTTCATGAGCAGCG ATGATGAAGCGACCG	PCR
<b>attB RIG-I CA Rv</b>	GGGGACCACTTTGTACAAGAAAGCTGGGTCTTATGAATTCT CACTAAGATTCTG	PCR

<b>BFP Linker</b>	CTCGAGATCTGAGTCCGGAATTAAGCTTGTGCCCCAG	PCR
<b>BFP linker p65 overlap Fw</b>	GGGGCACAAGCTTAATTCCGGACTCAGATCTCGAGAAGACG AACTGTTCCCCC	PCR
<b>BFP linker p65 overlap Rv</b>	GGGGGAACAGTTCGTCTTCTCGAGATCTGAGTCCGGAATTA AGCTTGTGCCCC	PCR
<b>cPPT F</b>	AAAAGAAAAGGGGG	PCR
<b>EMCV2 R</b>	CGGCAATATGGTGGAAAATAAC	PCR
<b>GAPDH Fw</b>	GAAGGTGAAGGTCGGAGC	qRT-PCR
<b>GAPDH Rv</b>	CAAGATGGTGATGGGATTTC	qRT-PCR
<b>IFIT1 Fw</b>	GAAGCAGGCAATCACAGAAA	qRT-PCR
<b>IFIT1 Rv</b>	GAAACCGACCATAGTGGAA	qRT-PCR
<b>IFN<math>\beta</math> Fw</b>	GACGCCGCATTGACCATCTA	qRT-PCR
<b>IFN<math>\beta</math> Rv</b>	GACATTAGCCAGGAGTTCTC	qRT-PCR
<b>IFN<math>\lambda</math> Fw</b>	GCAGGTCAAATCTCTGTCACC	qRT-PCR
<b>IFN<math>\lambda</math> Rv</b>	AAGACAGGAGAGCTGCAACTC	qRT-PCR
<b>IRF3 AsiS1 Rv</b>	ATAGATGCGATCGCTTAGCTCTCCCCAGGGCCCTGGAAATC	PCR
<b>Linker p65 Fw</b>	CCGGACTCAGATCTCGAGAAGACGAACTGTTCCCCCTCATC	PCR
<b>mCherry - p65 linker Fw</b>	GGCGGCCGCTCGAGTCTCCGGACTCAGATCTCGAGAAGACG AACTGTTCCCCC	PCR
<b>mCherry - p65 linker Rv</b>	GGGGGAACAGTTCGTCTTCTCGAGATCTGAGTCCGGAGACT CGAGCGGCCGCC	PCR
<b>Mcherry 2A overlap Fw</b>	CACAGTGGCGGCCGCTCGAGTCAACGGTAGAGCCGAGGGC	PCR
<b>Mcherry 2a Rv</b>	GCCCTCGGCTCTACCGGTGACTCGAGCGGCCGCCACTGTG	PCR
<b>mCherry Linker</b>	CTCGAGATCTGAGTCCGGAGACTCGAGCGGCCGCCACTG	PCR
<b>mTurquoise Asc1 Fw</b>	ATCTATGGCGCCCATGGGCGTGGCCGACCTGATCAAGAAG TTCG	PCR
<b>mTurquoise IRF3 linker overlap Fw</b>	GGACGAGCTGTACAAGTCCGGACTCAGATCTCGAGAAATGG GAACCCCAAAGCC	PCR
<b>mTurquoise IRF3 linker overlap Rv</b>	GGCTTTGGGGTTCCTTTCTCGAGATCTGAGTCCGGACTT GTACAGCTCGTCC	PCR
<b>mTurquoise IRF3 ovrlp Fw</b>	GGCATGGACGAGCTGTACAAGGGAACCCCAAAGCCACGGAT CCTG	PCR
<b>mTurquoise IRF3 ovrlp Rv</b>	CAGGATCCGTGGCTTTGGGGTTCCTTGTACAGCTCGTCCA TGCC	PCR
<b>mTurquoise linker overlap Fw</b>	GGACGAGCTGTACAAGTCCGGACTCAGATC	PCR
<b>mTurquoise linker overlap Rv</b>	GATCTGAGTCCGGACTTGTACAGCTCGTCC	PCR
<b>mVenus Apa1 Rv</b>	GCCCGTGGGCCCTTACTTGTACAGCTCGTCCATGC	PCR
<b>mVenus BamH1 Fw</b>	ACCCGGGATCCATGGTGTAGCAAGGGCGAGGAG	PCR
<b>p65 AsiS1 Rv</b>	ATAGATGCGATCGCTTAGGAGCTGATCTGACTCAGC	PCR
<b>pDONR primer F</b>	TCGCGTTAACGCTAGCATGGATCTC	PCR
<b>pDONR primer R</b>	GTAACATCAGAGATTTTGTAGACAC	PCR
<b>pLV-pwpi promoter module 1 Fw</b>	CGAGCGCTGTGCCTTGAATGCTAGTT	PCR
<b>pLV-pwpi promoter module 1 MscI Rv</b>	GGTATCGATGTGCAGATAATGGCCA	PCR
<b>pWPI mTurquoise-IRF3 deltaGAp4446 Fw</b>	GGATGCACAGCAGGAGGATTTCCGAATCTTCCAGGCCTGGG CCGAGG	PCR
<b>pWPI mTurquoise-IRF3 deltaGAp4446 Rv</b>	CCTCGGCCAGGCCTGGAAGATTCGAAATCCTCCTGCTGT GCATCC	PCR
<b>RIG-I CA delta G-A Fw</b>	GATAAGATGGAACTTCTGACATACAGATTTTCTACCAAGA AG	PCR

<b>RIG-I CA delta G-A Rv</b>	CTTCTTGGTAGAAAATCTGTATGTCAGAAGTTTCCATCTTATC	PCR
<b>Tag-BFP Asc1 Fw</b>	ATCTATGGCGCGCCATGAGCGAGCTGATTAAGGAGAACATG	PCR
<b>Tag-BFP p65 overlap Fw</b>	GCAAACCTGGGGCACAAGCTTAATATGGACGAACGTTCCCCCTCATCTTCCCGGCAG	PCR
<b>Tag-BFP p65 overlap Rv</b>	CTGCCGGGAAGATGAGGGGGAAACAGTTTCGTCCATATTAAGCTTGTGCCCCAGTTTGC	PCR
<b>v2 NLS Mcherry overlap Fw</b>	CGAAGAAAAAGCGCAAAGTGATGGTGAGCAAGGGCGAGGAG	PCR
<b>v2 NLS mCherry Rv</b>	CTCCTCGCCCTTGCTCACCATCACTTTGCGCTTTTCTTCG	PCR

## 2.10 Viruses

Table 11 viruses

Table of Viruses	
Name	Origin
<b>Influenza A virus (SCM35) (<math>\Delta</math>NS1_2A_Gaussia)</b>	Martin Schwemmler, University Freiburg
<b>Influenza A virus (WSN1)</b>	Georg Koch, University Freiburg
<b>Mengo Virus</b>	Frank Van Kuppefeld
<b>Sendai Virus</b>	Rainer Zawatzky, DKFZ

## 2.11 Bacteria and Bacterial cultures

Table 12 Bacteria

Table of Bacteria and Bacterial Cultures	
Name	Components
<b>Ampicillin</b>	100mg/mL in ddH <sub>2</sub> O, filter sterilised
<b><i>E.coli</i> DH5<math>\alpha</math></b>	Chemically competent bacteria
<b>Gentamycin</b>	50mg/mL (Gibco®)
<b>Kanamycin</b>	30mg/mL in ddH <sub>2</sub> O
<b>Lysogeny broth (LB) Agar</b>	30 g Bacto-Trypton, 15 g Yeast extract, 15 g NaCl, 15 g Agar in 3 l ddH <sub>2</sub> O and autoclaved
<b>Lysogeny broth (LB) medium</b>	50 g Bacto-Trypton, 25 g Yeast extract, 25 g NaCl in 5 l ddH <sub>2</sub> O and autoclaved
<b>One Shot® ccdB Survival™ 2 T1R (Invitrogen)</b>	Chemically competent bacteria

## 2.12 Software

Table 13 software

Table of Software		
Name	Supplier	Application
<b>Bio-Rad CFX Manager</b>	Bio-Rad Laboratories, Hercules, California, USA	qRT-PCR evaluation and quantification
<b>GraphPad Prism 6.0h</b>	GraphPad Software, San Diego, California, USA	Generation of graphs and figures
<b>ImageJ</b>	Wayne Rasband, NIH, USA	Western Blot evaluation and figure generation
<b>INTAS Chemostar</b>	INTAS Science Imaging, Göttingen, Germany	Western Blot image acquisition
<b>Labimage1D</b>	INTAS Science Imaging, Göttingen, Germany	Western Blot quantification
<b>SnapGene</b>	GSL Biotech LLC, Chicago, Illinois, USA	Plasmid design and <i>in silico</i> cloning

## 2.13 Equipment

Table 14 Equipment

Table of Equipment	
Name	Supplier
<b>Analytical balance LP-3102</b>	VWR International GmbH, Germany
<b>Analytical fine balance LA-124i</b>	VWR International GmbH, Germany
<b>Biological safety cabinet Safe 2020</b>	Thermo Fisher Scientific, Germany
<b>C1000 Touch Thermal Cycler</b>	Bio-Rad Laboratories GmbH, Germany
<b>Centrifuge 5424</b>	Eppendorf AG, Germany
<b>Centrifuge 5424 R</b>	Eppendorf AG, Germany
<b>Centrifuge 5810 R</b>	Eppendorf AG, Germany
<b>Centrifuge HeraeusMultifuge 3S-R</b>	Thermo Fisher Scientific, Germany
<b>Centrifuge Sorvall RC-5C plus</b>	Sorvall, Germany
<b>CFX Connect™ Real-Time PCR Detection System</b>	Bio-Rad Laboratories GmbH, Germany
<b>CO<sub>2</sub> Cell Incubator MCO-20AIC</b>	Panasonic Healthcare Co., Ltd., Japan
<b>CUY900-13-3-5 Cell-Culture-Plate Electrode</b>	Nepa Gene co. Ltd., Japan
<b>ECL ChemoCam imager 3.2</b>	INTAS Science Imaging Instruments, Germany
<b>Electric Power Supply EPI 500/400</b>	Amersham Pharmacia Biotech, Germany
<b>ELISA plate reader Multiskan Ex</b>	Thermo Fisher Scientific, USA
<b>Freezer Liebherr Premium</b>	Liebherr-International Deutschland GmbH, Germany
<b>Fridge Med Line</b>	Liebherr-International Deutschland GmbH, Germany
<b>Gel-iX-imager</b>	Intas Science Imaging Instruments, Germany
<b>GenePulser Xcell™</b>	Bio-Rad Laboratories GmbH, Germany
<b>Haemocytometer</b>	Brand GmbH, Germany
<b>Heidolph Duomax 1030</b>	Heidolph Instruments GmbH & Co. KG, Germany



<b>HI-2211 Bench Top pH &amp; mV Meter</b>	HANNA instruments Deutschland GmbH, Germany
<b>Ikamag Reo Magnetic stirrer</b>	IKA®-Werke GmbH & CO. KG, Germany
<b>Leica Fluorescence Microscope</b>	Leica CTR MIC Leica, Germany
<b>Microfuge B</b>	Beckman, Germany
<b>Microscope Primovert</b>	Zeiss, Germany
<b>Microwave Oven</b>	CLAtronic, Germany
<b>Mini Trans-Blot® Cell</b>	Bio-Rad Laboratories GmbH, Germany
<b>Mini-PROTEAN® Tetra Handcast Systems</b>	Bio-Rad Laboratories GmbH, Germany
<b>Mini-PROTEAN® Tetra Vertical Electrophoresis Cell</b>	Bio-Rad Laboratories GmbH, Germany
<b>Mithras LB 940 Multimode Microplate Reader</b>	Berthold Technologies, Germany
<b>Mithras<sup>2</sup> LB 943 Multimode reader</b>	Berthold Technologies, Germany
<b>Multi-Axle Rotating mixer</b>	NeoLab, Germany
<b>Multi-channel pipette 10-100</b>	Eppendorf, Germany
<b>Multi-channel pipette 10-300</b>	Eppendorf, Germany
<b>NanoDrop NP-1000</b>	Thermo Fisher Scientific, Germany
<b>neoLab Mini Vacuum pump and compressor</b>	NeoLab, Germany
<b>Nikon Eclipse Ti Fluorescence Microscope</b>	Nikon Corporation, Japan
<b>Olympus confocal Microscope</b>	Olympus Corporation, Japan
<b>PerfectBlue™ Gelsystem Mini S</b>	VWR International, Germany
<b>Pipetboy Acu 2</b>	Integra Biosciences GmbH, Germany
<b>Pipette P10</b>	Eppendorf AG, Germany
<b>Pipette P1000</b>	Eppendorf AG, Germany
<b>Pipette P20</b>	Eppendorf AG, Germany
<b>Pipette P200</b>	Eppendorf AG, Germany
<b>PowerPac™ Basic</b>	Bio-Rad Laboratories GmbH, Germany
<b>PowerPac™ Hc</b>	Bio-Rad Laboratories GmbH, Germany
<b>ThermoForma Incubator 3862</b>	Labotect, Germany
<b>Thermomixer Comfort 1.5 ml</b>	Eppendorf AG, Germany
<b>Thermomixer F1.5</b>	Eppendorf AG, Germany
<b>Trans-Blot® SD Cell</b>	Bio-Rad Laboratories GmbH, Germany
<b>Trans-Blot® Turbo™ System</b>	Bio-Rad Laboratories GmbH, Germany
<b>UV Transilluminator</b>	VilberLourmat, Germany
<b>Vacuubrand BVC professional</b>	Vacuubrand GmbH & Co. KG, Germany
<b>Vortex Genie 2</b>	Scientific Industries Inc., USA
<b>Waterbath GFL 1083</b>	GFL, Germany

## 2.14 Consumable materials

Table 15 Consumables

<b>Table of General Materials</b>	
<b>Name</b>	<b>Supplier</b>
<b>1,5 ml reaction tube</b>	Sarstedt AG & Co., Germany
<b>10 cm bacteria culture plate Falcon</b>	Corning GmbH, Germany

<b>12 well cell culture plate</b>	Corning GmbH, Germany
<b>15 ml Falcon</b>	Corning GmbH, Germany
<b>2 ml reaction tube</b>	Sarstedt AG & Co., Germany
<b>24 well cell culture plate</b>	Corning GmbH, Germany
<b>24 well glass bottom cell culture plate</b>	In vitro scientific (P24-1.5H-N)
<b>50 ml Falcon</b>	Corning GmbH, Germany
<b>6 well cell culture plate</b>	Greiner Bio-One GmbH, Germany
<b>96 well cell culture plate</b>	Corning GmbH, Germany
<b>96 well flat bottom plate</b>	Corning GmbH, Germany
<b>Cell scraper</b>	Sarstedt AG & Co., Germany
<b>CELLSTAR® Cell Culture Dishes 6cm</b>	Greiner Bio-One GmbH, Germany
<b>CELLSTAR® Cell Culture Dishes 10cm</b>	Greiner Bio-One GmbH, Germany
<b>CELLSTAR® Cell Culture Dishes 15cm</b>	Greiner Bio-One GmbH, Germany
<b>Cover slips</b>	Glaswarenfabrik Karl Hecht GmbH, Germany
<b>Cryo vials</b>	Greiner Bio-One GmbH, Germany
<b>Extra thick blotting paper</b>	Bio-Rad Laboratories GmbH, Germany
<b>Face mask</b>	Rösner-Mautby Meditrade Holding GmbH, Germany
<b>Filter 0,2 µm</b>	GE Healthcare, USA
<b>Filter 0,45 µm</b>	GE Healthcare, USA
<b>Glas slides Superfrost™</b>	Thermo Fisher Scientific Inc., USA
<b>Hard-Shell® 96-Well PCR Plates</b>	Bio-Rad Laboratories GmbH, Germany
<b>Neubauer counting chamber</b>	Neolab, Germany
<b>PVDF Western Blot membrane</b>	Bio-Rad Laboratories GmbH, Germany
<b>Scalpel</b>	B. Braun Melsungen AG, Germany
<b>Sealing sheets PCR plates</b>	Bio-Rad Laboratories GmbH, Germany
<b>Stericup® 0,22 µm</b>	Thermo Fisher Scientific Inc., USA
<b>Stericup® 0,45 µm</b>	Millipore, Germany
<b>Stripetten 2, 5, 10, 25 and 50 ml</b>	Corning GmbH, Germany
<b>Syringe 5, 10, 20 ml</b>	BD, Germany
<b>Tips 10, 100 and 1000, filtered</b>	STARLAB GmbH, Germany
<b>Tips 10, 200 and 1000 µl, refill pack</b>	Greiner Bio-One GmbH, Germany
<b>Tips 10, 200 and 1000, Stecksystem</b>	STARLAB GmbH, Germany
<b>Whatman filter paper</b>	GE Healthcare Life Sciences, UK
<b>XCEED Nitrile Gloves, S</b>	Barrier Safe Solutions International, Inc., USA

# 3.0 Methods

## 3.1 Cloning and bacterial culturing

### *3.1.1 Transformation of competent bacteria*

100  $\mu$ L of chemically competent *E.coli* DH5 $\alpha$  bacteria were thawed on ice and mixed with 100-500 ng plasmid DNA for retransformations, with 5  $\mu$ L of ligation reaction, or with the total volume of LR/BP reaction. DNA was incubated with bacteria for 20 min on ice followed by 45 sec at 42°C (heat shock). After a recovery period of 2 min on ice, 200  $\mu$ L of LB medium was added and bacteria were incubated on a shaker for 1h at 37°C. Bacteria were plated onto LB-agar plates containing restriction antibiotics (Ampicillin (0.1 mg/mL), Kanamycin (0.3 mg/mL), Gentamicin (7  $\mu$ L/mL) or spectinomycin (50  $\mu$ g/mL)).

### *3.1.2 Plasmid amplification and purification*

Plasmid DNA was amplified in *E.coli* DH5 $\alpha$ . Clones were picked from plates and grown in LB medium supplemented with plasmid-specific restriction antibiotics overnight at 37°C while shaking.

### *3.1.3 Small scale plasmid purification*

Transformed bacterial clones were incubated in 3 mL of LB medium containing the respective restriction antibiotics. Overnight cultures were centrifuged at 11,000 x *g* for 5 mins and LB medium was removed. DNA was purified from bacterial pellets using the Nucleospin <sup>®</sup> plasmid purification kit according to manufacturer's instructions. Concentrations were determined using the Nanodrop photospectrometer.

### *Large scale plasmid purification*

Transformed bacterial clones were pre-cultured for 8 hrs in 9 mL antibiotic-containing LB medium. Bacterial cultures were centrifuged at 10,000 x *g* and plasmid DNA was

extracted from overnight cultures using the Nucleobond® PC 500 plasmid purification kit according to manufacturer's instructions. DNA pellets were resuspended in sterile ddH<sub>2</sub>O and concentrations were determined using the Nanodrop photospectrometer.

### 3.1.4 Polymerase chain reaction

Polymerase chain reactions (PCRs) were performed using the Q5® High-Fidelity DNA Polymerase according to the manufacturers protocol:

Q5® PCR reaction mix

Table 16 PCR reaction mix

Component	50 µL reaction
<b>10 mM dNTPs</b>	1 µL
<b>10 µM Primer fw</b>	2.5µL
<b>10 µM Primer rv</b>	2.5 µL
<b>5x Q5® GC Enhancer</b>	10 µL
<b>5x Q5® reaction buffer</b>	10 µL
<b>Nuclease-free ddH<sub>2</sub>O</b>	ad 50 µL
<b>Q5® High-Fidelity Polymerase</b>	0.5 µL
<b>Template DNA</b>	variable (~ 100 – 500 ng)

PCRs using the Q5® High-Fidelity polymerase were incubated according to the following protocol.

Q5 PCR program:

Table 17 PCR program

Step	Temperature (°C)	Seconds	Cycles
<b>Initial denaturing</b>	98	30	1
<b>Denaturing</b>	98	5 – 10	25
<b>Annealing</b>	50 - 72	10 – 30	25
<b>Elongation</b>	72	20 – 30	25
<b>Final elongation</b>	72	120	1

PCR products were resolved on 1% agarose gels and purified using the PCR and Gel clean up kit.

### *3.1.5 Overlap-extension PCR*

In order to combine two ssDNA fragments into one dsDNA fragment of a given sequence, overlap-extension PCR was carried out. For the combining of two ssDNA fragments, the two respective dsDNA fragments were amplified together using the PCR protocol described previously, however, the 5'-3' ssDNA (sense orientation) fragment produced from the first dsDNA fragment during the PCR protocol was designed to overlap with the 3'-5' ssDNA (antisense orientation) from the second dsDNA fragment, which was produced during the PCR protocol. Fw and Rv primers specific for the 5' end of the sense strand and the 3' of the antisense strand allowed for the amplification of a single strand of dsDNA which would be the combination of two dsDNA fragments. The PCR fragments were resolved on a 1% agarose gels to confirm the correct height of the product. Products were then purified from the gel using the using PCR and Gel clean up kit and eluted in 30  $\mu$ L ddH<sub>2</sub>O. The final PCR product was either ligated into a specific vector or used for BP recombination by Gateway® cloning technology.

### *3.1.6 Gateway™ cloning*

Gateway™ cloning is a system that employs a two-step selection reaction to generate recombinant DNA plasmids. Firstly, it is used to shuttle any PCR product or gene of interest into a vector known as an "entry vector". From this entry vector the PCR product/gene of interest can be shuttled, in one reaction step, from the entry vector into a variety of template destination vectors. These destination vectors allow for the rapid generation of recombinant plasmids that are equipped with various tags from different vector systems. The BP reaction (first step) mediates the recombination of PCR fragments flanked by attB sites into pDONR vectors harbouring attP sites. This reaction results in an entry vector containing the PCR product/gene of interest flanked by attL sites. As a side product, a linear fragment (encoding for bacterial toxin ccdB) is removed from the vector. In case of a non-successful recombination bacteria transformed with non-recombined pDONR plasmids will express the ccdB gene and die, thereby selecting for positive colonies. pDONR vectors can be used in an LR

reaction to shuttle the gene of interest into a destination vector (pDEST) that again harbours the *ccdB* gene flanked by *attR* sites. As with the pDONR vector, non-recombined pDEST will be negatively selected by the expression of the *ccdB* gene.

### 3.1.6.1 Generation of entry clones (BP reaction)

Primers were designed which harboured the *attB* sites necessary for recombination. A start codon was added to the fw primer and a stop codon to the rev primer.

Table 18 GW primers

Name	Sequence 5' – 3'
<b>attB fw</b>	GGGGACAAGTTTGTACAAAAAAGCAGGCTTC
<b>attB rev</b>	GGGGACCACTTTGTACAAGAAAGCTGGGTC

By PCR amplification *attB*-flanked inserts were generated, separated on a 1% agarose gel and purified. DNA inserts were resuspended in 30  $\mu$ l ddH<sub>2</sub>O. BP reactions were set up according to the following protocol.

Table 19 GW reaction

Component	10 $\mu$ L reaction
<b>pDONR/pENTR</b>	150 ng
<b>attB-flanked Insert</b>	150 ng
<b>BP clonase</b>	1 $\mu$ L
<b>1x TE buffer</b>	To 10 $\mu$ L

BP reactions were incubated for at least 2 hrs at 25°C and subsequently transformed into competent DH5 $\alpha$  bacteria. Successful BP cloning was visualised by digesting pDONR plasmids with BsrGI which, due to cutting both recombination sites and the vector backbone, generated three specific fragments. Plasmids were sequenced to ensure the desired sequence was amplified.

### 3.1.6.2 Generation of expression clones (LR reaction)

LR reactions were carried out by combining desired destination vectors with generated pDONR vectors. LR reactions were set up according to the following protocol.

Table 20 GW shuttling

Component	10 $\mu$ L reaction
pDONR/pENTR	150 ng
pDEST	150 ng
LR clonase	1 $\mu$ L
1x TE buffer	ad 10 $\mu$ L

LR reactions were incubated for at least 2 hrs at 25°C and subsequently transformed into competent DH5 $\alpha$  bacteria. Successful LR cloning was visualised by digesting pDEST plasmids with BsrGI which, due to cutting both recombination sites, generated two specific fragments. Plasmids were sequenced to ensure the desired sequence was cloned.

### 3.1.7 Sequencing analysis of plasmid DNA

Purified plasmid DNA was diluted to 100ng/ $\mu$ L. 5 $\mu$ L of the plasmid was mixed with 5mL of 5 $\mu$ M sequencing primer. The DNA/primer mixture was sent to GATC Biotech Ltd. for LIGHTrun<sup>®</sup> sequencing. The returned sequence was analysed using the Snapgene<sup>®</sup> program.

## 3.2 Cell Culture

### 3.2.1 Cell culturing

All cell lines were cultured in DMEM+++ (standard cell culture medium) and kept at 37 °C, 95% relative humidity, and 5% CO<sub>2</sub>. For passaging cell lines, medium was

removed and cells were washed with 1X PBS. Cells were detached by adding Trypsin-EDTA and incubating for up to ~5 min at 37°C. Detached cells were washed off the dish using FCS containing DMEM to halt trypsinisation, diluted to desired concentration, and added to a new cell culture dish. Cells were passaged before confluency was reached. Stable expression of recombinant plasmids within cell lines were grown in presence of 1 mg/mL G418, 5 µg/mL puromycin, µg/mL zeocin and/or 5 µg/ml blasticidin, respectively, unless stated otherwise for a specific cell line.

### *3.2.2 Cryopreservation of mammalian cells*

For the cryopreservation of mammalian cells, a confluent 15 cm dish was detached as described previously. Detached cells were spun down and resuspended in 9 ml fetal calf serum containing 10% DMSO which was distributed to 9 cryovials before they were stored at -80°C for at least 48h. For long term storage cells were then transferred to liquid nitrogen (-180°C). Revival of mammalian cells was achieved by quickly thawing contents of cryovials. Semi-thawed cells were added to pre-warmed standard cell culture medium and incubated until they had attached to the plate. Medium was changed to remove DMSO the following day.

### *3.2.3 Determining cell numbers in solution*

From a cell suspension, the number of cells per mL was determined by using a hemocytometer. 10µL of single cell suspension were loaded to the chamber and living cells (determined by morphology) within the four large quadrants were counted using an inverted light microscope. Given that the space over each quarter section has a defined volume of 0.1 µL, the number of counted cells multiplied by 10,000 and divided by 4 is the number of cells per mL.



### 3.2.4 Transfection of recombinant DNA

#### 3.2.4.1 Lipofectamine 2000<sup>®</sup>

Cells were transfected with recombinant DNA plasmids for transient expression of specific genes of interest using lipofectamine 2000<sup>®</sup> reagent mixed with OptiMEM. For a 24-well format, per well, 1  $\mu\text{L}$  of lipofectamine 2000<sup>®</sup> mixed with 49  $\mu\text{L}$  of OptiMEM, and separately, up to 1000  $\mu\text{g}$  of the respective recombinant DNA plasmid mixed to a total volume of 50  $\mu\text{L}$  OptiMEM. These mixtures were allowed to warm to room temperature and after 5 mins, the lipofectamine 2000<sup>®</sup> mixture was combined with the DNA mixture and incubated for a further 20 mins. During this incubation time, a media change was carried out for the target cells, fresh DMEM+++ was added to each target well and allowed to warm to 37°C. Finally, 100  $\mu\text{L}$  DNA/lipofectamine 2000<sup>®</sup> mixture was added to a single 24-well. The target cells were incubated with the transfection reagent mixture for at least 6 hours before changing media again to DMEM+++. Expression of the recombinant gene of interest can then proceed.

#### 3.2.4.2 jetPEI<sup>®</sup>

Cells were transfected with recombinant DNA plasmids for transient expression of specific genes of interest using jetPEI<sup>®</sup> reagent mixed with 150 mM NaCl. For a 24-well format, per well, 8  $\mu\text{L}$  of jetPEI<sup>®</sup> mixed with 42  $\mu\text{L}$  of 150 mM NaCl, and separately, up to 2000  $\mu\text{g}$  of the respective recombinant DNA plasmid mixed to a total volume of 50  $\mu\text{L}$  150 mM NaCl. These mixtures were allowed to warm to room temperature and after 5 mins, the jetPEI<sup>®</sup> mixture was combined with the DNA mixture and vortexed for 5 secs and then incubated for a further 20 mins. During this incubation time, a media change was carried out for the target cells, fresh DMEM+++ was added to each target well and allowed to warm to 37°C. Finally, 100  $\mu\text{L}$  DNA/jetPEI<sup>®</sup> mixture was added to a single 24-well. The target cells were incubated with the transfection reagent mixture, no media change is required. Expression of the gene of interest can then proceed.

### 3.2.5 Transduction of recombinant DNA

#### 3.2.5.1 Lentiviral mediated stable integration of recombinant DNA

Stable indiscriminate expression of a gene of interest was achieved by lentiviral transduction of target cells. Lentiviral particles were produced by a combination transfection of a lentiviral vector (e.g pWPI containing the gene of interest), with two packaging plasmids (gag-pol and VSV-G expression plasmid). Lentiviral particles were produced in 293T cells, harvested, and used to infect target cells. To produce lentiviral particles  $0.8 \times 10^6$  293T cells were seeded in a 6cm dish. Medium was changed the next day and cells were transfected with pWPI lentiviral vector, gag-pol (psPAX2) and VSV-G expression plasmid (pMD2.G) using CalPhos™ Mammalian transfection kit. 6.4 µg pWPI, 6.4 µg psPAX2 and 2.1 µg pMD2.G were diluted in a final volume of 438 µl sterile H<sub>2</sub>O and 62 µL 2M CaCl<sub>2</sub> were added on top. 500 µL 2X HBS were added drop wise to the mix while air was blown into the liquid to provide oxygen aiding precipitate formation. The transfection mix was added slowly and drop-wise to 293T cells. 8 hrs post transfection medium was changed. 48 hrs after transfection supernatants were collected and passed through a 0.45 µm-pore filter to prevent contamination with particle producing 293T cells. Filtered supernatants were added onto target cells that were seeded the day before. Supernatants of transfected 293T cells were harvested again after 8 hrs and 24 hrs and handled the same way as described above. After 1-3 rounds of target cell infection the medium was replaced with standard cell culture medium containing the appropriate restriction antibiotic. Antibiotics were kept while passaging stable cell lines, as described previously, to ensure constitutive expression of the gene of interest, unless experiments were performed on the target cells.

### 3.2.6 *In vitro* transcription

*In vitro* transcription of RNA was carried out using T7 RNA polymerase to transcribe RNA from DNA using the following reaction mixture:

Table 21 *in vitro* transcription of RNA

<b>Component</b>	<b>50 <math>\mu</math>L reaction</b>
<b>25 mM rNTPs</b>	12 $\mu$ L
<b>5x buffer RRL</b>	20 $\mu$ L
<b>RNAsin (40U/<math>\mu</math>L)</b>	2.5 $\mu$ L
<b>T7 RNA polymerase</b>	4 $\mu$ L
<b>DEPC treated ddH<sub>2</sub>O</b>	51.5 $\mu$ L
<b>Template DNA</b>	variable (~ 500-1000 ng)

### 3.2.7 *Generating Double Stranded RNA*

Double stranded RNA (dsRNA) was generated using the TLR3 template DNA. Primers were designed to amplify the sense and antisense orientation of the specific sites within the TL3 DNA sequence, using various positions of annealing, different lengths could be generated. The primers used generated two sets of dsDNA with lengths of 100, 200, and 400 base pairs. These dsDNA fragments were used as templates for *In vitro* transcription of ssRNA fragments (described previously). The ssRNA fragments from both dsDNA templates are complimentary for each other, the resulting products of the *In vitro* transcription are mixed together in a 1:1 ratio. This mixture is then mixed again in a 1:1 ratio with annealing buffer (see materials). This mixture is incubated at 98°C for 1 min, the heat is turned off and allowed to slowly cool until room temperature is reached. The dsRNA that is the product of the annealed ssRNA fragments was purified by size exclusion chromatography by Dr. Stefan Seitz, Molecular Virology, Heidelberg University, Heidelberg.

The following primers were used to amplify specific segments of the TLR3 gene sequence (1=Fw primer, 2=Rv primer, S=Sense, A=antisense):

Table 22 dsRNA primers

Primer	Sequence
<b>Primer T7</b>	TAATACGACTCACTATAGGGAGATGCTTTCTCTTGGTTGGGC
<b>Primer T7.2</b>	GGGAGATGATGCTTTCTCTTGGTTGGGC
<b>1S40</b>	GGGAGATAGGTGGCCCAACCAAGAGAAAGCATCATCTCCCTATAG
<b>1A40</b>	TAATACGACTCACTATAGGGAGATGATGCTTTCTCTTGGTTGGGC
<b>2S40</b>	GGGAGATGATGCTTTCTCTTGGTTGGGCCACCTATCTCCCTATAG
<b>2A40</b>	TAATACGACTCACTATAGGGAGATAGGTGGCCCAACCAAGAGAAA
<b>1-100</b>	GGGAGATCTCCATTCCTGGCCTGTGA
<b>2-100</b>	TAATACGACTCACTATAGGGAGATCTCCATTCCTGGCCTGTGA
<b>1-200</b>	GGGAGAGCATCAGTCGTTGAAGGCTTG
<b>2-200</b>	TAATACGACTCACTATAGGGAGAGCATCAGTCGTTGAAGGCTTG
<b>1-400</b>	GGGAGAACCACCAGGGTTTCGCTGTTT
<b>2-400</b>	TAATACGACTCACTATAGGGAGAACCACCAGGGTTTGCCTGTTT

### 3.3 Biochemical and Molecular Biological Assays

#### 3.3.1 Protein Complementation Assay

##### 3.3.1.1 PCA Constructs

Developing the constructs for the application of protein complementation assay (PCA) involved the separation of *Gaussia princeps* luciferase (GLuc) protein into two fragments, N1 and N2, where by N1 corresponds to amino acids 1-93, and N2 corresponds to amino acids 94-169, excluding the 16 amino acids of the N terminal end that correspond to the secretion signal sequence. GLuc N1 and GLuc N2 are then tagged by way of Gateway™ cloning (described previously) to pairs of proteins of interest, such that protein X is linked to GLuc N1 and protein Y is linked to GLuc N2. Sequence identity is confirmed prior to application.

### 3.3.1.2 Assay procedure

To perform PCA, two constructs pertaining to the proteins of interest, linked to GLuc N1 and GLuc N2 respectively, are transfected into 293T cells using a 96-well format, with  $3 \times 10^4$  cells seeded per well and cultivated in 100  $\mu$ L DMEM +++. It is essential to ensure even distribution of cells within the 96-well. This is most easily achieved when seeding the cells by stabilising the plate flat and horizontal and to move swiftly and thoroughly back and forth. Then, rotating the plate on its axis so that it is now still flat, but vertical in comparison, performing the same shaking manoeuvre as before achieves a perfect distribution of the cells within the 96-well. Optimal transfection conditions involve the application of the jetPEI® transfection reagent protocol, combining 100ng of the respective proteins of interest linked GLuc N1 and GLuc N2 DNA plasmids for a total transfection of 200ng DNA per well. The cells can then be incubated for 24-96 hours, however, 48 hours was chosen as the optimal length of incubation time. To control for random interaction of the respective proteins, GLuc N1 linked to no protein is co-transfected with GLuc N2 linked to the protein of interest, and separately, the reverse is also applied (GLuc N2 linked to no protein, GLuc N1 linked to protein). Each condition, of which there are three (X-GLuc N1 + Y-GLuc N2, Empty-GLuc N1 + Y-GLuc N2, X-GLuc N1 + Empty-GLuc N2), is performed in triplicate on the 96-well plate as described previously, the inclusion of these “empty” partner controls allow for the calculation of the normalised luminescence ratio (NLR) outlined by Madden *et al*, 2011 (REF#). The NLR is the basis on which the protein:protein interaction is analysed, a high NLR compared to negative control suggests a strong, rapid, or stable interaction (due to the transient nature of full GLuc reconstitution).

To optimise the sensitivity of NLR acquisition, it is essential to perform a kinetics assay, whereby the luminescence ratio is measured every 0.1-1 secs post substrate addition for up to 600 secs. The time at which the peak NLR is reached will vary slightly from PPI to PPI, and may greatly affect positive signals. Furthermore, it is essential to measure the luminescence using a high sensing filter for the emission wavelength of *Gaussia princeps* luciferase post substrate addition, as this too, increases the sensitivity of NLR acquisition. Additionally, several parameters were examined that failed to alter the sensitivity of the assay to any meaningful extent; lysis conditions, not

lysing the cells, substrate concentration/saturation, alternative cell line origins, and alternative substrate derivatives.

### 3.3.2 Luciferase Assay

On day 0, cells are seeded on a 24-well format ( $0.75-1.5 \times 10^5$  cells/well). On day 1, cells are transfected using the Lipofectamine 2000® protocol described previously. The DNA reporter plasmids (Firefly-IFIT1 and Renilla-SV40) are co transfected. 9 hours later cells were stimulated either by poly(I:C), or plasmid transfection, or by SeV infection (MOI 5). If not indicated otherwise, cells were stimulated for 16h before medium removal and lysis in 100  $\mu$ L/24-well luciferase lysis buffer (day 2). Plates can be stored at -80°C until measurement. Samples were measured using Mithras<sup>2</sup> LB 943 Multimode reader or Mithras LB 940 Multimode Microplate Reader. Measuring Firefly-IFIT1 based luminescence was achieved using luciferase assay buffer supplemented with 1:20 D-luciferin stock solution, 1:100 100 mM ATP and 1:1000 1 M DTT (see materials). Additionally, the Renilla substrate, Coelenterazine, was diluted 1:700 in luciferase assay buffer to measure Renilla-SV40 based luminescence. Enzymatic reactions were halted using the addition of 10% SDS. 24-well plates were measured using the following protocol on a well-by-well basis, and each sample was performed in triplicate:

Table 23 luciferase assay protocol

<b>Luciferase Assay Program</b>	
<b>Action</b>	<b>Procedure</b>
Dispense firefly substrate	4x100 $\mu$ L
Shake	2 sec
Measure (No filter)	10 sec
Dispense Renilla substrate	4x100 $\mu$ L
Shake	2 sec
Measure (480nmBRET-hisense filter)	10 sec
Dispense 20% SDS	100 $\mu$ L
Shake	2 sec

### 3.3.3 Western Blot

#### 3.3.3.1 Sodium Dodecyl Sulphate Polyacrylamide Gel Electrophoresis

Sodium Dodecyl Sulphate polyacrylamide gel electrophoresis (SDS PAGE) resolving gels containing 6-15% polyacrylamide (PAA) were prepared using 40% acrylamide/bisacrylamide (ratio 29:1) stock solution diluted in resolving gel buffer (see materials). N,N,N',N'-Tetramethylethylenediamine (TEMED) and saturated ammonium peroxydisulfate (APS) solution were added (1:500 each) to initiate the polymerisation reaction. The Solution was immediately cast using the Mini-PROTEAN® Tetra Handcast System (Bio-Rad) and carefully overlaid with 100% isopropanol to ensure a level and consistent resolving gel portion. 4% PAA stacking gel solution was prepared using 40% acrylamide/bisacrylamide (ratio 29:1) stock solution diluted in stacking gel buffer. TEMED and APS supplemented gel solution was cast on top of the resolving gel after residual isopropanol was removed, and specific combs (either 10-well or 15-well) were used to form the stacking gel portion. Cell lysates for protein sample analysis were extracted using either a final concentration of 2X Laemmli buffer, or RIPA buffer supplemented with protease inhibitors (see materials). Samples in RIPA buffer were immediately frozen, thawed and debris was pelleted by centrifugation at full speed for 10 min.

Cells with DMEM --- were mixed with 6X Laemmli to a final working concentration of 2X in order to immediately lyse whole cells for protein analysis. Protein samples were denatured by boiling for 5 min at 95°C, unless stated otherwise. If necessary, samples were treated with Benzonase ® prior to gel loading. Equal volumes of samples were loaded into each lane within the SDS-PAGE gels. A lane with pre-stained protein marker was included to determine size of detected proteins (see materials). Gels were run in 1X TGS buffer for 30 min at 70-80V and 1 – 1.5h at 125V, or until proteins were adequately resolved.

### 3.3.3.2 Western Blot Electrophoresis

SDS-PAGE gels with resolved proteins embedded in the gel were transferred to a Western Blot chamber (see materials). The gels were transferred onto a membrane (PVDF (requires Methanol or ethanol activation) or nitrocellulose), and separated from the housing cassette by filter paper and sponges. The proteins were subsequently transferred to the membrane using electrophoresis by applying a constant ampage of 0.3 A, which resulted in a variable voltage of between 40-60 V. Transfers of protein was carried out for 2 hours under these conditions. Western Blot transfers were carried out using 1X wet transfer buffer supplemented with 20% methanol.

### 3.3.3.3 Western Blot staining

Protein transferred to either PVDF membranes or Nitrocellulose membranes were stained using specific primary antibodies to visualise and quantify proteins of interest. To achieve this, PVDF membranes were taken directly after transfers and soaked in 100% methanol for 5 seconds. The membranes were then hung to dry until no longer translucent. Once dried, membranes were rehydrated using 80% ethanol, and washed 3x using wash buffer (1X TBS/PBS 0.2% Tween-20). For Nitrocellulose membranes, the membranes were directly transferred to blocking buffer after transfers were completed and incubated for 2 hours at room temperature, and subsequently wash 3x 5mins with the appropriate wash buffer. Membranes were then incubated overnight at 4°C with the primary antibody (see materials for list) in either 1X TBS with 5% BSA and 0.2% tween-20 or 1X PBS with 5% Milk and 0.2% tween-20. Membranes were then washed 3x 5mins with the corresponding wash buffer before applying the appropriate secondary antibody for 2 hours at room temperature or overnight at 4°C. The membrane was again washed 3x 5mins with the appropriate wash buffer. Western Blots were then developed using the ECL Western Blot detection solution (see materials) to induce chemiluminescence whereby proteins of interest were imaged by Intas ChemoCam ECL imager and quantification could be consequently carried out.



#### *3.3.3.4 Western Blot Quantification*

Proteins of interest were quantified in terms of their expression levels for specific samples by their luminescence signal strength that was imaged, as described previously, using Lab Image 1D software. Quantification of samples includes the protein of interest, and additionally an appropriate general protein to act as a sample loading control, these loading control proteins include GAPDH,  $\beta$ -Actin,  $\gamma$ -Tubulin, and Calnexin.

#### *3.3.4 Synchronised Dynamics Analysis*

##### *3.3.4.1 Synchronised Dynamics Sample Acquisition*

In order to measure the dynamics of proteins of interest, quantitative Western Blotting must be applied. The problem, dynamics, arises when comparing samples over a time course, this is negated by using a synchronised grouped cell response system. The following methodology describes the approach to synchronising PRR (in this case RIG-I) mediated signal transduction and harvesting protein for quantitative Western Blot analysis.  $12 \times 10^6$  A549 cells are harvested for each experiment. The cells are centrifuged and resuspended in 1.2 mL cytomix buffer containing 2mM ATP and 5mM Glutathione (see materials). The cytomix cell suspension is distributed into 3 0.4cm electroporation cuvettes (Bio-rad). Each cuvette contains 400  $\mu$ L of the cytomix cell suspension. Prior to adding the cell suspension to each cuvette, 0.8 pmol of purified dsRNA of a defined length is added to each cuvette (2 nM). Each cuvette is entered into the CE module of the Bio-rad GenePulser Xcell™ electroporator. The cuvette is pulsed with an electrical current for 10 ms (150V exponential decaying pulse), immediately proceed with the next cuvette to be electroporation, and once all are pulsed, take up all the cells in the cytomix with a glass pipette tip and transfer to a 15 mL Falcon containing 2 mL DMEM +---. It is absolutely essential that this media is pre-warmed to 37°C. Once the pulsed cells have been transferred, quickly distribute the cells in a pre-warmed 37°C cell culture plate, according the experimental design. For

short, fine time courses, cells were distributed into 14 wells of a 24-well plate (200  $\mu$ L per well). In order to take a 0 hour time point, 200  $\mu$ L is immediately added to a 1.5 mL eppendorf tube containing 100  $\mu$ L 6X Laemmli buffer for a final concentration of 2X Laemmli buffer, containing whole cell lysate. The plate is incubated at 37°C. Heat management must be carefully maintained/regulated. For each time point where protein must be harvested, 100  $\mu$ L 6X Laemmli buffer is added to the well in question and whole cell lysate is transferred to a 1.5 mL eppendorf tube. All samples are then denatured at 95°C for 5 mins, whereby they can then be loaded on to an SDS-PAGE gel for Western Blot analysis. Samples can be kept frozen at -20°C for an extended period of time (>1 year).

### *3.3.5 Live Synchronised Cell Imaging*

Fluorescently labelled proteins stably expressed in cells can be imaged in terms of their localisation over time using a synchronisation approach. A cell culture plate electrode (see materials) purchased from Nepa Gene company was modified to be compatible with the Bio-rad GenePulser Xcell™ electroporator.  $0.75 \times 10^5$  A549 cells stably expressing eGFP-IRF3 and mCherry-RelA were seeded on high performance cover glass bottom black 24-well plates (In vitro scientific). The following day the media is removed and cells are stained with Hoechst 33258 (see materials) for 10 mins at room temperature at a dilution of 1:10000 in 1X PBS. Cells are wash with 1X PBS and fresh media is added and the plate is placed back into the incubator to bring the cells back 37°C . After 30 mins, the media is removed and 100  $\mu$ L cytomix buffer is added on the cells. 0.1-1pmol dsRNA of a defined length is added to the cytomix buffer and carefully shaken back and forth to ensure even coverage of the buffer on the cells. The in-well electrode is placed in position in the well and steadily held while the electrical pulsing program is initiated. The in-well electrode pulses the cells with 150V for 10 ms with the block pulse protocol. Immediately after pulsing the cells, pre-warmed microscope media (37°C) is added on the cells and the plate is placed in the microscope incubator for live cell imaging (at 37 °C, 95% relative humidity, and 5% CO<sub>2</sub>). Imaging of the 405 nm w/v, 488 nm w/v, and 565 nm w/v channels are carried

out every 0.5-2 mins using the Olympus FV1000 confocal microscope to determine the localisation of the tagged proteins over time, in a synchronised manner.

### *3.3.6 ELISA*

ELISA (enzyme linked immunosorbent assay) was used to measure the production of IFN $\beta/\lambda$ . The follow protocol pertains to IFN $\beta$  (LumiKine<sup>TM</sup>, invivogen) and incubation times may differ for IFN $\lambda$ . Capture antibodies diluted in 1X PBS were incubated overnight at room temperature on the appropriate 96-well plate. Excess liquid was removed and the plates were dried by gently patting the plate on paper towels. Blocking buffer (5% BSA 0.05% Tween-20) was then added to each well and incubated for 2 hours at 37°C. This solution was removed and the plate dried as described previously. Samples, including standards, were appropriately diluted in reagent diluent (see materials/manufacturers protocol), and added to coated wells of the plate. The samples and standard were incubated for 2 hours at 37°C. each well was then washed 3x using wash buffer (1X PBS 0.05% Tween-20) and the plate was dried as described previously. A linked detection antibody, in the case of IFN $\beta$ , a biotinylated detecting antibody is incubated for 2 hours at 37°C. Samples are washed again as before, and finally the signalling antibody is incubated for 30 mins at 37°C before a final washing step. The plate can now be measured for the abundance of the protein of interest relative to the standard, using the appropriate measuring instrument.

### *3.3.7 RNA and quantitative PCR*

#### *3.3.7.1 RNA isolation*

RNA isolation was performed using the Nucleospin<sup>®</sup> RNA Plus kit according to the manufacturer's instructions. Cells were washed with 1X PBS prior to lysis in LBP buffer. Lysates were stored at -80°C until RNA extraction. Purified RNA was resuspended in nuclease-free ddH<sub>2</sub>O and used for Expand<sup>TM</sup> RT or cDNA preparation for quantitative Real-Time PCR. Reverse transcription was performed using the High

Capacity cDNA Reverse Transcription kit (Applied Biosystems). Reaction mixes were prepared according to the following protocol:

Table 24 A and B cDNA synthesis protocol

Component	6.6 $\mu$ L reaction
<b>100 mM dNTPs</b>	0.25 $\mu$ L
<b>10X random hexamer primers</b>	0.66 $\mu$ L
<b>10X reaction buffer</b>	0.66 $\mu$ L
<b>Nuclease-free H<sub>2</sub>O</b>	1.07 $\mu$ L
<b>Reverse Transcriptase</b>	0.33 $\mu$ L
<b>Isolated RNA</b>	3.3 $\mu$ L
<b>RNase inhibitor</b>	0.33 $\mu$ L

Temperature ( $^{\circ}$ C)	Time
25	10 min
37	2 hrs
85	5 min

All cDNA samples were diluted with ddH<sub>2</sub>O 1:20 or 1:10 depending on the yield.

### 3.3.7.2 Quantitative Real-Time PCR

Quantitative Real-Time PCR (qPCR) was performed using the iTaq<sup>TM</sup> Universal SYBR<sup>®</sup> Green Supermix and a Bio-Rad CFX Connect<sup>TM</sup> Real-Time PCR Detection System (see materials). All samples were measured in triplicates. Non-amplification and non-target controls were included to control for specific amplification.

qPCR reactions were prepared and carried out from each cDNA sample as previously described according to the following protocols:

Table 25 A and B qPCR protocol

Component	15 $\mu$ L reaction
<b>2x iTaq SYBR<sup>®</sup> Green</b>	7.5 $\mu$ L
<b>cDNA sample</b>	3 $\mu$ L
<b>Nuclease-free H<sub>2</sub>O</b>	1.5 $\mu$ L
<b>Primer fw</b>	1.5 $\mu$ L
<b>Primer rev</b>	1.5 $\mu$ L

Step	Procedure	Description
1	95°C	3 min
2	95°C	10 sec
3	60°C	30 sec
4	Quantify	-
5	Continue from Step 2	45 cycles
6	65°C increase to 95°C	0.5°C/0.05 sec
7	Measure every 0.5°C	-

qPCR data was analysed using the Bio-Rad CFX Manager software. Relative mRNA expression was calculated using the  $2^{-\Delta\Delta Ct}$  method as described in REF#(find in Julia thesis)

### 3.3.8 Illumina HumanHT-12 Chip expression profiling

RNA was harvested according to section 3.3.7.1 using the synchronised stimulation approach described in section 3.3.4. Samples were generated in duplicate for A549 wild type cells, and in addition, A549 IFN alpha/lambda Receptor knock-out cells, and sent to the Genomics and Proteomics core facility of the DKFZ in Heidelberg, Germany, where illumine Human HT-12 chips were used to analyse the expression mRNAs across the genome in response to dsRNA, over 24 hours with time intervals of 0, 1, 2, 4, 6, 8, 12, 18, and 24 hours.

### 3.3.9 Proteome analysis

$2.4 \times 10^7$  A549 wild type cells were resuspended in cytomix containing ATP and glutathione, and evenly divided into 9 cuvettes. Cuvettes were each rapidly electroporated in the presence of 2 nM 400 bp dsRNA (taking 1min 57s). cells were transferred to 37°C media (totalling 9mL) and seeded evenly between 3 6cm cell culture dishes. At each specific time point, cells were harvested from 6cm dishes by forcefully pipetting 4°C sterile 1X PBS until all cells were lifted, cells were then spun down at 300 x g for 3 min, supernatant was removed and cell pellet was snap frozen in liquid nitrogen for storage at -80°C.

# 4.0 Results

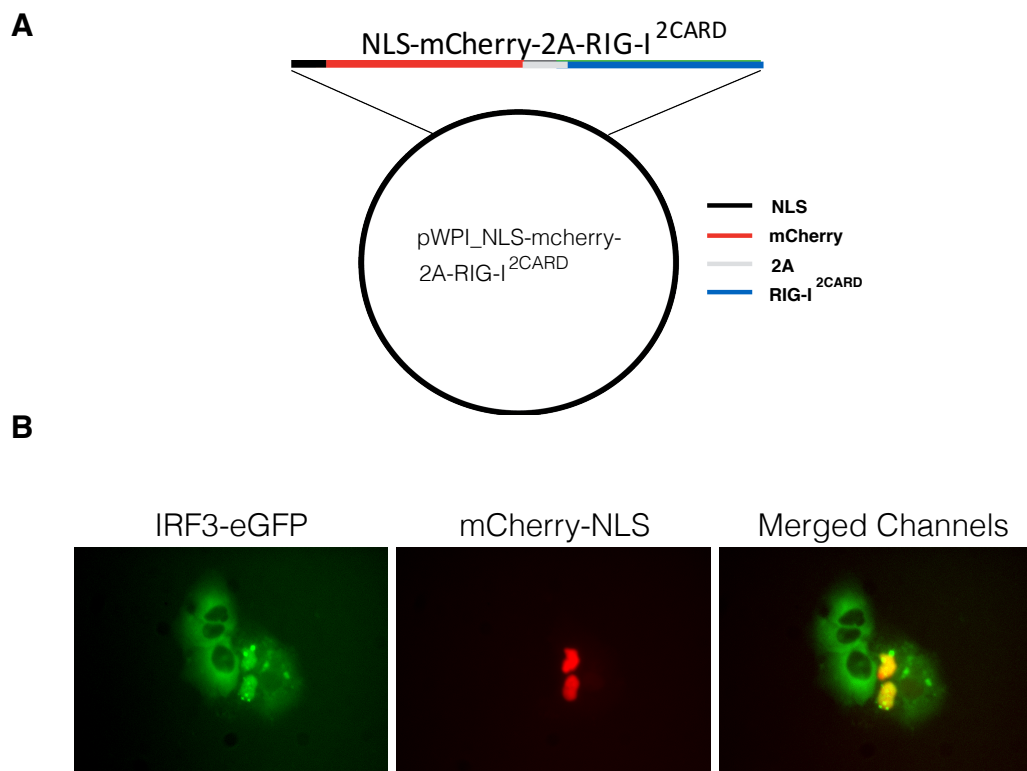
This study attempts to enhance our fundamental understanding of the antiviral signalling network through the characterisation of the regulation RIG-I signalling, and the characterisation of the dynamics of the RIG-I signalling events in response to the detection of dsRNA. Toward this, and taking into account the major role that ubiquitination has on the regulation of RIG-I signal transduction, as discussed previously, we designed an siRNA based screen that targeted a fully annotated list of functional and putative E3 ubiquitin ligases to determine the impact they had on the activation of IRF3 and NF $\kappa$ B. For the characterisation of the dynamics of RIG-I signalling, we sought to understand whether RIG-I signalling was indeed stochastic, as had been reported, and to characterise the kinetics of individual steps within the network in order to generate the fundamental data that could be used to build a mathematical model. Furthermore, we sought to understand the strict dependence ISGs had on the RIG-I/IRF3 signalling pathway and the IFN/JAK/STAT signalling pathway, we further hypothesised that these ISG inductions might differ in their kinetics and amplitudes depending on whether IFN/JAK/STAT signalling was present. This, we sought to characterise the kinetics of the host cellular responses triggered by the detection of dsRNA in extensive detail, and providing an excellent background for which mathematical modelling can be applied in order to quantitatively describe the molecular events involved in antiviral signalling, which will represent a strong tool to study the foundations of molecular basis for successful/unsuccessful viral infections.

## 4.1 Identifying novel regulators of the RIG-I signalling network

In order to identify novel regulators of the RIG-I signalling pathway, a robust read-out for activation of the signalling pathway needed to be developed. Initially, an ambitious project was planned to develop a cell line that would act as a multispectral read out for distinct aspects of RIG-I activation, using a five-channel fluorescence read-out. The initial cell line being developed would include the transcription factors IRF3 and NF $\kappa$ B fused to respective fluorescent proteins. In addition to this, a constitutively active

recombinant RIG-I protein (RIG-I<sup>2CARD</sup>), fused a fluorescent protein tagged with a nuclear localisation signal (NLS), but separated by a 2A signal sequence, would be used (Figure 4.1.1A). Thus, active RIG-I (and by extension the number of activated cells) could be quantified by measuring fluorescence in the nucleus. Upon initial testing it was observed that the NLS-mCherry-2A-RIG-I<sup>2CARD</sup> construct was successful in activating the RIG-I signalling cascade when transfecting Huh7.5 cells expressing IRF3-eGFP, and furthermore, was quantifiable (mCherry fluorescent signal in the nucleus) (Figure 4.1.1 B)

**Figure 4.1.1 RIG-I induction construct**



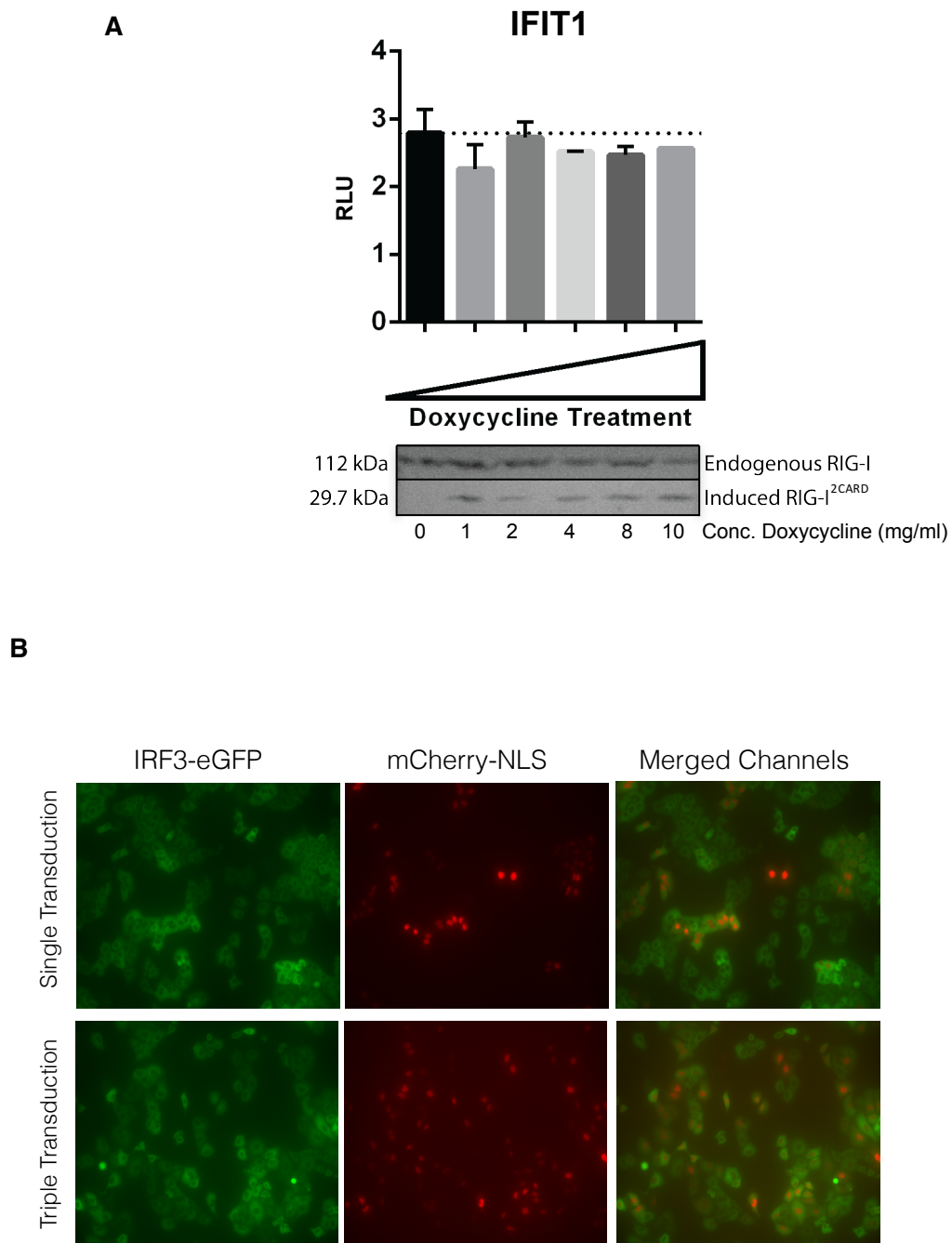
**Figure 4.1.1:** Constitutively active RIG-I construct. **A)** Graphic showing the recombinant gene construct of the pWPI plasmid comprising of the nuclear localisation signal tagged fluorescent protein mCherry, separated from the constitutively active form of RIG-I (RIG-I<sup>2CARD</sup>) by the cleavage signal site 2A. **B)** Proof of concept of the NLS-mCherry-2A-RIG-I<sup>2CARD</sup> functioning as intended in Huh 7.5 cells stably expressing RIG-I and IRF3-eGFP. Activated cells can be differentiated from non-activated by either a cytoplasmic IRF3-eGFP signal (inactive) or a nuclear IRF3-eGFP signal (active). Activation is due to the expression of RIG-I<sup>2CARD</sup> and can additionally

be marked by the nuclear signal of mCherry fluorescence, which overlaps with activated IRF3-eGFP signal.

This construct was overexpressed in the A549 cell line already overexpressing IRF3-eGFP. NLS-mCherry-2A-RIG-I<sup>2CARD</sup> was stably expressed in this cell line with a transactivator that would only activate expression in the presence of doxycycline (Tet-on system). This is due to a tet-response element (TRE). A TRE is 7 repeats of a 19-nucleotide tetracycline operator (tetO) sequence, and is specifically recognized by the tetracycline repressor (tetR) which is stably co-expressed with NLS-mCherry-2A-RIG-I<sup>2CARD</sup>. Endogenously, if doxycycline/tetracycline are present, tetR will bind to doxycycline and not to the TRE and therefore allowing transcription to proceed. Western Blotting shows the construct is technically functional in the A549 cells, such that mCherry (~27 kDa) separates from RIG-I<sup>2CARD</sup> (~29.7 kDa) due to the 2A signal sequence, and that it is specifically induced upon treatment with doxycycline (Figure 4.1.2 A), however expression of the recombinant gene(s), using increasing concentrations of doxycycline, appeared to not reach a high enough threshold in order to activate the RIG-I signalling cascade, despite the mCherry nuclear fluorescent signal (Figure 4.1.2 A). This was not overcome by increasing the gene copy numbers within the cells and was subsequently removed from the reporter cell line generation project entirely (Figure 4.1.2 B).



**Figure 4.1.2 RIG-I<sup>2CARD</sup> induction**

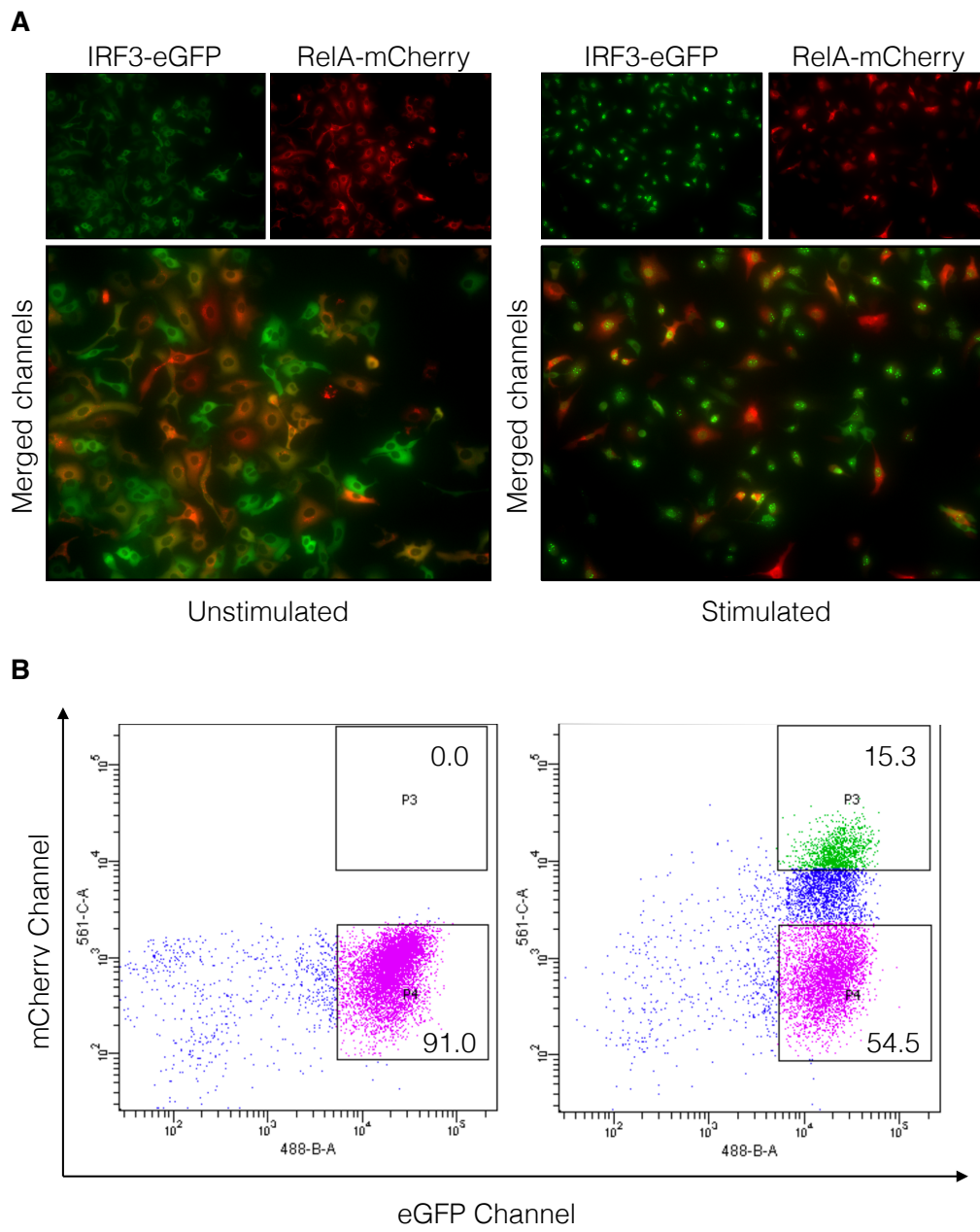


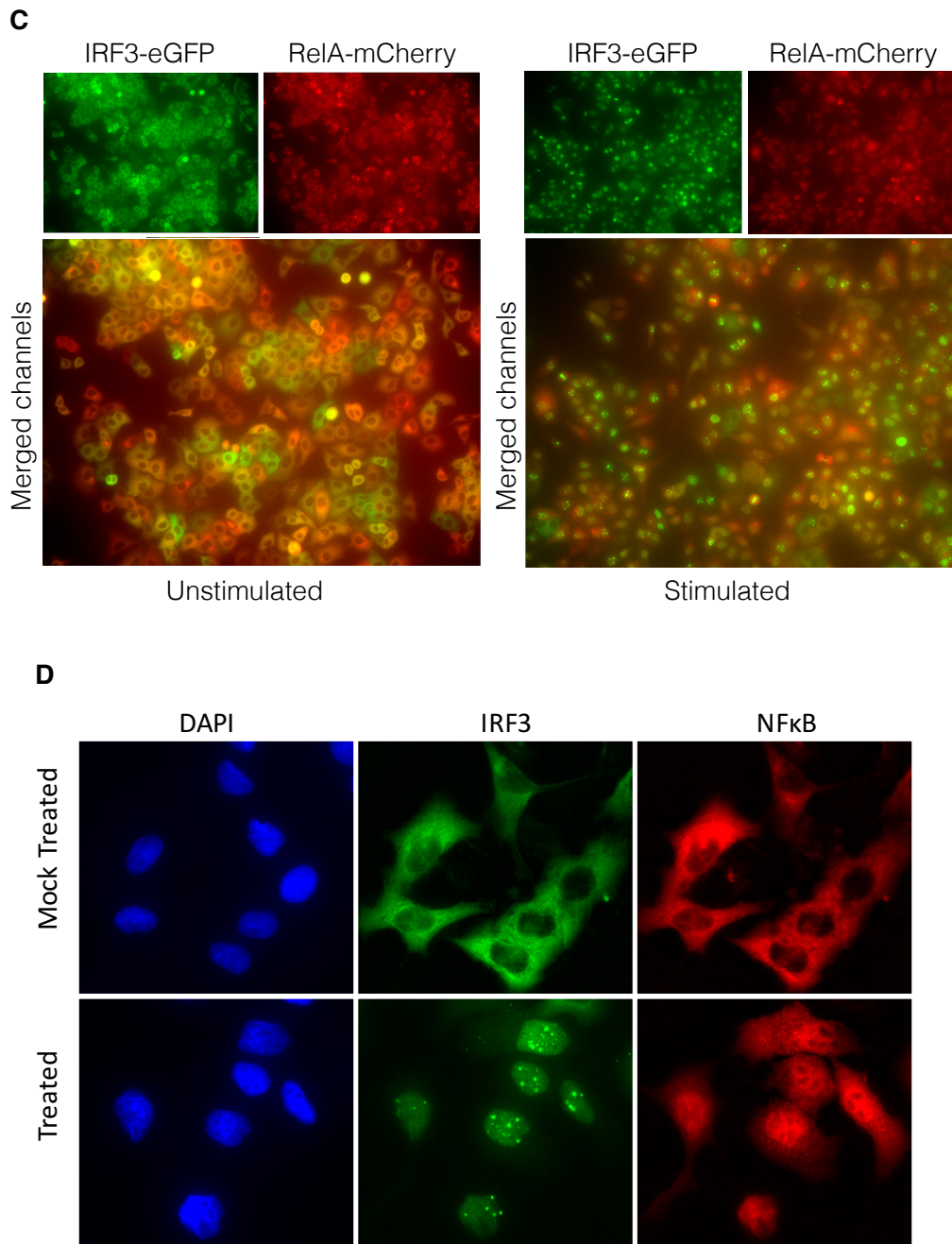
**Figure 4.1.2:** Specific induction of NLS-mCherry-2A-RIG-I<sup>2CARD</sup>. **A)** A549 cells stably expressing the transactivator which induces expression of NLS-mCherry-2A-RIG-I<sup>2CARD</sup> upon doxycycline treatment were tested for their ability to express the construct and activate the RIG-I mediated antiviral signalling pathway. Increasing concentrations of doxycycline were used for induction, however, despite successful

induction of NLS-mCherry-2A-RIG-I<sup>2CARD</sup>, no activation was seen compared to non-treated cells. **B)** Fluorescence microscopy images of A549 cells stably expressing IRF3-eGFP and NLS-mCherry-2A-RIG-I<sup>2CARD</sup> under the regulation of the tetR. The top row panel of images depict cells that were treated with a single round of transduction and the bottom row panel depicts cells that were treated with three rounds of transduction in order to increase copy numbers of the gene of interest.

Despite these technical road blocks, the cell line persevered in the form of a straightforward and facile read out; IRF3-eGFP and NF $\kappa$ B-mCherry, two transcription factors which are both activated upon RIG-I stimulation. Activation and translocation to the nucleus results in transcription of type I and III interferons, interferon stimulated genes, and pro inflammatory cytokines. IRF3-eGFP was stably overexpressed in A549 cells and the subunit of NF $\kappa$ B that translocates to the nucleus, RelA (p65), was N-terminally fused to mCherry and also stably overexpressed in this cell line. It was seen that expressing RelA too highly would result in non-specific translocation of the protein, most likely due to over-exceeding the levels of its negative regulator (I $\kappa$ B $\alpha$ ) (data not shown). Rather than express higher levels of RelA-mCherry in the cells and risk non-specific activation, a transduction titration was carried out with the cells in order to yield cells expressing different intensities of mCherry that would not spontaneously activate without any treatment. The cells were then sorted by fluorescence intensity using fluorescence activated cell sorting (FACS). This resulted in a more homogenous expression of both IRF3-eGFP and RelA-mCherry in the A549 cells (Figure 4.1.3A-D) (henceforth these sorted cells will be referred to as A549<sup>IRF3-488/RelA-575</sup>). This cell line was then used for screening purposes to identify the efficiency of translocation for either IRF3 and NF $\kappa$ B.

**Figure 4.1.3 FACS sorting dual fluorescent cells**



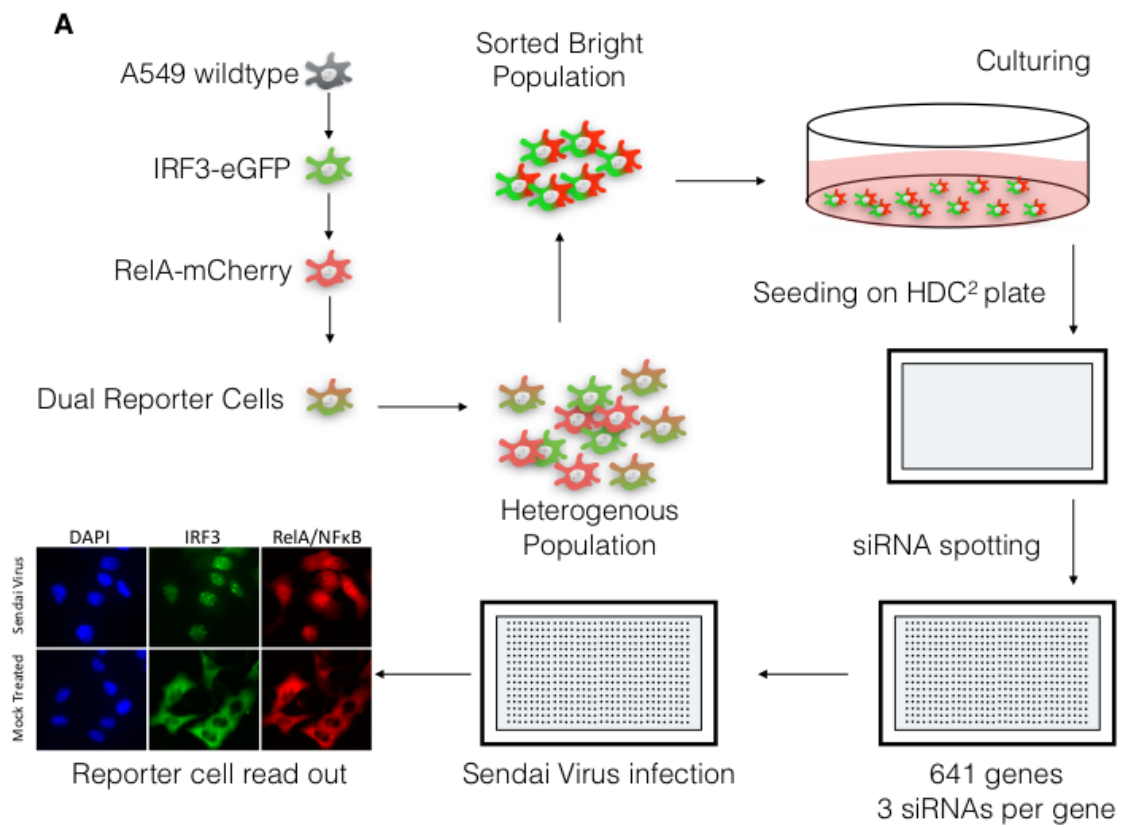


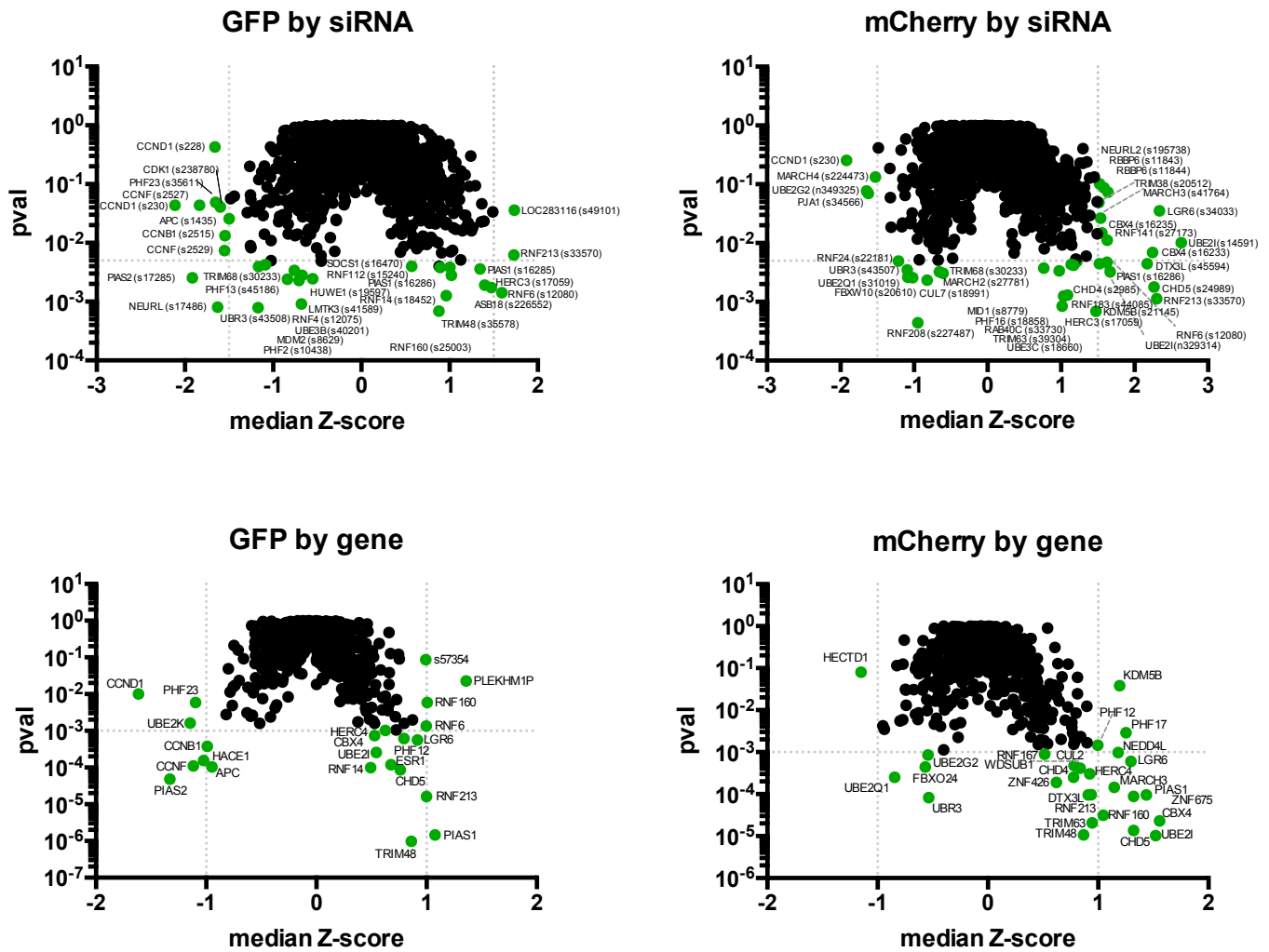
**Figure 4.1.3:** Cell line testing and FACS. **A)** A549 cells stably expressing IRF3-eGFP were transduced in a 1:1 ratio of supernatant containing lentivirus containing recombinant mCherry-RelA and fresh DMEM and tested for activation by assessing nuclear translocation of both IRF3 and RelA. A strong heterogeneous population was observed with this stable cell line. **B)** Fluorescence Activated Cell Sorting (FACS) of the brightly expressing cells for eGFP (488 nm w/v) and mCherry (561 nm w/v), respectively. **C)** FACS sorted cells were tested for their homogeneity and activation profile. **D)** Final cell line to be used for the siRNA screen for E3 ligases, depicting the nuclear translocation of activated cells for both IRF3 and RelA.

Once the cells were prepared and tested for their functionality as a read-out for RIG-I activation, an siRNA library was designed to identify novel E3 Ligase enzymes that are positively or negatively regulating RIG-I signalling, for either the canonical IRF3 or NF $\kappa$ B pathways. Li *et al*, 2008 annotated 617 putative functional E3 Ligase enzymes within the human genome, based on signature catalytic domains ([193]), and this was used as the basis for the customised siRNA targeting E3 Ligases. In total, 616 genes were targeted for knockdown by siRNA, with 3 siRNAs per gene. Including positive and negative controls, a total of 641 genes were targeted. The siRNAs were spotted, in combination with lipofectamine 2000® on a high-density cell chip with microscopy quality glass plating (HDC<sup>2</sup>), which was developed in-house by group of Dr. Holger Erfle, head of ViroQuant-Cell Networks RNAi screening facility, at the Bioquant institute, Heidelberg, Germany. siRNAs/lipofectamine were spotted on each HDC<sup>2</sup> using a spotter obtained from Graffinity pharmaceuticals. A549<sup>IRF3-488/RelA-575</sup> were then seeded 48 hours after spotting and a further 24 hours later were infected with Sendai virus, a virus that is specifically recognised by RIG-I. The cells were inoculated with the virus for approximately 4 hours prior to fixing and nuclear staining. The HDC<sup>2</sup> chips, using channels 420/460nm Ex/Em, 488/515nm Ex/Em, and 587/610nm Ex/Em were imaged using an Olympus IX 81 ® microscope, for Hoechst staining, eGFP, and mCherry respectively (Figure 4.1.4 A).

Images were then processed and analysed using an automated high throughput fluorescence microscopy system [194]. Image analysis determined nuclei of Hoechst stained cells and measured the intensity and localisation of eGFP and mCherry fluorescence respectively, such that if RIG-I is activated, cells will have a stronger nuclear signal for their respective transcription factor. Thus, the number activated cells, in addition to the extent of activation, can be quantified by measuring the ratio of the nuclear signal and the cytoplasmic signal (Figure 4.1.4 B). Screening analysis was carried out by the group of Dr. Karl Rohr, Head of the Biomedical Computer Vision Group (BMCV), at the Bioquant institute, Heidelberg.

**Figure 4.1.4 siRNA screening**



**B**

**Figure 4.1.4:** siRNA screen. **A)** Schematic overview of the siRNA screen development, application, and analysis. **B)** statistically significant hits (by p-value) that are either positively or negatively regulating (median Z-score) the translocation of IRF3 (GFP) and NF $\kappa$ B (mCherry), by either a specific siRNA (labelled “by siRNA”) or by gene hits encompassing all three siRNA’s (labelled “by gene”).

Interestingly, PIAS1 from the protein inhibitor of STAT family, is a significant hit as a negative regulator of both IRF3 and NF $\kappa$ B activation, and so far, is only characterised as an inhibitor of the JAK/STAT signalling cascade, indicating a novel role for this protein in the RIG-I signalling cascade. Further, PIAS2 is one of the strongest hits as a positive regulator of IRF3 activation, with a stronger Z-score for positive regulation than that of TRIM25 and RNF123, both hits in our screen, and both published as positive regulators of RIG-I signalling [72, 195]. Deeper analysis and further work will

be carried out to define the role these hits have on RIG-I mediated signal transduction. A list of candidate genes that are not known to regulate RIG-I signalling can be found in the following table:

Table 26 siRNA screen candidates

siRNA	Mean Z-score activation	SD	P-value	Gene
s1435	-1.1584	1.2702	2.56E-02	APC
s226552	1.2047	0.6066	1.91E-03	ASB18
s2515	-1.6790	1.4422	1.32E-02	CCNB1
s230	-1.4205	1.7808	4.36E-02	CCND1
s228	-0.6059	2.1847	4.3E-01	CCND1
s2527	-1.3443	1.6868	4.38E-02	CCNF
s2529	-1.7248	1.3097	7.41E-03	CCNF
s238780	-1.1897	1.4642	4.07E-02	CDK1
s17059	1.2391	0.8065	1.74E-03	HERC3
s19597	-0.6788	0.4688	2.46E-03	HUWE1
s41589	-0.5656	0.3316	9.10E-04	LMTK3
s49101	1.1777	1.1575	3.60E-02	LOC283116
s8629	-0.7097	0.5178	3.38E-03	MDM2
s17486	-1.5706	0.9031	8.05E-04	NEURL
s45186	-0.8802	0.6683	4.23E-03	PHF13
s10438	-0.9743	0.6697	2.40E-03	PHF2
s35611	-1.5522	1.4710	4.92E-02	PHF23
s16286	1.1930	0.8419	2.79E-03	PIAS1
s16285	1.2166	0.8970	3.59E-03	PIAS1
s17285	-1.8338	1.2736	2.55E-03	PIAS2
s46606	1.2198	0.9590	5.12E-03	PRICKLE2
s15240	0.8514	0.6342	3.80E-03	RNF112
s18452	1.2061	0.7449	1.26E-03	RNF14
s25003	0.7858	0.5867	3.85E-03	RNF160
s32087	-0.5164	0.3608	4.88E-03	RNF20
s33570	1.5179	1.2372	6.21E-03	RNF213
s12075	-0.6500	0.4588	2.80E-03	RNF4
s12080	1.4681	0.6979	1.43E-03	RNF6
s16470	0.7774	0.5842	4.00E-03	SOCS1
s35578	0.9687	0.5438	6.90E-04	TRIM48
s30233	-0.9232	0.6928	3.96E-03	TRIM68
n329314	0.8464	0.6365	4.01E-03	UBE2I
s40201	-0.6837	0.4664	2.29E-03	UBE3B
s43508	-1.2465	0.7150	7.93E-04	UBR3
s43507	-0.9281	0.5686	4.99E-03	UBR3

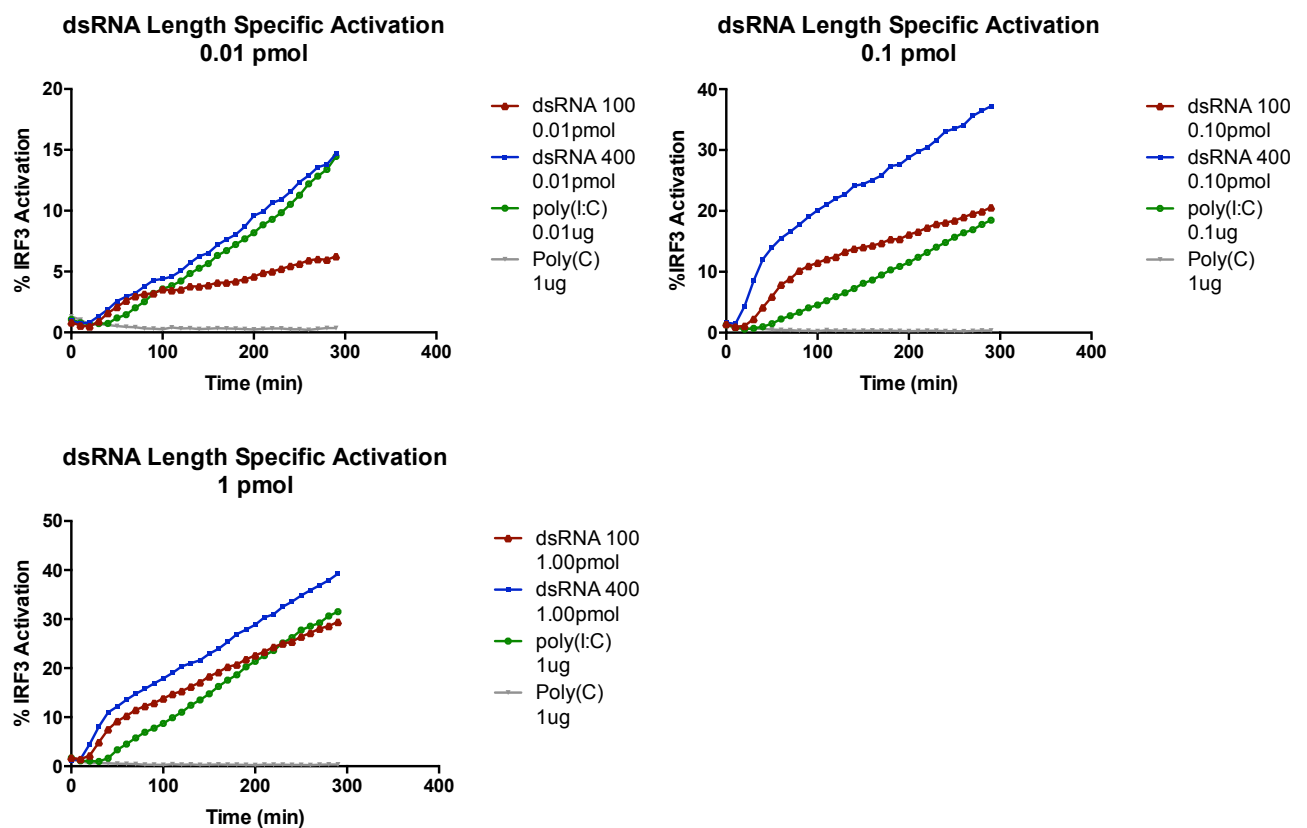
**Table 26:** siRNA screen list of candidate genes that may significantly positively or negatively regulate the RIG-I signalling pathway leading to the activation of IRF3/NF $\kappa$ B.



## 4.2 RIG-I Signalling – From Tools to Dynamics Data

Despite RIG-I signalling having been extensively studied, the dynamics and regulation of the signalling steps has been somewhat overlooked. In order to fully understand the relationship between the host and an invading virus, in terms of pathogenesis and disease progression, dynamics of a successful antiviral signalling response must be analysed. Using A549 cells stably expressing IRF3 tagged with eGFP and fluorescence imaging, we could track the activation of the RIG-I signalling pathway using transcription factor translocation in response to dsRNA as a read out. Toward understanding the regulation and kinetics of IRF3 activation in response to dsRNA, we used different concentrations (0.01-1 pmol dsRNA/well) and different lengths of dsRNA (100 base pairs or 400 base pairs) using a lipoma-transfection approach (figure 4.2.1).

**Figure 4.2.1 IRF3 translocation tracking**



**Figure 4.2.1:** IRF3 activation tracking by microscopy. Individual cells were imaged every 15 min in response to dsRNA liposome-transfection and the % of cells that were activated over time was calculated, using poly(I:C) as a positive control and poly(C) as negative control.

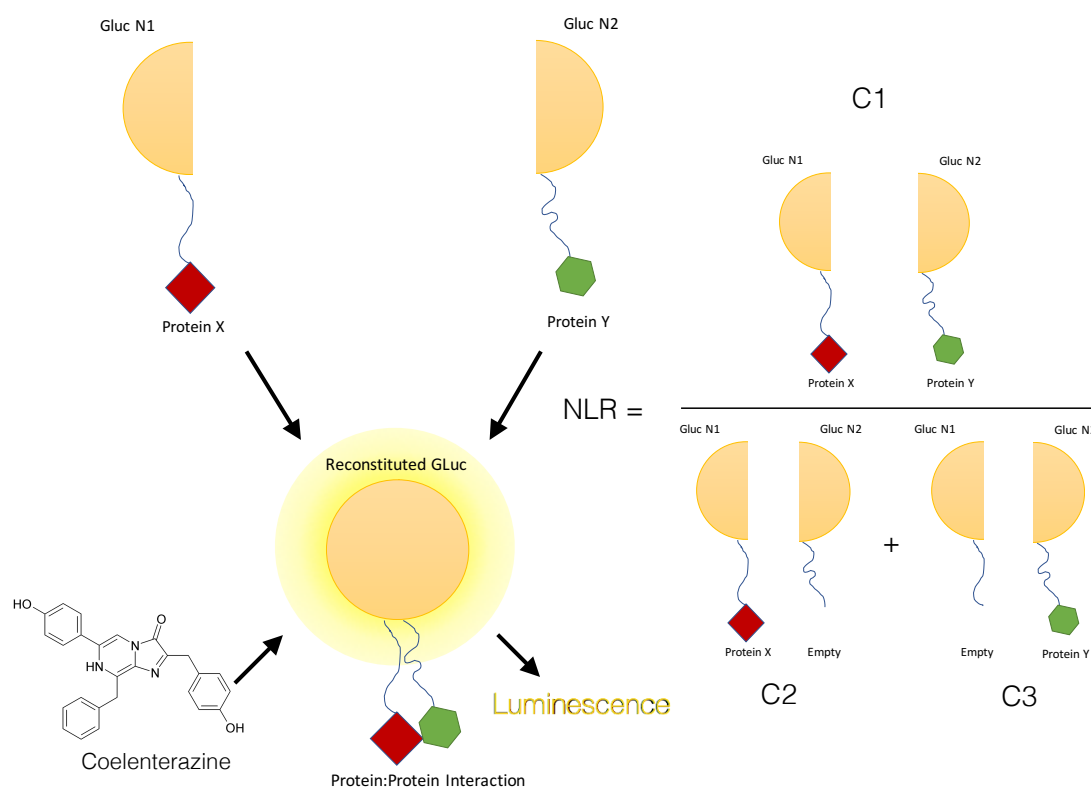
We could see a clear dose dependent and length dependent response to dsRNA in A549 cells, where 400 bp dsRNA at all three concentrations acted as a stronger and faster inducer of IRF3 translocation when compared to 100 bp dsRNA. We observed a strong heterogeneity in terms of the time of translocation of IRF3 between the cells that were tracked, and while we were able to track individual cells, the experiment highlighted specific aspects of RIG-I signalling measurements that needed to be addressed. We speculated that the observed heterogeneity of IRF3 translocation in response to dsRNA delivery was due to staggered uptake (endocytosis) of the liposome-dsRNA transfection complex. Using IRF3 translocation in response to dsRNA-liposome transfection, we limited ourselves to observing the very downstream point in signalling. Further, we could not determine the moment in time of endocytosis of the liposome-dsRNA complex by each cell, and thus, without knowing this point in time, the dynamics of IRF3 activation could not be compared. In order to characterise the RIG-I signalling dynamics, we would have to extend our observations to the detection of dsRNA, as well as including the individual proteins involved prior to the activation of IRF3. To achieve a thorough analysis of RIG-I signalling, we would need to synchronise the delivery of dsRNA in order to compare the activation of IRF3 and other proteins involved. If RIG-I signalling was a stochastic event, as suggested by Rand *et al.* 2012, single cell read-outs would be necessary.

Thus, toward understanding the dynamic process of the RIG-I signalling cascade, the activation kinetics of the intermediate steps within the signalling cascade must be examined using a quantitative approach. Data published in Nature Methods (Remy & Michnick, 2006 and Madden *et al.*, 2011) [196, 197] outlined a method for quantitatively measuring protein:protein interactions (PPIs). The method was based off of the luminescent potential of enzyme *Gaussia princeps* luciferase (henceforth abbreviated as GLuc). In the case of Protein Complementation Assay (PCA), GLuc is split into two fragments, N1 and N2, where by N1 corresponds to amino acids 1-93, and N2 corresponds to amino acids 94-169, excluding the 16 amino acids of the N

terminal end that correspond to the secretion signal sequence. In order to measure PPIs, GLuc N1 and GLuc N2 are fused to proteins of interest that are known to interact. Upon close proximity, GLuc structure reconstitutes to form its functional native structure, where by its enzymatic activity is restored. Therefore, upon PPI, GLuc enzymatic activity is directly proportional to the affinity and rate of occurrence of the specific PPI. Since the read-out for GLuc activity is luminescence based, PPIs can be quantitatively measured using interacting proteins fused split GLuc and measuring luminescence.

In order to account for random reconstitution of the GLuc within cells, control assays are included to calculate a normalised luminescence ratio (NLR). The assay involves the input of a protein of interest fused to GLuc N1, in addition to its interacting partner (putative or known), fused to GLuc N2 (henceforth this construct mix is referred to as C1). Separately, these proteins of interest are, in addition, used as input with their cognate GLuc fragment fused to no protein, such that Protein X-GLuc N1 + Empty-GLuc N2 will be measured (henceforth referred to as C2). Additionally the reverse is also measured; Empty-GLuc N1 + Protein Y-GLuc N2 (henceforth referred to as C3). C1, if the protein partners do interact, will give a positive luminescent signal, the strength of which will be based on protein interaction affinity and rate of occurrence. C2 and C3 however, should not give a strong positive interaction signal due to the fact that the GLuc fragments will be separated by the empty control and should not specifically reconstitute to their native structure and therefore should not be able to produce a luminescent signal. It cannot be ruled out however that random close proximity of the protein fused GLuc fragment and the empty GLuc fragment occurs. This results in the generation of a base line luminescent signal to normalise to for the positive interaction input (C1). Thus, the normalised luminescent ratio is the quantification of the C1 input divided by the combination of the quantification C2 and C3 (illustrated and summarised in figure 4.2.2).

**Figure 4.2.2 PCA overview**

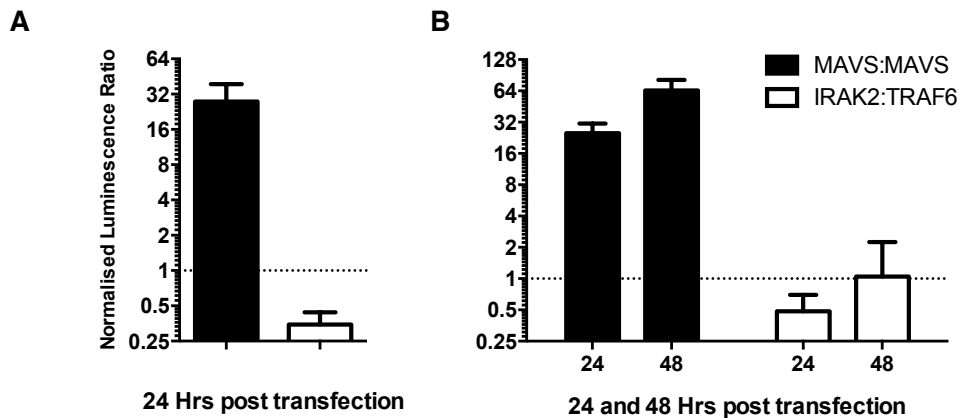


**Figure 4.2.2:** Split *Gaussia princeps* luciferase based protein complementation assay illustration, and how normalised luminescence ratio (NLR) is calculated. Two proteins of interest are linked with each half of the split *Gaussia princeps* luciferase protein, upon addition of the substrate, if the two proteins are interacting the luciferase activity is reconstituted and a luminescence signal can be detected. Normalisation controls are also measured to verify for protein interaction specific signals.

In order to examine whether PCA could be used to quantitatively measure the kinetics of PPIs within a cell, it was first tested if results obtained by Madden *et al*, 2011 could be reproduced using the same approach (figure 4.2.3). It was demonstrated that various incubation times post transfection of the cells yielded varying luciferase signals based upon PPIs (figure 4.2.3 A, C, and B). Despite the varying luminescence signal, it was determined that protein interactions could be detected and quantified using split *Gaussia princeps* luciferase, but that the sensitivity of the assay was not as reproducible as published by Madden *et al*, 2011 (figure 4.2.3D).

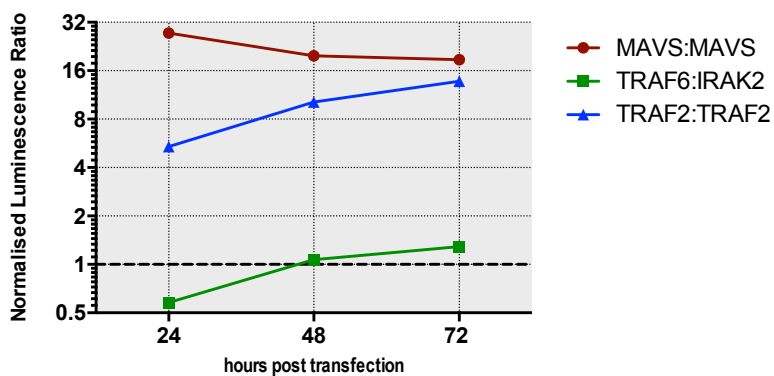
Figure 4.2.3 PCA preliminary results

### Protein Complementation Assay Luminescence Signal



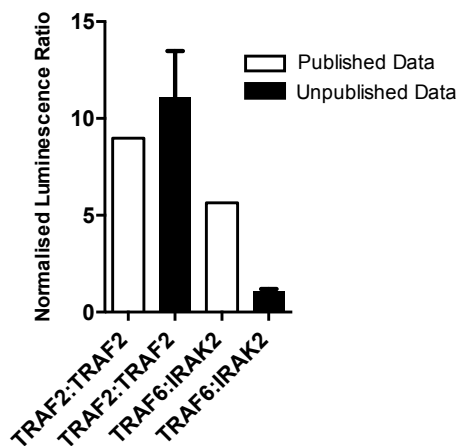
**C**

### Comparison Between Different Incubation Times for Luminescence Signal Strength



**D**

### Comparison of Published Data and Our Generated Data

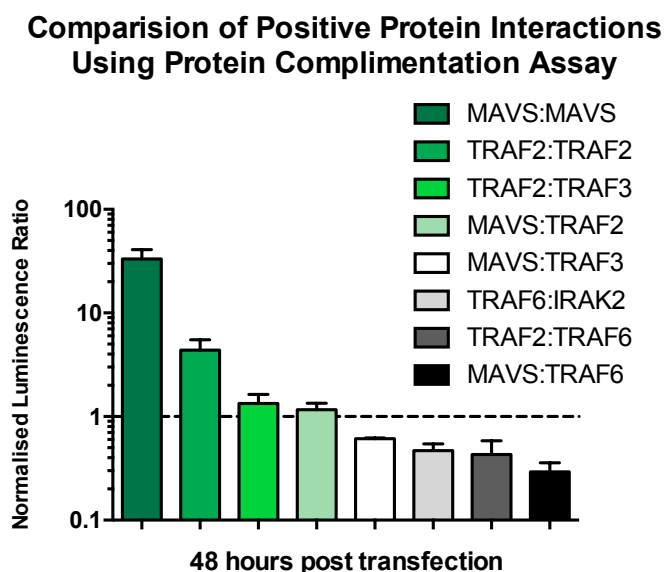


**Figure 4.2.3:** Split *Gaussia princeps* luciferase linked to proteins of interest were tested for their luciferase activity (Protein Complementation Assay) as an experimental basis to quantify protein Interactions *In vitro*. HEK293T cells were transfected with 50ng DNA constructs of proteins of interest, known to interact, linked to the N1 or N2 fragments respectively of *Gaussia princeps* luciferase prior to incubation times and cell lysis by freeze-thawing. **A)** Analysis of protein interaction partners after 24 hours of transfection. **B)** Comparison of protein interaction partners after 24 or 48 hours. **C)** Analysis of luminescence over 24, 48, and 72 hours using positive interaction partners, assuming a background signal noise threshold of 1.0 as a cut off point for a positive interaction signal. **D)** Comparison of the data published for positive interaction partners versus data generated in our lab for the same interaction partners (labelled unpublished data), using the same methodology. Values are expressed as a mean +/- SD, except for (C) where only the mean is expressed, all conditions were carried out in triplicate, for (A and B) n=3, (C) n=1.

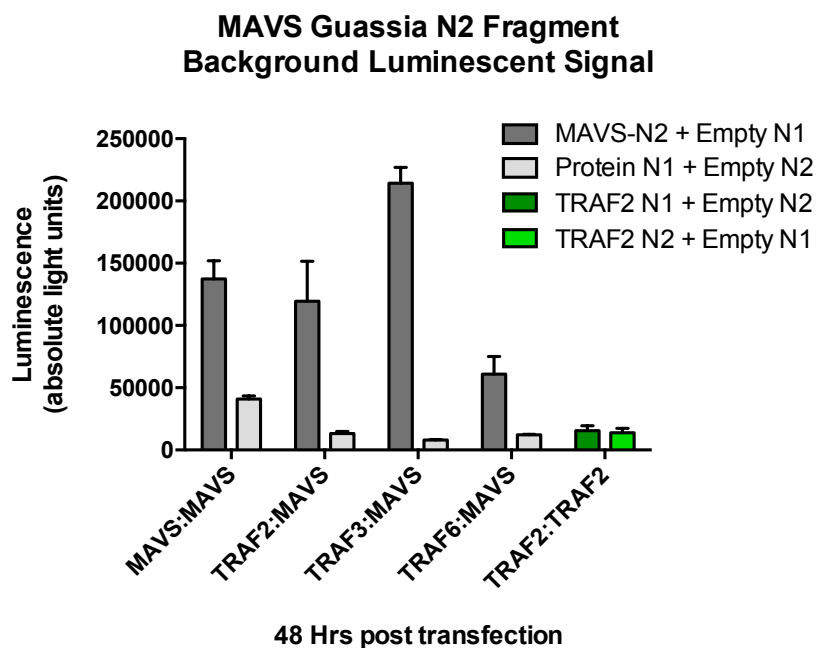
To determine how the lack of reproducibility of the results shown in figure 4.2.3 D occurs, it was examined whether the technical application of the assay could be optimised in order to increase the sensitivity to a “benchmark” point where positive interactions could give a robust luminescence signal. The benchmark for positive interaction signals was given the arbitrary unit of 1, with regards to normalised luminescence ratio (NLR). Using an optimised assay approach (REF# appendix figure PCA), a panel of positive interaction protein partners were tested for their ability to approach the benchmark in terms of their positive luminescence signal. Despite an overall better signal for MAVS:MAVS regarding the newly optimised approach, only 50% of PPIs tested were able to reach the benchmark (Figure 4.2.4 A). This may have been due, in part, to the unusually high signal to background noise ratio of a single plasmid construct: MAVS-N2 (C3 control). When examining the individual luminescence signals that are used to calculate the NLR, it was determined that MAVS, fused to GLuc N2, would give a positive luminescence signal despite not being co-transfected with a protein interaction partner (empty GLuc N1). This appeared to only affect MAVS, as it can be seen that TRAF2, when fused to either N1 or N2, and co-transfected with its cognate empty control, would give a remarkably low background luminescence signal when compared to MAVS-N2/empty-N1 (figure 4.2.4 B).

Figure 4.2.4 PCA controls

A



B



**Figure 4.2.4:** Positive protein interaction partners were tested for their reconstituted linked luciferase activity, using a threshold of 1 RLU as a baseline for a positive interaction signal over background noise. HEK293T cells were transfected with 100ng DNA constructs of proteins of interest, known to interact, linked to the N1 or N2 fragments respectively of *Gaussia princeps* luciferase. **A)** The range of signals for positive interaction partners and, for some, their lack of positive luciferase signal (signifying protein:protein interaction). **B)** A breakdown of the negative control

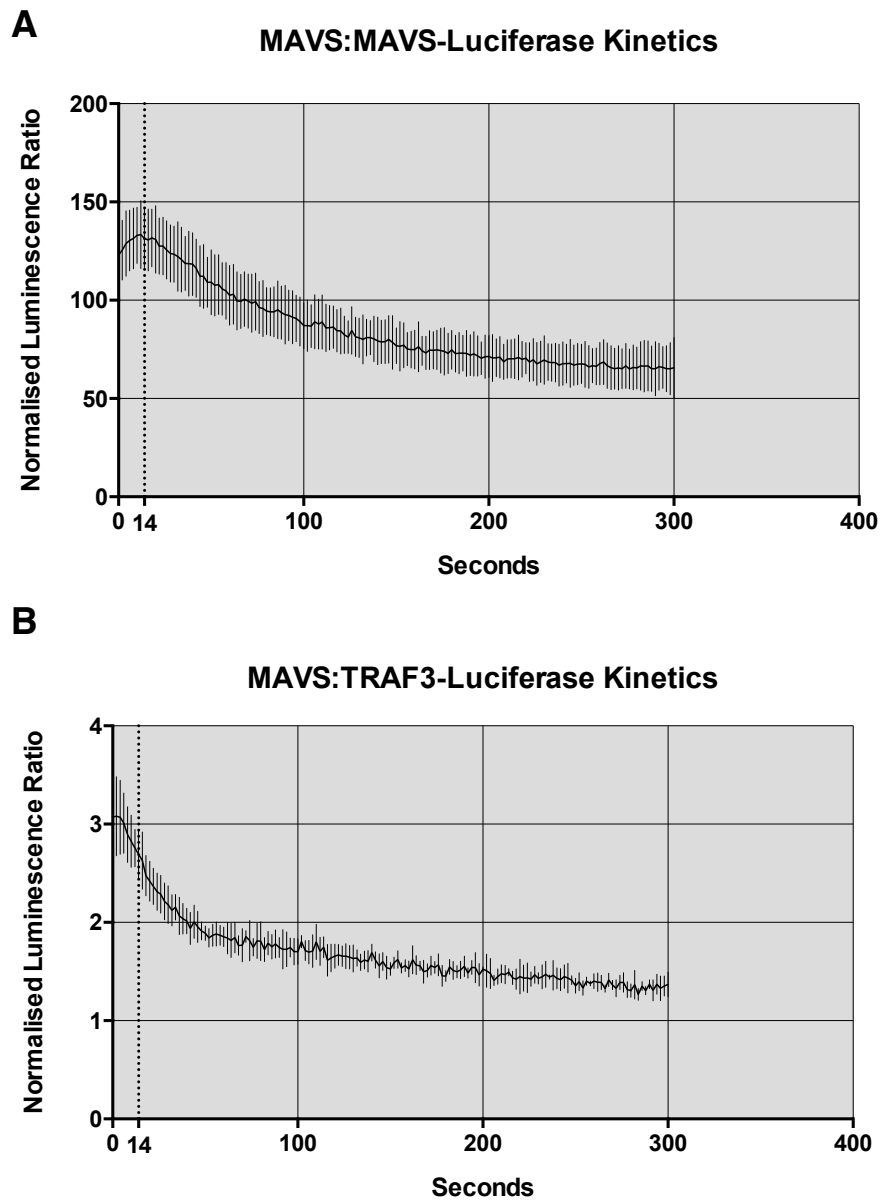
luciferase activity (absolute light units) signals used to normalise the positive control. Dark grey signifies that MAVS is linked to the N2 fragment of *Gaussia princeps* luciferase, light grey signifies that a positive interaction partner of MAVS (here TRAF2, TRAF3, and TRAF6) is linked to the N1 fragment of *Gaussia princeps* luciferase. TRAF2:TRAF2 is shown in green as a MAVS-free control, highlighting the occurrence of a high background signal due to MAVS-*Gaussia* N2 binding empty N1. Values are expressed as a mean +/- SD (n=3).

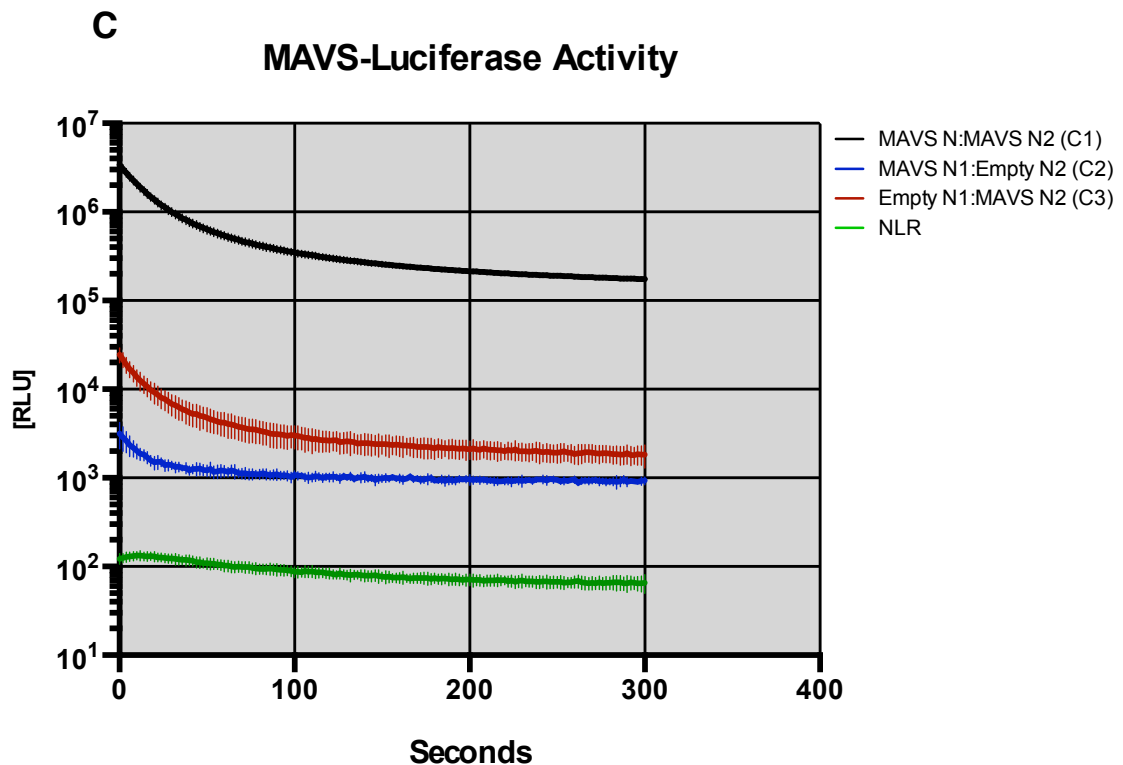
Given that PCA would be used to measure PPIs over time in order to analyse the dynamics of RIG-I mediated signal transduction, MAVS:MAVS and MAVS:TRAF3, two robust positive interactions regarding PCA, were analysed in terms of quantitative kinetic measurements, in order to determine if PCA was a suitable approach. It was demonstrated that, indeed, luminescence could be measured over time, but that the initial substrate binding resulted in a peak signal in the early seconds of the time course, but that the NLR appeared to reach a stable plateau (figure 4.2.5 A and B). Furthermore, it was demonstrated that re-addition of the substrate after 100 seconds from the original addition of substrate, resulted in only a minimal and very short spike in the NLR, such that it would return to its stable plateau (data not shown). A break down of the individual kinetics of MAVS:MAVS (C1, C2, C3 and NLR), display a robust measurement, and suggest the “peak” signal is due to a more rapid degradation of the C2 and C3 signals respectively (figure 4.2.5 C).



Figure 4.2.5 PCA based luciferase activity over time

### Kinetics of Protein:Protein Interaction Mediated Reconstitution of Luciferase Activity





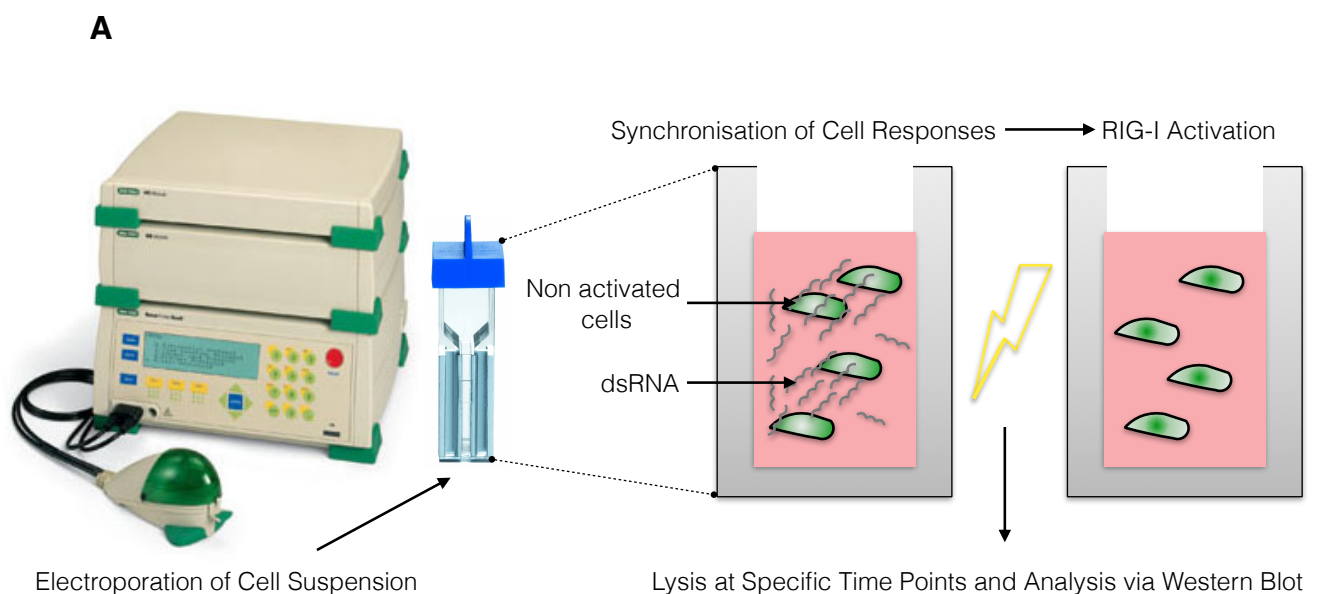
**Figure 4.2.5:** Time course experiment to analyse the potential for quantitative kinetics analysis using PCA. HEK293T cells were transfected with 100ng DNA for each respective construct and 10 $\mu$ M Coelenterazine was used to induce a luminescent signal from time point 0 (seconds), luminescence was then measured every 2 seconds for 300 seconds total. **A)** MAVS:MAVS interaction based reconstituted luciferase kinetics. **B)** MAVS:TRAF3 interaction based reconstituted luciferase kinetics. **C)** Break down of the individual kinetics of each condition for MAVS:MAVS measured in order to calculate the normalised luminescence ratio (NLR). Values are expressed as a mean  $\pm$  SD, all conditions were carried out in triplicate, data representative from one of two experimental replicates.

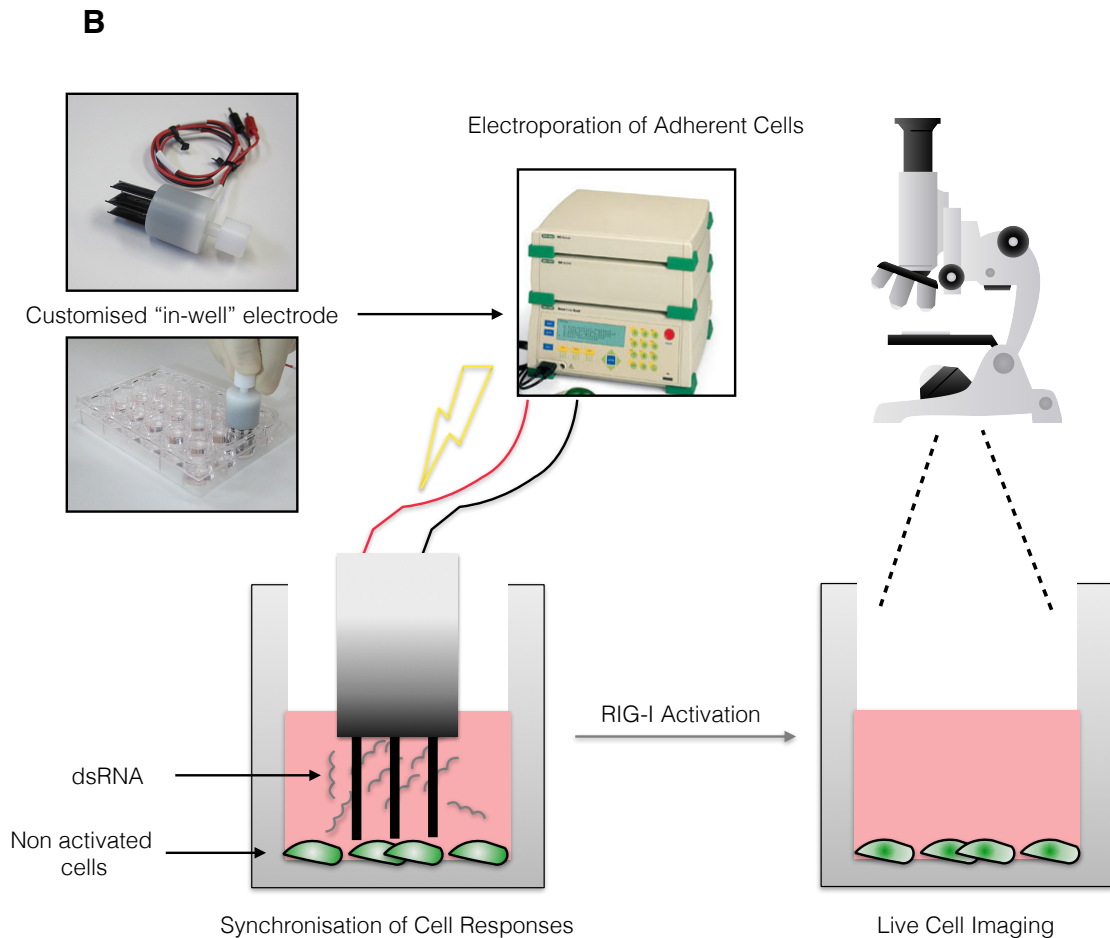
Given the appearance of a significant peak signal, it was examined whether varying delay and measurement times would affect the luminescent signal strength of MAVS:MAVS. It was observed that the varying delays and measurement windows results in dramatic changes to the NLR (data not shown). Thus, the measuring window may be specific for each individual interaction, which is highlighted by the peak in signal seen between the MAVS:MAVS interaction and the MAVS:TRAF3 interaction (figure 4.2.5 A and B). As such, it was decided that this tool would not be appropriate to measure the dynamics of RIG-I signalling, and an alternative approach was necessary. Since using infection with virus or liposome-transfection of dsRNA leads to an asynchronous activation dynamic within the cell pool due to the unknown time

point at which each cell was infected/activated (we speculated that dsRNA delivery by endocytosis of the dsRNA-liposome complex/virus particle occurs randomly on a cell to cell basis), and that we further could not effectively measure PPIs quantitatively, a synchronous activation approach was designed in order to analyse grouped cells efficiently regarding activation kinetics.

Cell suspensions were electro-transfected in the presence of dsRNA. Electroporation of cells results in the influx of the surrounding solution, in this case, dsRNA containing solution for the duration of the electrical pulse. The cells are exposed to an electrical pulse (150V) for a mere 10ms, thus, the influx of dsRNA into electro-transfected cells occurs at the exact moment in time for each cell. This ultimately results in the synchronisation of cell responses and allows for the analysis of kinetics regarding RIG-I signalling (Figure 4.2.6).

**Figure 4.2.6 Cell electroporation overview**



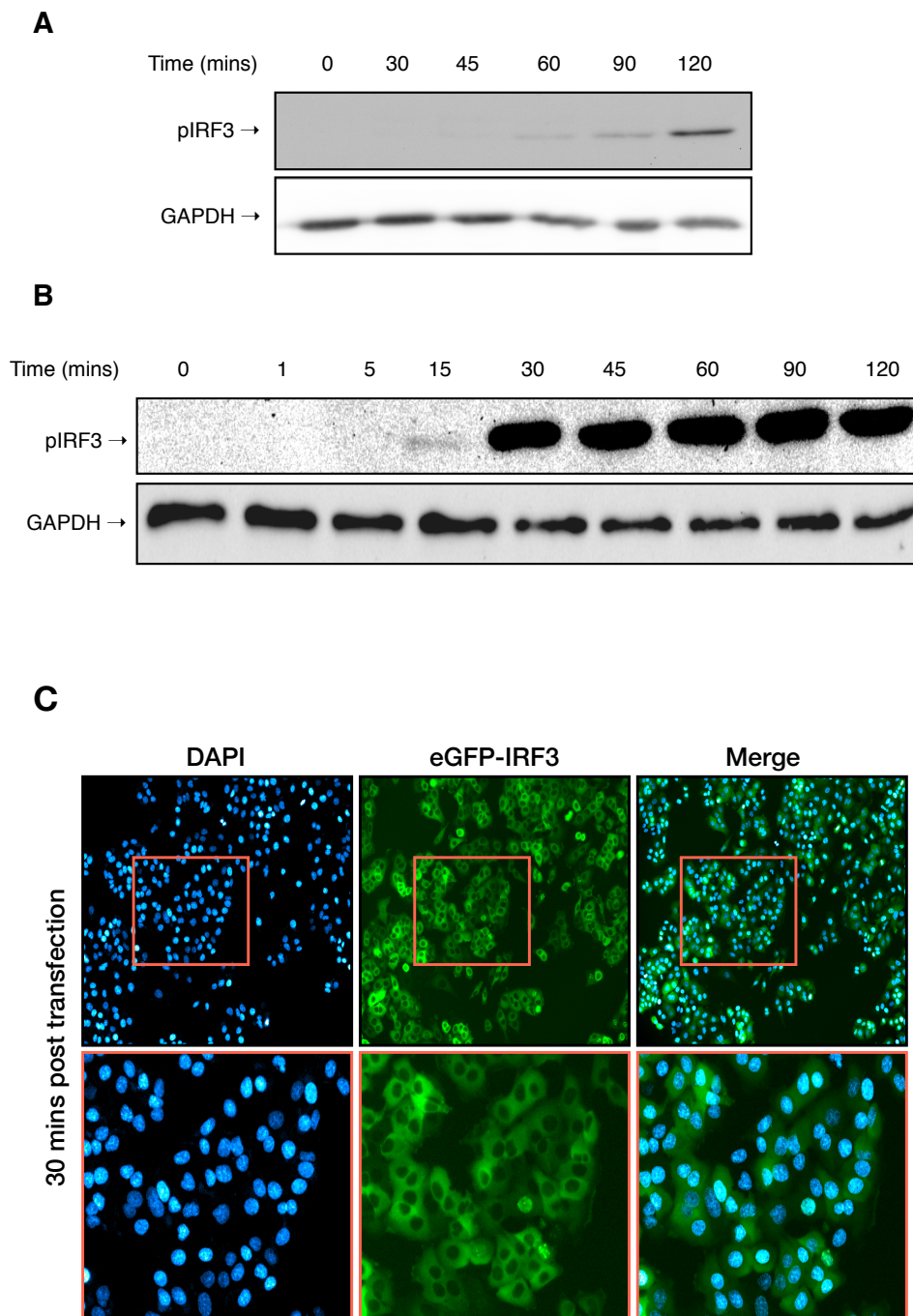


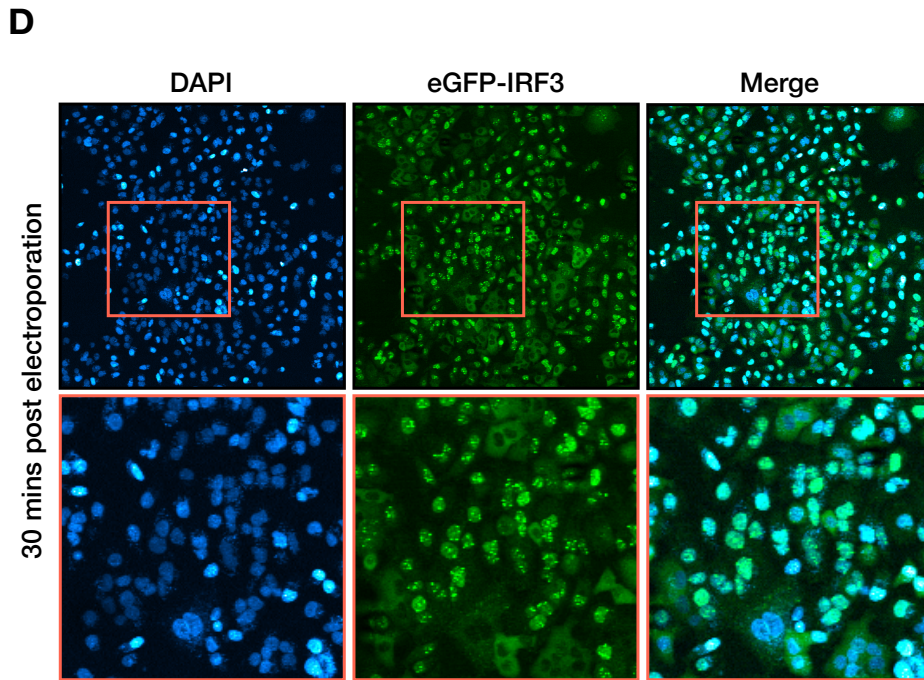
**Figure 4.2.6: A)** Schematic overview of the electroporation of mammalian cells. Cells are suspended in electroporation buffer (cytomix containing 0.8pmol (2nM) dsRNA, and  $4.0 \times 10^6$  A549 cells) in a 0.4mm cuvette. Cuvettes are pulsed with a block pulse of 150V for 10ms. dsRNA enters the cells and synchronises the RIG-I signalling cascade in activated cells. **B)** Schematic overview of the electroporation of mammalian cells adherent to a 24-well glass-bottom plate. Cells are electro-transfected using a customised "in-well" electrode with 100uL buffer (cytomix containing 0.8pmol (8nM) dsRNA). Wells are pulsed with a block pulse of 150V for 10ms. dsRNA enters the cells and activates the RIG-I signalling cascade, allowing for live cell imaging of synchronised responses.

### 4.3 RIG-I Signalling Dynamics

Using an electro-transfection based approach to delivering dsRNA into the cells, we negate the random and unknown delivery kinetics by endocytosis, which would in theory synchronise RIG-I detection of dsRNA across all activated cells. In order to confirm the robustness of the synchronisation, a comparison was made between dsRNA liposome-transfected cells, which would mimic the kinetics/dynamics of a viral infection assay, and dsRNA electro-transfected cells. (Figure 4.3.1). There was a stark contrast between the kinetics of IRF3 activation, which was analysed based upon its phosphorylation at S396 and using GAPDH and total protein control, which is required prior to translocation to the nucleus, and in addition, the live cell imaging of IRF3-eGFP localisation. When comparing liposome-transfection against electro-transfection, we observed a much faster response for both phosphorylation, and nuclear localisation of IRF3 using the electro-transfection approach. As depicted in figure 4.3.1, under a transfection approach (asynchronous) IRF3 begins to be phosphorylated roughly 60 minutes to 90 minutes post transfection, with a relatively strong phosphorylation signal seen after 120 minutes. Compared to the electroporation approach (synchronous), IRF3 begins to be phosphorylated much more rapidly, with a weak signal seen as early as 15 minutes, and quite a strong signal at 30 minutes after electroporation. Moreover, this strong signal is maintained, and even increases slightly for up to 120 minutes, as opposed to the more gradual and overall weaker signal increase seen in the transfection approach. Further, when analysing the localisation of IRF3-eGFP, it was seen that after 30 minutes post-treatment of the cells, there was a strong difference in the number of cells that had IRF3 localised to the nucleus when comparing liposome-transfection and electro-transfection of dsRNA, where electroporation resulted in much higher number of activated cells.

**Figure 4.3.1 Liposome- vs electro-dsRNA transfection**

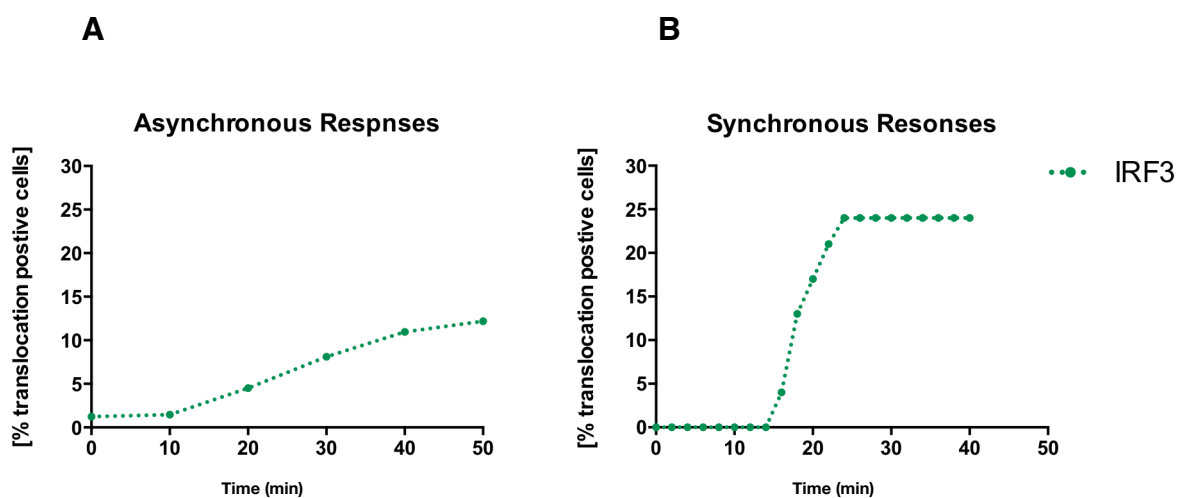




**Figure 4.3.1:** Comparison between transfection and electroporation of dsRNA using A549 cells. **A)** 2nM dsRNA liposome-transfected into A549 cells, which were lysed at specific time points and phosphorylated IRF3 was analysed by Western Blot. **B)** 2nM dsRNA electro-transfected into A549 cells, which were lysed at specific time points and phosphorylated IRF3 was analysed by Western Blot. **C) and D)** Analysis of eGFP-IRF3 translocation from the cytoplasm to the nucleus 30 mins post liposome-transfection (C) or electro-transfection (D) of 2nM 400 bp dsRNA.

Thus, we decided to track the localisation of IRF3 over time in response to dsRNA delivery by either liposome-transfection or electro-transfection (figure 4.3.2).

**Figure 4.3.2 IRF3 nuclear translocation quantification**



**Figure 4.3.2:** Comparison between liposome-transfected **(A)** 2nM 400 bp dsRNA (Asynchronous Responses – 10 min intervals) and electro-transfected **(B)** 2nM 400 bp dsRNA (Synchronous Responses – 2 min intervals) using live cell imaging to measure and quantify the percentage of cells that have IRF3 in the nucleus.

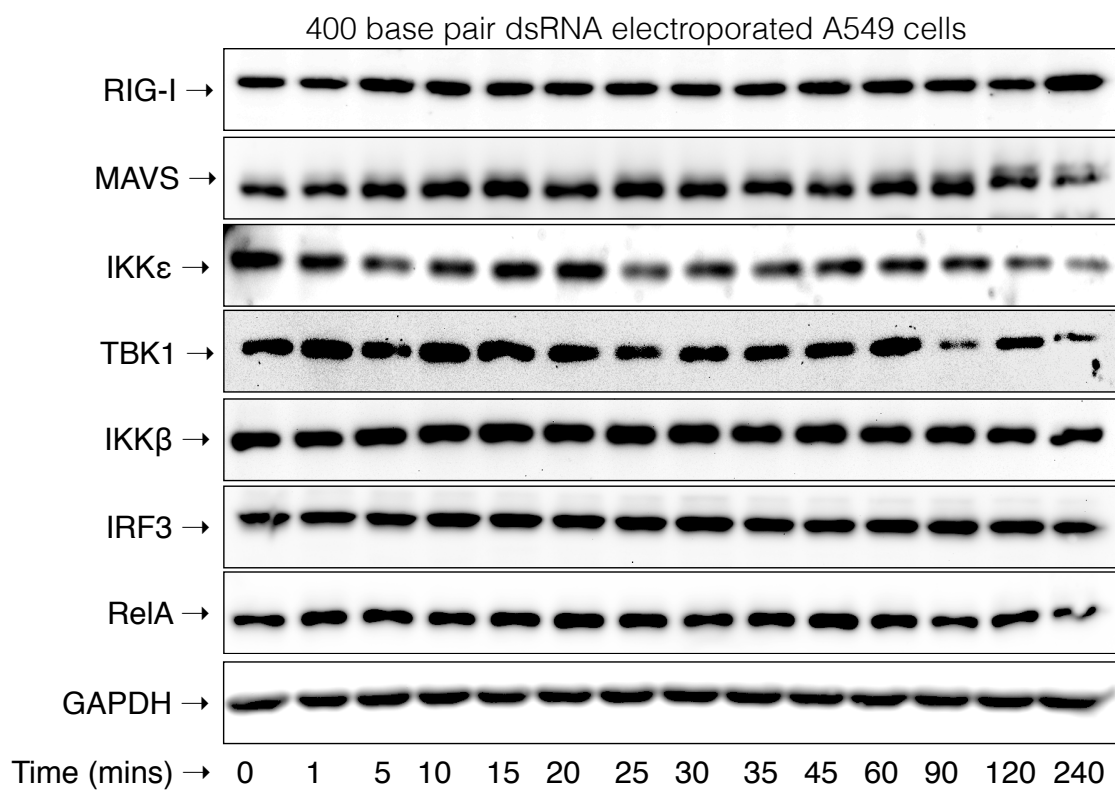
As depicted, when analysing IRF3 translocation over time, under a transfection approach, IRF3 translocation is more gradual, and somewhat delayed. This is in contrast to the electroporation approach, where IRF3 translocation appears to be earlier/rapid and simultaneous, as opposed to staggered/gradual. Thus, we could confirm the robustness of the synchronisation of RIG-I activation and the downstream activation of IRF3. Therefore we decided to endogenously measure the activation states, by quantitative phospho-specific Western Blots, of the canonical proteins involved in RIG-I signalling using the synchronisation approach (described in section 1.3.1.3).

The electroporation of cells in suspension (outlined in figure 4.2.6 A) was used to stimulate the cells synchronously to allow for the measurement of activation markers (post translational modifications) for the specific sub steps of the RIG-I signalling cascade. These sub steps include TBK1, I $\kappa$ K $\epsilon$ , I $\kappa$ B $\alpha$ , I $\kappa$ K $\beta$ , IRF3, and RelA (subunit of NF $\kappa$ B). Due to technical difficulties regarding multiple antibodies targeting the same protein and poor signal acquisition of total protein controls, the native protein was not used as a control measurement when quantifying phosphorylation levels of each protein in the Western Blots, instead GAPDH/calnexin was used. Thus, it was pertinent to determine if the increase/decrease in phosphorylation levels of specific proteins over time was not due to increase or decrease of the target protein itself. As such, phosphorylated protein and native protein was measured separately and GAPDH or Calnexin was used as loading control in each case (Figure 4.3.3).

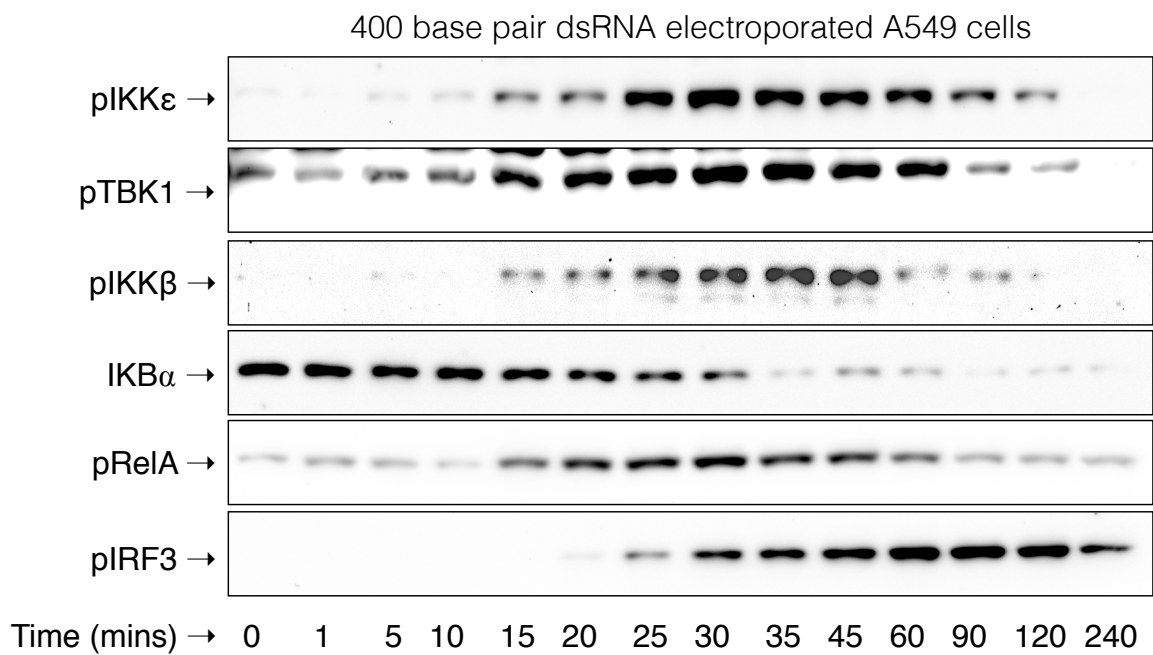


**Figure 4.3.3 Canonical RIG-I signalling protein dynamics analysis**

**A**



**B**



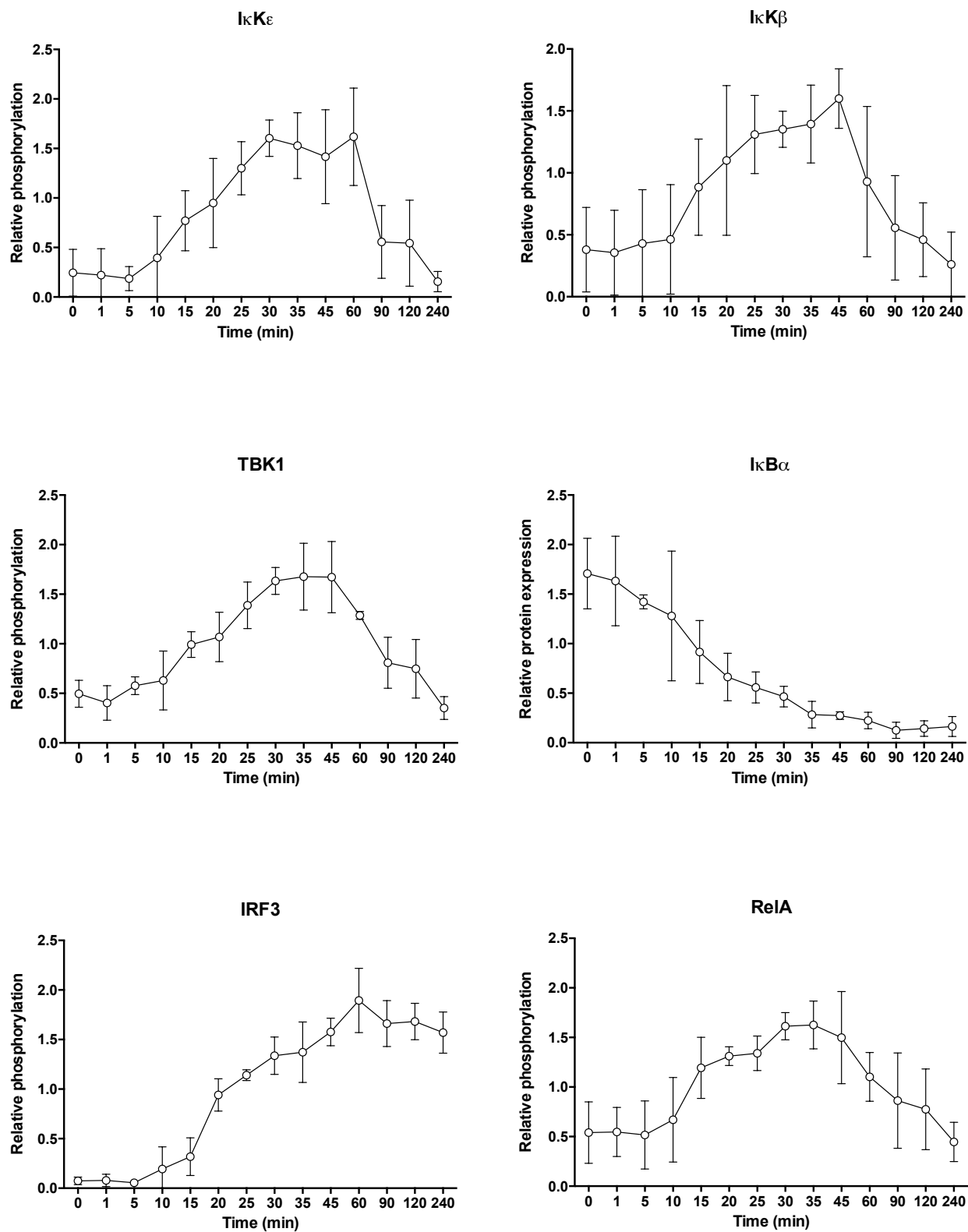
**Figure 4.3.3:** Analysis of expression profiles of major RLR pathway components upon synchronous stimulation of A549 cells by electroporation of 2 nM dsRNA (400 bp). Total protein levels **(A)** or phosphorylated proteins **(B)** were detected by immunoblotting at specific time points after electro-transfection (as indicated).

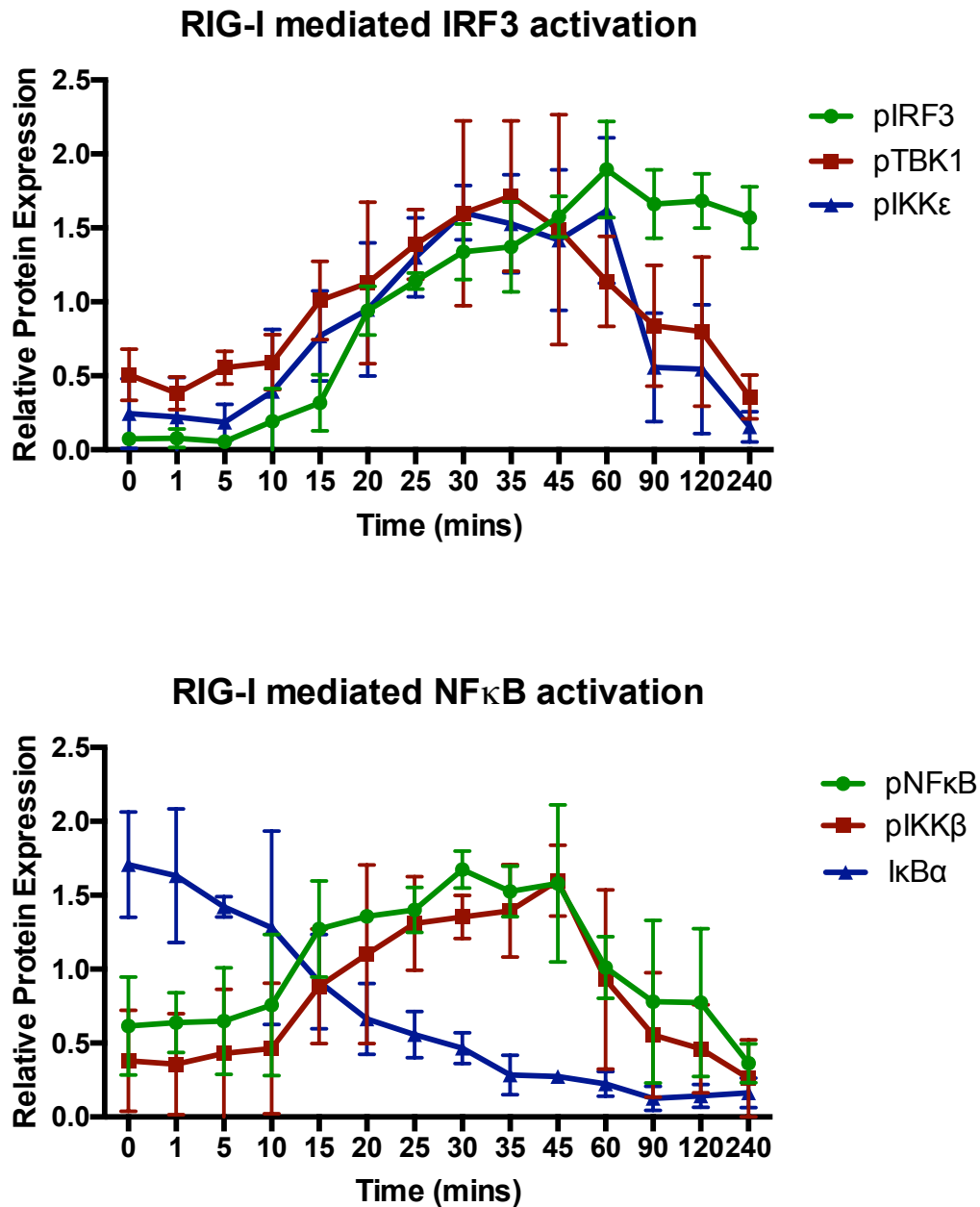
As depicted, the total protein controls appear to not increase or decrease dramatically such that it would majorly effect the quantification of the activation markers for each protein of interest. Furthermore, as indicated from figure 4.3.1, the activation markers under a synchronised approach appear to occur more rapidly and in unison, suggesting a robust and valid read-out. For example, it can be seen that IRF3 only becomes phosphorylated (15-20mins) after TBK1 and I $\kappa$ K $\epsilon$  are increasing in their phosphorylation levels (5-15mins), further verifying synchronicity the assay. Similarly, for I $\kappa$ K $\beta$  and RelA, the activation state of these proteins requires the degradation of I $\kappa$ B $\alpha$ . it can be seen that the phosphorylation of both I $\kappa$ K $\beta$  and RelA occurs only after the initial decrease in total protein of I $\kappa$ B $\alpha$ . Thus, we can see in almost real time, the events of the signalling cascade happen from time point 0 mins (initial recognition of dsRNA), allowing us to follow the flow of the signalling steps from one “checkpoint” to another with respect to RIG-I signalling.

The electroporation of mammalian cells (A549 cells) used to generate the phoso-specific Western Blots of the activation markers were quantified using Lab-image 1D in the time resolved manner depicted in figure 4.3.3 in order to obtain accurate kinetic data regarding RIG-I signalling sub-steps leading to transcription factor activation (Figure 4.3.4A). The canonical pathways for IRF3 and NF $\kappa$ B are displayed separately for a more straightforward interpretation of each signalling cascade (Figure 4.3.4B).

**Figure 4.3.4 Canonical RIG-I signalling protein dynamics quantification**

**A**



**B**

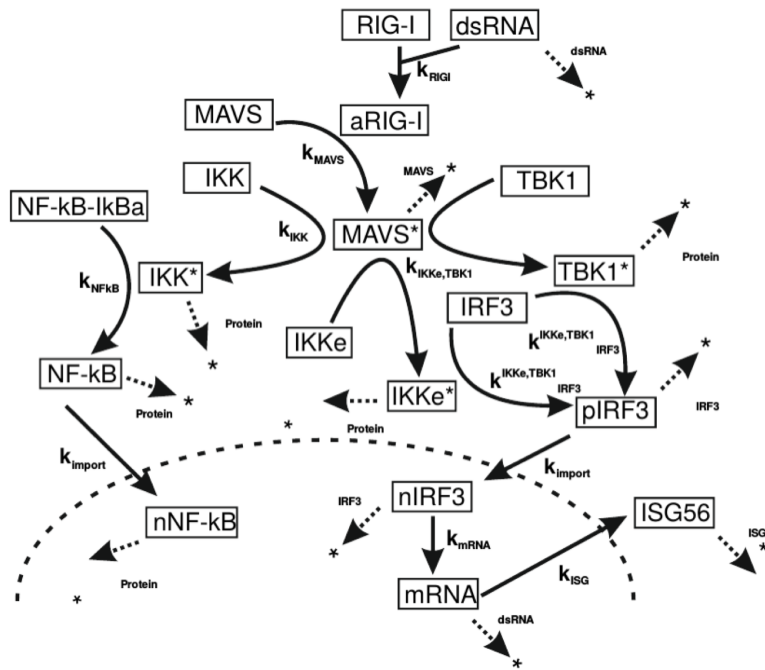
**Figure 4.3.4:** Quantification of the phosphorylation dynamics of the proteins of interest within the RIG-I signalling cascade. **A)** Quantitative data regarding the activation profile of the indicated protein after electroporation of 0.8pmol dsRNA at the indicated time points. **B)** Collation and overlay of the quantitative phospho-specific Western Blot data for the downstream RIG-I dependent canonical IRF3 and NFκB signalling pathways. Data points are mean values (+/- standard deviation) of four independent biological replicates. Values were normalised to the mid-range values for each protein analysed within each individual experiment.

Upon analysis of the canonical proteins and their activation profiles under synchronised RIG-I signalling, it was found that indeed signalling was not a stochastic event, and as depicted, appears to have pre-determined set of kinetics that is rapid and very predictable (deterministic event). We therefore believed that RIG-I mediated signal transduction was an ideal candidate for the application of mathematical modelling, as deterministic processes provide a more straightforward approach compared to stochastic processes. Teaming up with a Ph.D. student from the University of Greifswald, Darius Schweinoch in the group of Dr. Lars Kaderali, we set about designing a mathematical model that assess the kinetics of key signalling events within the RIG-I signalling cascade, extending from solely RIG-I mediated signal transduction to encompass gene transcription and IFN signalling.

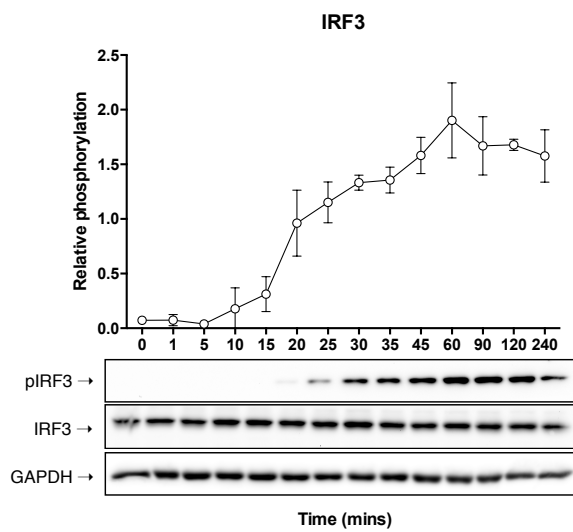
Using synchronised cell responses as a basis for examining activation markers, the kinetic data generated was used to examine various parameters that would model, analyse, and simulate the cells responses that would most closely fit the experimental results (regarding RIG-I signalling – figure 4.3.4). Ultimately this combines theory with experimental data and achieves the simulation of complex molecular networks of a biological system. Modelling, carried out by Darius Schweinoch, simulates the rate of change ( $K$ ) from one protein state to another (for example, non-phosphorylated protein to its phosphorylated state). Using ODEs, multiple parameters of each specific protein were tested. Specifically, the unknown rate constants, which describe the rate of change, were tested such that the model best describes the experimental data provided (deterministic parameters). It is important to note that multiple parameters may fit the experimental data, and therefore it is unknown which model truly reflects the natural molecular events within the cell. An overview of the modelling scheme and its basis can be seen in figure 4.3.5.

Figure 4.3.5 Mathematical modelling

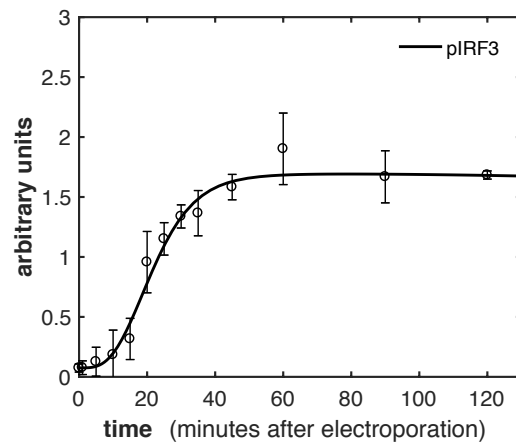
A



B



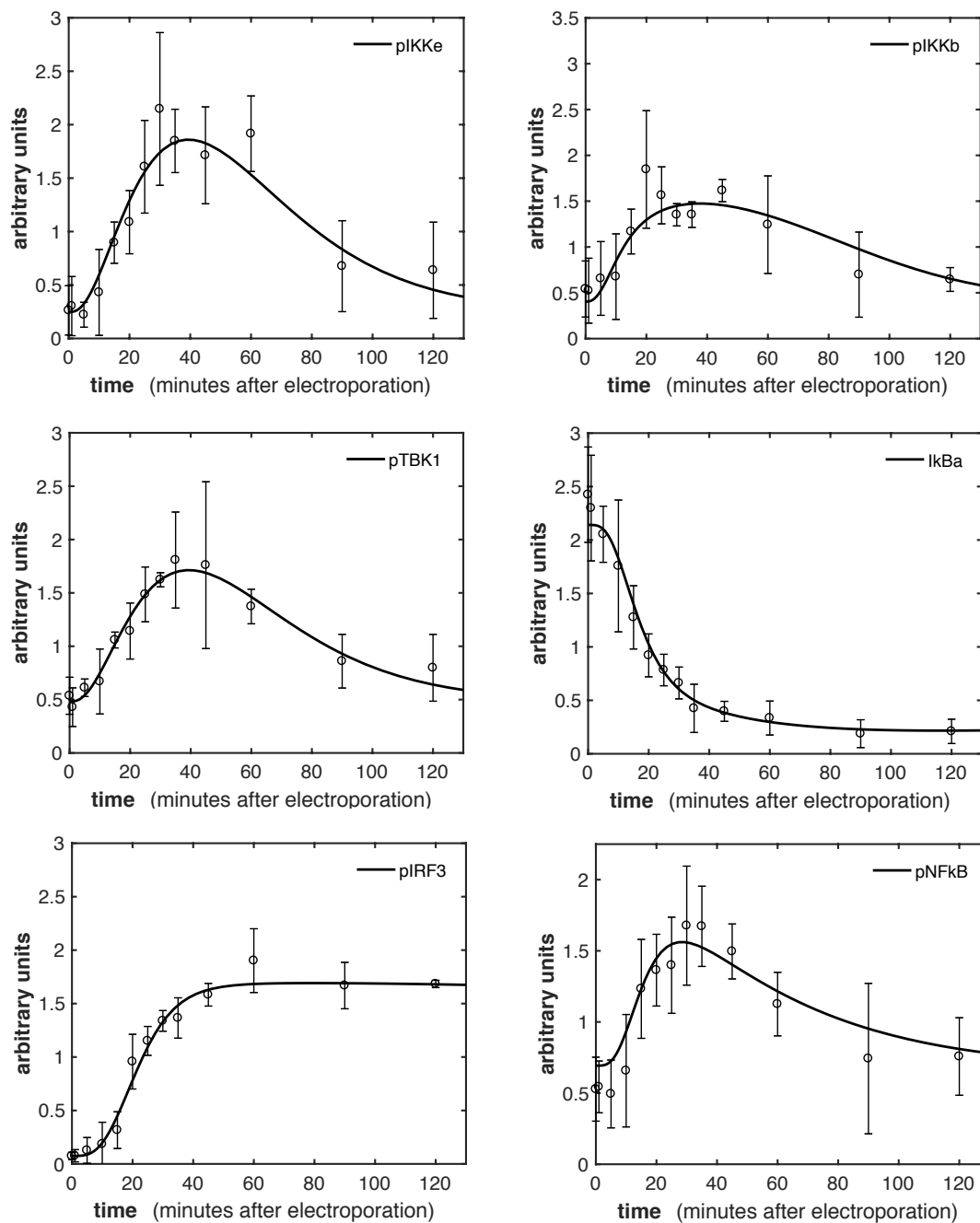
C



**Figure 4.3.5:** Dynamic pathway model for RIG-I signalling pathway. **A)** Graphical illustration of a mathematical model for the RIG-I signalling pathway. The model consists of ordinary differential equations (ODEs) based on mass action kinetics and describes each of the major steps of signal transduction from RNA sensing by RIG-I to transcription of target genes and the production of their mRNAs. Kinetic rates of the individual reactions (i.e. model parameters) were taken from literature where possible (e.g. rate of mRNA synthesis) or estimated by model fitting to experimental data. **B)** As an example of quantitative, time-resolved data that was used to “train” the mathematical model, the time-course of IRF3 phosphorylation is shown, including the total protein control and GAPDH as a loading control. Data points in the graph represent means and SD from four independent experiments (see figure 4.3.4). **C)** After fitting of the model to measured data of all protein species (see figure 4.3.4), the ODE system can rather accurately simulate the dynamics of IRF3 activation upon stimulation with dsRNA. The solid black line is the model simulation, black crosses represent measured data used for fitting (without the 240 min value). All mathematical modelling was performed by Darius Schweinoch in the group of Prof. Lars Kaderali (University Medicine Greifswald).

These parameters were then fit for each of the proteins analysed in figure 4.3.4, such that that the kinetics of the activation of each individual sub-step could be simulated by mathematical modelling (figure 4.3.6).

**Figure 4.3.6 Parameter fitting**

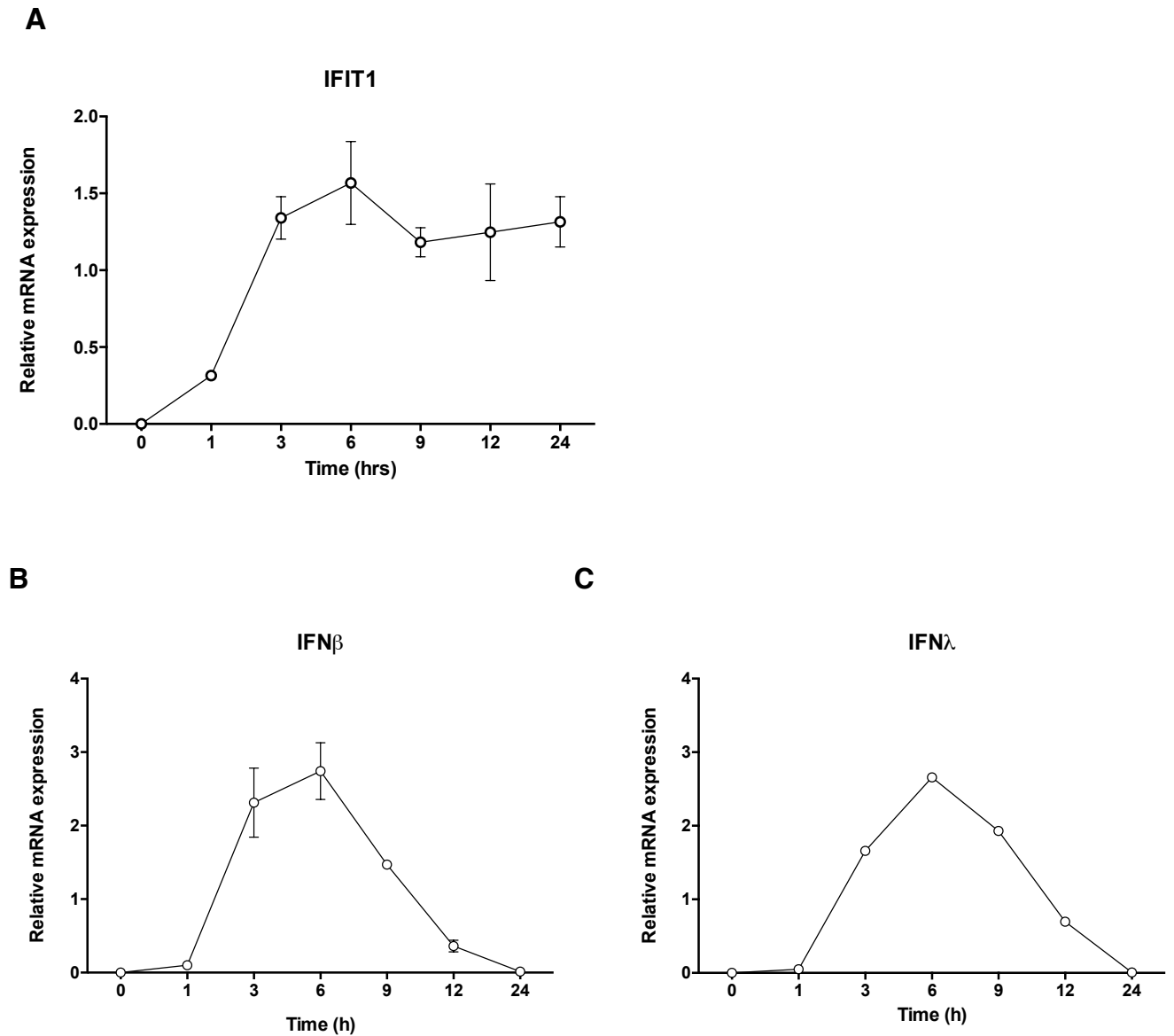


**Figure 4.3.6:** Parameters that were fit for each individual sub-step of the RIG-I signalling cascade (by Darius Schweinoch) compared with experimental data obtained in our lab.



Having generated the basis for a mathematical model describing the dynamics and kinetics of RIG-I signal transduction, a more comprehensive overview of the antiviral innate immune response was desired. Therefore it was decided to extend the data analysis further such that it would encompass not only RIG-I dependent signal transduction, but additionally IRF dependent transcription of specific mRNAs, translation of these mRNAs, and ultimately include IFN dependent signal transduction too, which leads to further production ISGs. This could be incorporated in the mathematical model to provide an extensive overview of the processes involved in mounting an antiviral response. The electro-transfection experimental set up was used to analyse the mRNA expression profile of the synchronised cells over a period of 24 hours. IFIT1, an ISG which is both expressed by the activation of RIG-I in addition to the stimulation of IFN receptors, was measured by qRT-PCR (Figure 4.3.7 A). Using the same experimental set up as previously described, mRNA for IFN $\beta$  and IFN $\lambda$ , which is specific to RIG-I signalling in this experimental set up, was also measured (Figure 4.3.7 B-C).

**Figure 4.3.7 ISG mRNA analysis**



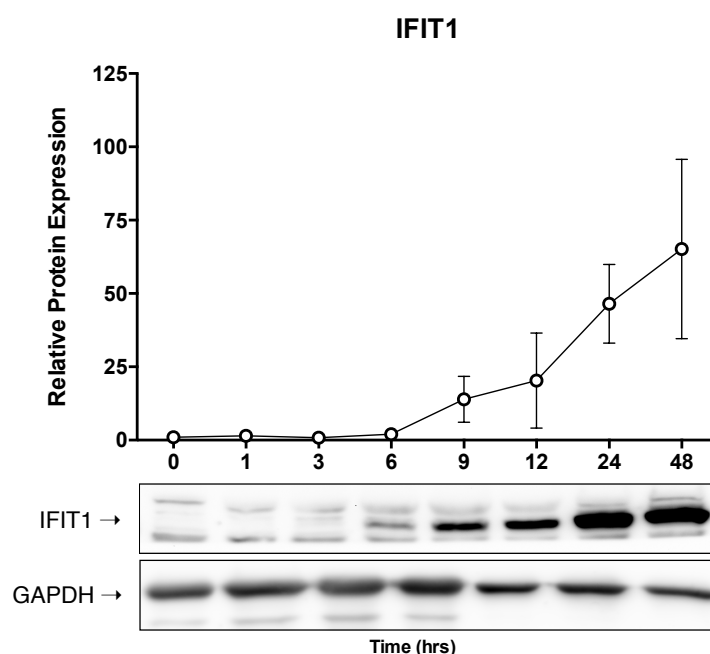
**Figure 4.3.7:** Time-resolved quantification of target gene transcription. A549 cells were electro-transfected with 2nM 400 bp dsRNA and RNA was harvested at the indicated time points post electro-transfection. Production of mRNA downstream of IRF3 activation was determined by gene-specific qRT-PCR against A) IFIT1 (n=3 +/-SD), B) IFN $\beta$  (n=2 +/-SD) or C) IFN $\lambda$  (n=2 +/-SD).

Interestingly, it can be seen for IFIT1 that the mRNA, under a synchronised approach, peaks at 6 hours under this time course, where it begins to decrease at 9 hours, but increases again and stabilises between 12-24 hours. This, in comparison to IFN $\beta/\lambda$  mRNA produced under the same settings, shows a similar peak at 6 hours, but rather than decreasing at 9 hours and increasing again 12 hours, IFN $\beta/\lambda$  mRNA decreases at 9 hours, and continues to decrease until no mRNA is detected after 24 hours. With respect to IFIT1 mRNA and its increase from 9-12 hours, this is most likely due to the amplification effect of IFN protein that is translated by this time and then activates IFN signalling which results in expression of IFIT1, this amplification of mRNA is not seen for the IFNs because IFN signalling does not result in IFN mRNA expression.

To further extend the comprehensiveness of the data, and indeed the model, we wanted to analyse the downstream events of IRF3 activation, which is mainly the expression of type I/III IFNs. We then proceeded to measure expression of IFIT1 protein, which is thought to be similar to the expression kinetics of IFN $\beta$  (figure 4.3.8). We further tried to measure the production of IFN $\beta$  by ELISA and by an indirect bio-assay (4.3.9)

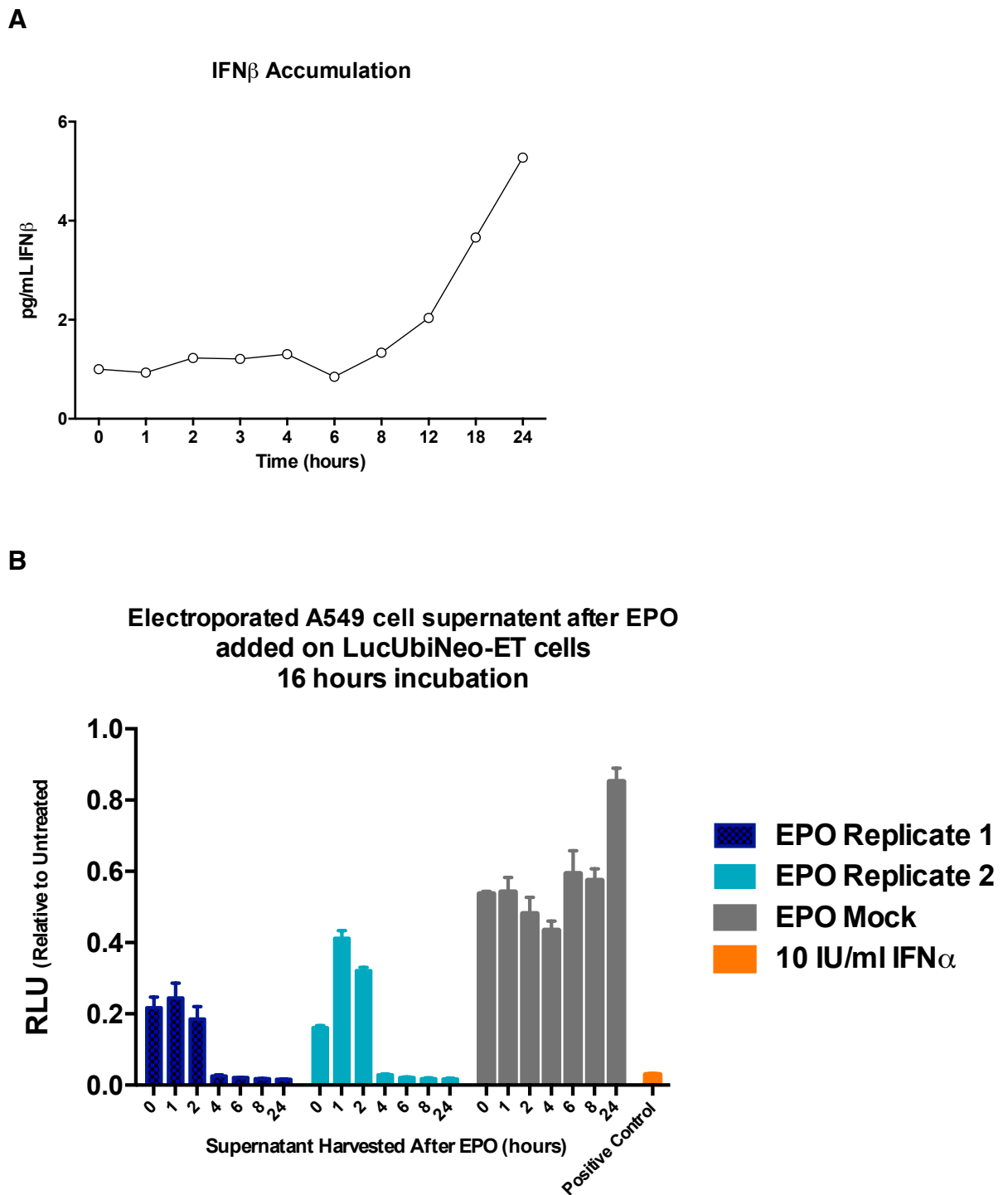
**Figure 4.3.8 IFIT1 protein expression**

**A**



**Figure 4.3.8:** Time-resolved quantification of target protein production. A549 cells were electro-transfected with 2nM 400 bp dsRNA and cells were lysed at the indicated time points post electro-transfection. Protein amounts of IFIT1, a major ISG, were determined by Western Blotting, and quantification of protein amounts is relative to GAPDH (values are expressed as mean +/- SD where n=3).

**Figure 4.3.9 IFN $\beta$  analysis**



**Figure 4.3.9** Time-resolved quantification of target protein production. A549 cells were electro-transfected with 2nM 400 bp dsRNA and supernatant was harvested at the indicated time points. **A)** ELISA based quantification of the production and accumulation of IFN $\beta$  in the supernatant of stimulated cells, data normalised to 0 hr value (n=1). **B)** Antiviral activity of secreted factors. Supernatants from 2nM 400 bp dsRNA electro-transfected A549 cells (two separate replicates) or supernatant from mock (no RNA) electro-transfected cells were collected at the indicated time points after electro-transfection. Stable HCV replicon cells (Huh7-LucUbiNeo/ET) were treated with supernatants for 16hrs and HCV luciferase activity was measured as an inversely proportional correlate of antiviral efficacy of the conditioned supernatants. 10 IU/ml of IFN $\alpha$  were used as a positive control. Values are means +/- SD of 3 technical replicates (wells).

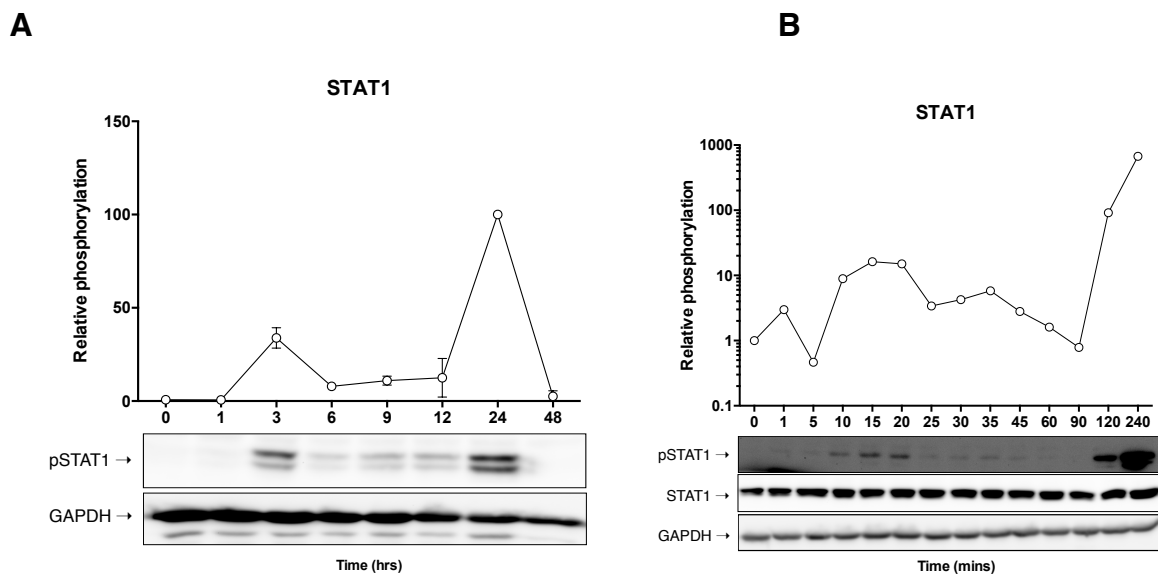
Using the same synchronised experimental approach described thus far, the expression of IFIT1 protein was measured by Western Blot and quantified by Densitometry. As shown in figure 4.3.8, translation of IFIT mRNA can be seen as early as 6 hours, and continues to increase in expression for up to 48 hours. This data is corroborated with the data that depicts the IFIT1 mRNA peaking in its expression at 6 hours.

Furthermore, using supernatant from dsRNA electro-transfected cells, which would eventually contain secreted IFN protein (type I/III) from RIG-I activated cells, we attempted to quantify the accumulation of IFN $\beta$  over time. Using an ELISA based read-out, we could detect IFN $\beta$ , but there was a high background and thus values were normalised to the 0 hour data point, this however resulted in very low sensitivity for IFN $\beta$  detection, with less than 6 pg/mL after 24 hours (4.3.9 A). We also measured IFN production indirectly using the HCV replicon system (4.3.9 B). It was seen that after 4 hours this supernatant could block replication of the HCV using the HCV replicon system [198], which has Firefly luciferase incorporated into the genome, and thus replication can be measured by luminescence. A strong luminescent signal represents strong replication of HCV, and vice versa. This suggests expression and excretion of IFN protein as early as 4 hours post electroporation, as depicted by the weak luminescent signal, which is not supported by the ELISA results. Although it is possible that this is a type III IFN specific effect.

We then went on to examine the activation of IFN signalling itself, which further upregulates the expression of ISGs. These ISGs include RIG-I itself, as well as many of the factors involved in signalling, thereby constituting an important positive feedback that might contribute to the observed signalling quite significantly. Further, negative feedback regulators may also be upregulated as a response to IFN signalling, dampening ISG expression. Darius Schweinoch and Lars Kaderali then set out to build a model that would incorporate these factors and thus intertwine the RIG-I mediated signalling cascade with the IFN mediated signalling cascade. To support this, we examined activation markers of IFN signalling.

IFN receptor signalling results in the phosphorylation of STAT1 and STAT2, allowing the STAT proteins to form homodimers (STAT1:STAT1) and heterotrimers (STAT1:STAT2:IRF9 – ISG3). STAT1 and STAT2 were examined in terms of their phosphorylation status over time following the activation of RIG-I. Interestingly, we saw a strong peak in the activation of STAT1 as early as 3 hours after RIG-I activation (figure 4.3.10 A), arguing for a strong early feedback response by IFN signalling on the dynamics of RIG-I signalling that we observe. Furthermore, this peak in the phosphorylation status of STAT1 is reduced from 3-6 hours, and stays reduced for up to 12 hours, where a much stronger level of phosphorylation is seen at 24 hours, peaking at 36 hours (data not shown). This phosphorylation is again reduced to background levels after 48 hours. To further investigate this early phosphorylation of STAT1, a finer time course (down to 5 min intervals) was applied within the first 4 hours of electroporation (figure 4.3.10 B).

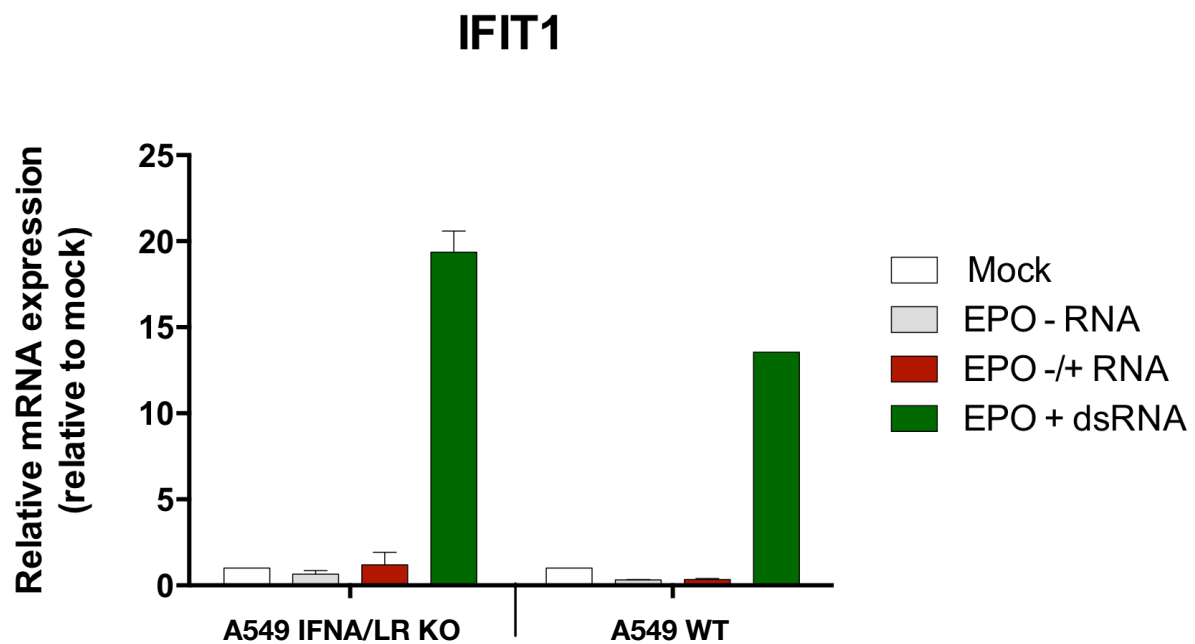
### Figure 4.3.10 STAT1 analysis



**Figure 4.3.10:** Quantitative and time-resolved analysis of STAT1 phosphorylation. A549 cells were electro-transfected with 2nM 400 bp dsRNA and lysed after the indicated time points, either **A**) short-term high-resolution, or **B**) over a longer time course of 48 hrs. Phosphorylation of STAT1 was assessed by phosphorylation-specific western blotting. Data are from a representative experiment out of 3 independent repetitions.

Strikingly, not only was there a strong phosphorylation of STAT1 between exactly 2 and 4 hours, which, according to the previous experiment shown in figure 4.3.10A, is not present after 6 hours, but furthermore, there was a slight phosphorylation of STAT1 seen between 10-20 mins after electroporation, which is extremely fast considering the previously shown dynamics of RIG-I/IFN signal transduction, indicating that there is another factor other than the RIG-I activation dependent production of IFN that is stimulating the phosphorylation of STAT1. To completely rule out that IFN is mediating this early activation on STAT1, supernatant from electro-transfected cells was immediately harvested (within 5 mins) and added on to freshly seeded A549 wildtype cells in addition to A549 IFN $\alpha/\lambda$  double receptor knock-out cells (A549 IFN $\alpha/\lambda$  LR KO cells) to examine their expression profile of IFIT1. It was seen that the supernatant induced expression of IFIT1 in both WT and A549 IFN $\alpha/\lambda$  LR KO cells, suggesting IFN is not the origin of this early STAT activation (Figure 4.3.11).

Figure 4.3.11 Electro-transfection controls



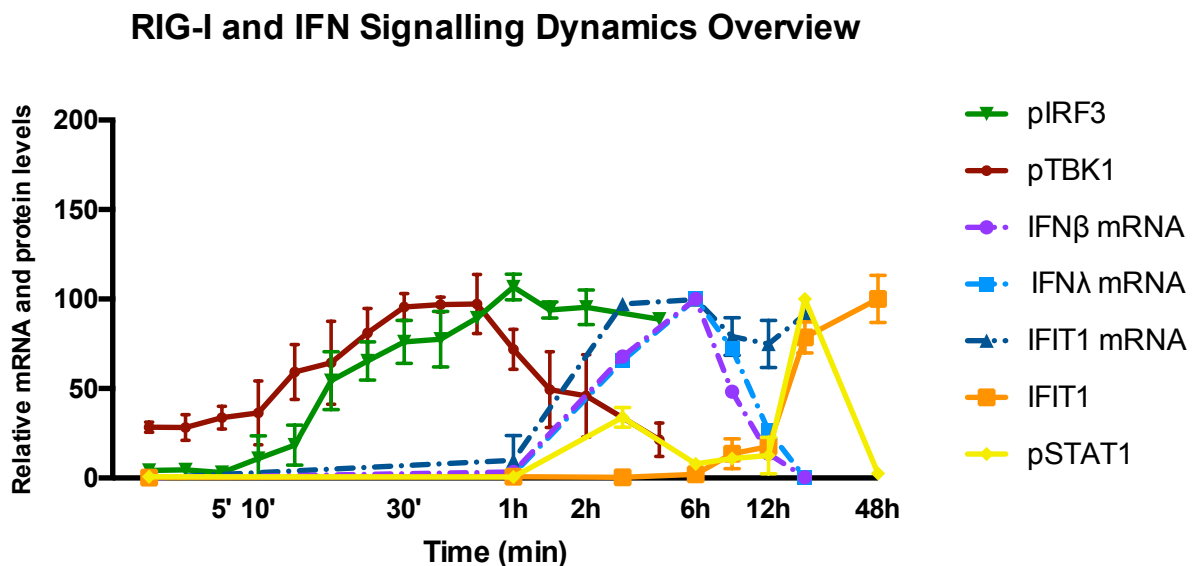
**Figure 4.3.11:** Control experiment for artefactual liberation of antiviral factors by electroporation of cells. A549 cells were electro-transfected either with 2nM 400 bp dsRNA as in the experiments before (EPO +RNA), or electro-transfected in the absence of RNA (EPO -RNA), electro-transfected in the absence of RNA with 2 nM 400 bp dsRNA supplemented immediately after electroporation (EPO +/- RNA) or left non-electro-transfected (mock). Cell supernatants were collected after 30 min and transferred to new A549 cells (A549 WT) or A540 IFNAR/IFNLR double-knockout cells (A549 IFNA/LR KO).

Upon further examination of this induction by supernatant that was immediately harvested from electro-transfected cells, it was determined that very specific factors were necessary to provide this activation ability. dsRNA must be present during the moment of electrical pulsing of the cells (EPO+RNA), if it is not present (EPO-RNA), or added after electrical pulsing of the cells (EPO-/+RNA), then no induction is seen. Furthermore, only freshly harvested supernatant (harvested within 5 mins) post electroporation has the ability to induce activation, supernatant that has been frozen and thawed loses this ability to induce activation (data not shown). Due to dsRNA being essential during the moment of electrical pulsing, in addition to the fact that freeze thawing of supernatant negates the induction ability, it is possible that the RNA is being endocytosed through other means in order to initiate RIG-I dependent signalling.



An overview of the RIG-/IFN signalling dynamics can be seen in figure 4.3.12. We can see from time point 0 min the flow of signalling the dynamics of specific factors and their activation over time, TBK1 becomes rapidly activated, between as early as 5-10 min, following this IRF3 becomes activated, starting at 10-15 min and peaking in its activation at around 60 min, activated IRF3 then mediates the transcription of ISGs such as IFIT1 (ISG56), IFN $\beta$ , and IFN $\lambda$ . Here we can see transcripts beginning to be detected almost simultaneously after about 60 min, and peaking in their expression after 6 hrs, where the IFN mRNA diverge from the ISGs, being depleted after 24 hours where as ISG56 continues to be transcribed. Translation of ISG56 can be detected as early as 6 hours and is rapidly translated between 12-24 hrs, with translation continuing for up to 48 hrs. IFN mediated signal transduction appears to be detected as early as 60 min, however this is diminished between 4-12 hrs, where STAT1 activation is strongest after 24 hrs.

**Figure 4.3.12 RIG-I dynamics overview**



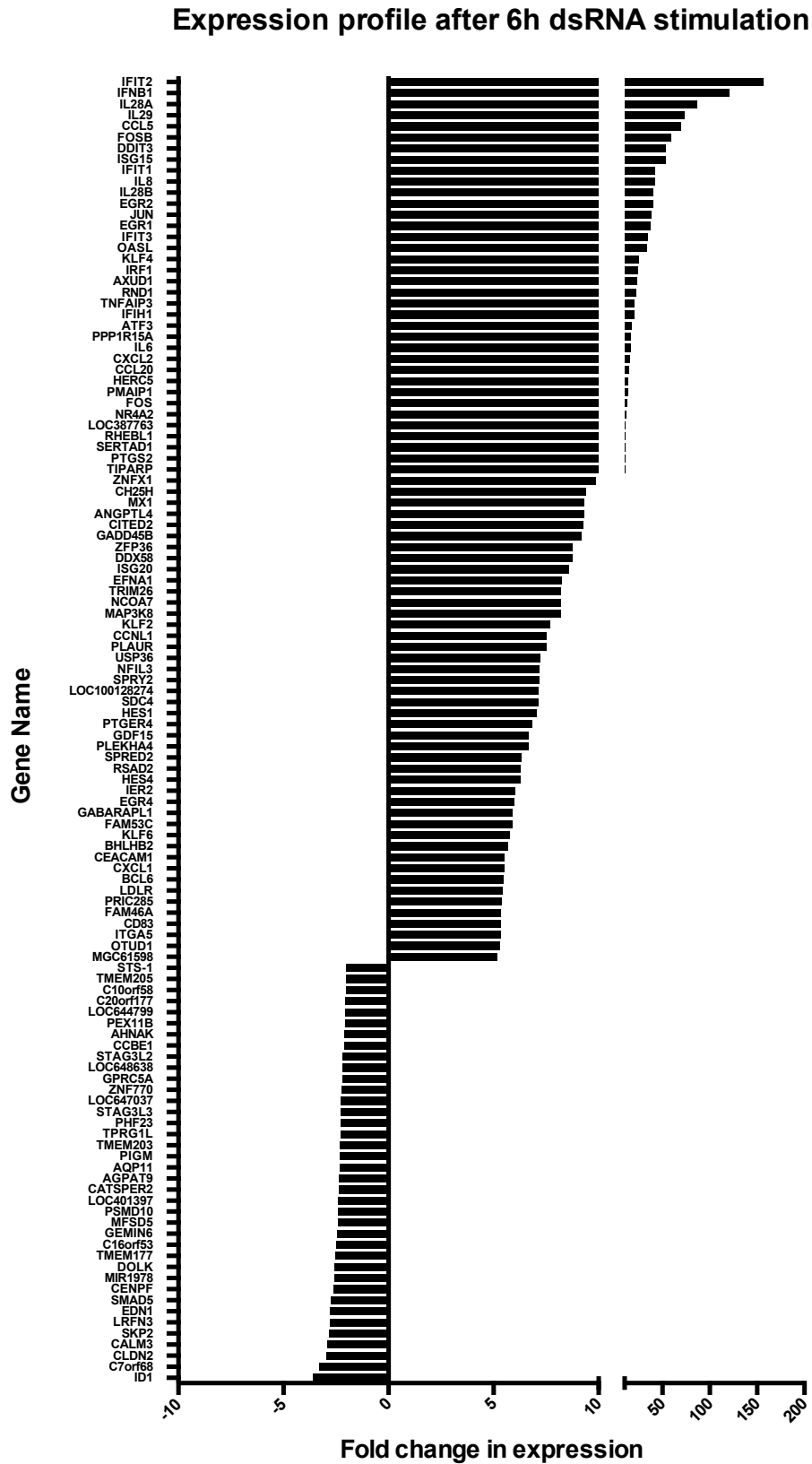
**Figure 4.3.12:** Compilation of time-course data for major signalling components. All values are normalized to the mean of their respective three most maximum values. Shown are mean  $\pm$  SD of three independent biological replicates ( $n=2$  for IFN $\beta$  and IFN $\lambda$  qRT-PCR).

In light of the synchronicity experiments for the quantification of the production of mRNAs measured from the moment cells activated, an opportunity presented itself; to examine the dynamics of ISG expression over time in wild type (WT) cells versus cells that did not express either IFNAR1 or IFNLR1 (IFNRKO), since we hypothesised that the ISGs induced by RIG-I/IRF3 might be different in their kinetics and dynamics compared to IFN/ISGF3. Furthermore, surprisingly little is known about ISGs that are specifically induced by IRF3, other than the IFNs and IFIT1. Thus, with IFNRKO cells we could determine which ISGs were dependent on which signalling cascade (RIG-I or IFN), and to what extent. Full time dependent transcriptome profiling upon synchronised RIG-I activation was carried out using WT cells and IFNRKO cells. Illumina humanHT-12 chips were used for the expression profiling and was carried out by the Genomics and Proteomics core facility of the DKFZ in Heidelberg, Germany.

This data-heavy analysis provided a significant and unique insight into antiviral signalling. Figure 4.3.13 A depicts the genes that were up or down regulated after 6 hours, using 0 hours as a normalisation control. The threshold for cut-off were 5 fold for upregulated genes and -3 fold for downregulated genes. Using a gene ontology tool powered by PANTHER ([www.pantherdb.org](http://www.pantherdb.org)), the genes that were upregulated by dsRNA stimulated RIG-I, were organised into gene ontologies (cellular function categories) based on their enrichment score defined by panther (figure 4.3.13 B). As we can see, the majority of genes upregulated by dsRNA stimulated RIG-I are specific for immune system responses against viral infection and regulation of these immune system responses (e.g. regulation of T<sub>H</sub>2 type responses, response to endogenous dsRNA, negative regulation of viral genome replication, negative regulation of type I IFN responses etc.). This validates the data set as a tool to compare the IFNRKO data set with the WT data set.

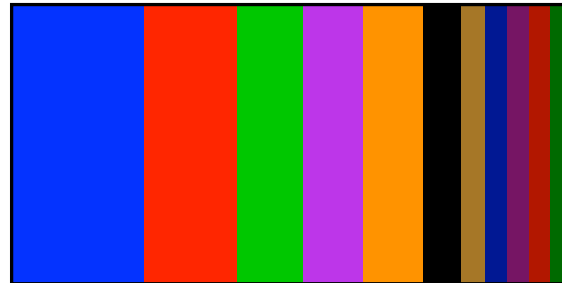
Figure 4.3.13 ISG expression after 6 hours

A



**B**

**Gene Ontology Analysis by PANTHER:  
Upregulated Cellular Processes by Enrichment Score  
6h post stimulation compared to 0H**



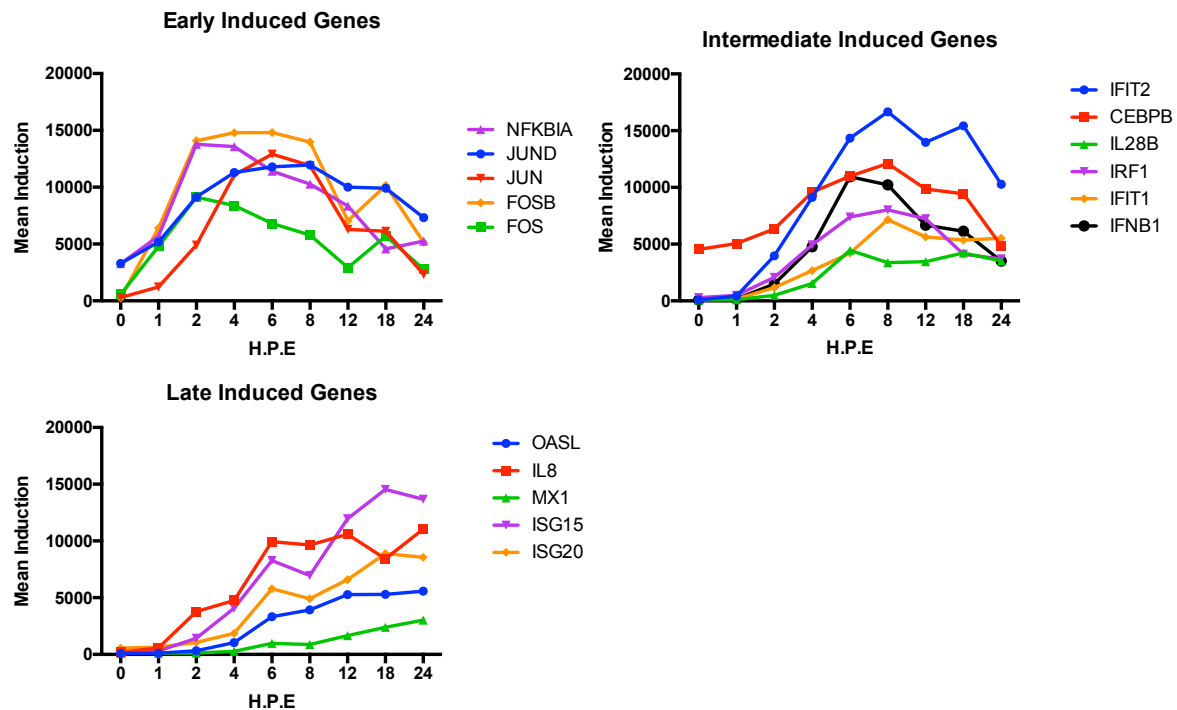
**Total Enrichment Score =421.73**

- regulation of T-helper 2 cell cytokine production (pval=3.6e-3)
- cellular response to endogenous dsRNA (pval=3.2e-4)
- regulation of type 2 immune response (pval=6.3e-5)
- negative regulation of viral genome replication (pval=5.3e-9)
- type I interferon signaling pathway (pval=1.6e-11)
- negative regulation of type I interferon production (pval=8.5e-4)
- cellular response to interleukin-1 (pval=1.0e-3)
- negative regulation of cytokine production (1.44e-10)
- regulation of cytokine biosynthetic process (pval=1.7e-3)
- regulation of transcription from RNA polymerase II promoter in response to stress (pval=2.0e-4)
- negative regulation of lymphocyte activation (pval=5.0e-4)

**Figure 4.3.13:** ISG expression analysis of transcriptome profiling upon electrotransfection of 2 nM 400 bp dsRNA. **A)** ISGs upregulated or downregulated 6 hours post-delivery of dsRNA in wild-type cells (normalised to 0 hr value). **B)** Gene Ontology analysis of the genes upregulated, designated by enrichment score via PANTHER.

We have compared the genes and categorically certain ISGs organised into “early” (within 4 hours) induced genes, “intermediate” (within 12 hours) induced genes, and “late” (within 24 hours) induced genes (figure 4.3.14).

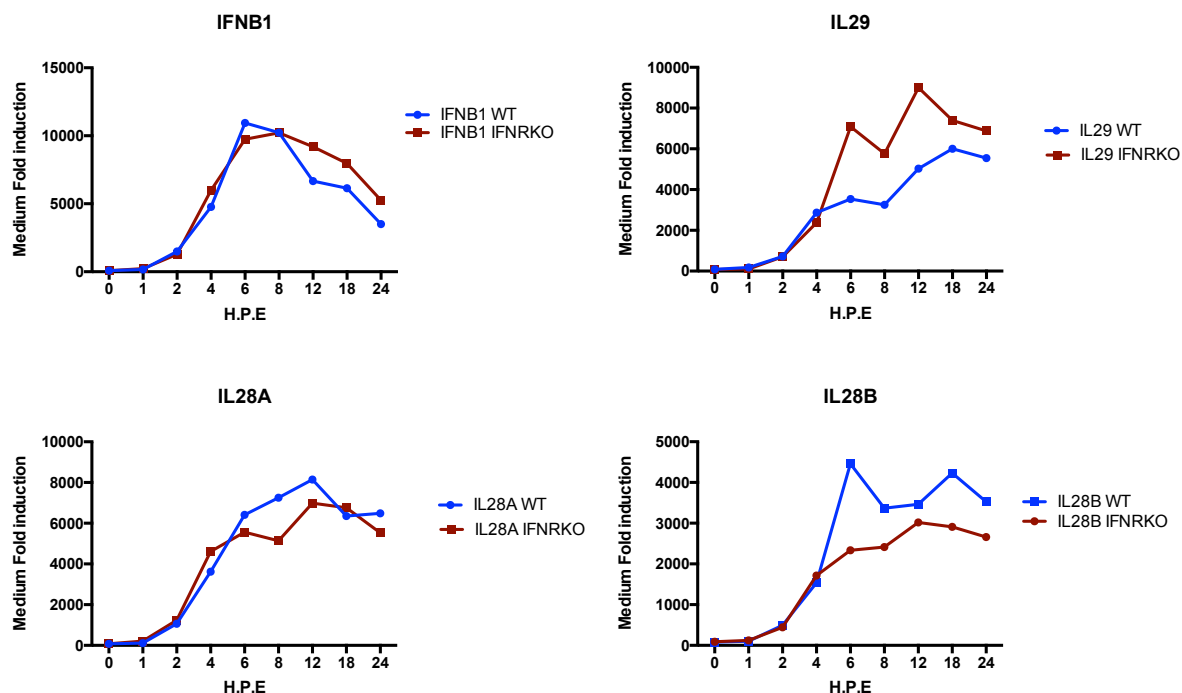
**Figure 4.3.14 Different phases of ISG induction**



**Figure 4.3.14:** ISG expression analysis of transcriptome profiling upon electrotransfection of 2 nM 400 bp dsRNA. ISGs upregulated at different phases of the antiviral response using WT cells only.

Further, we have compared the mean induction over time of the different IFN mRNAs induced in response to RIG-I signal transduction, and thus IRF3 transcription, compared to the IFNRKO cells which exclude IRF9 transcription (figure 4.3.14). Interestingly, there were contrasting results; IFNB1 and IL28A appeared to be largely unaffected by IFN mediated signal transduction, but the results for IL29 indicate that its expression is negatively regulated by IFN signalling, such that when you knock out the IFN receptors, IRF3 mediated transcription of IL29 is unhindered over time. The opposite is true for IL28B, where knocking out the IFN receptors results in a marked reduced expression of IL28B.

**Figure 4.3.15 Type I/III IFN expression**

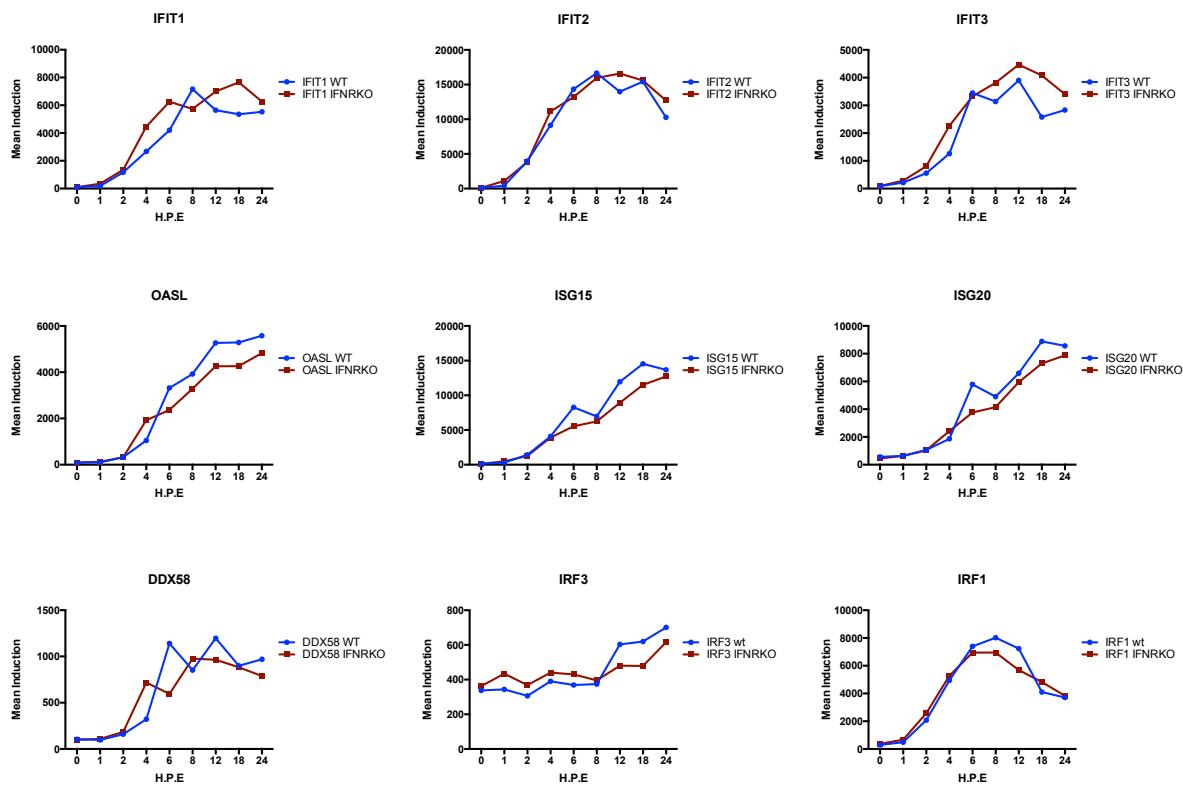


**Figure 4.3.15:** ISG expression analysis of transcriptome profiling upon electrotransfection of 2 nM 400 bp dsRNA. IFN mRNA upregulated upon dsRNA treatment in WT vs IFNA/LR KO cells.

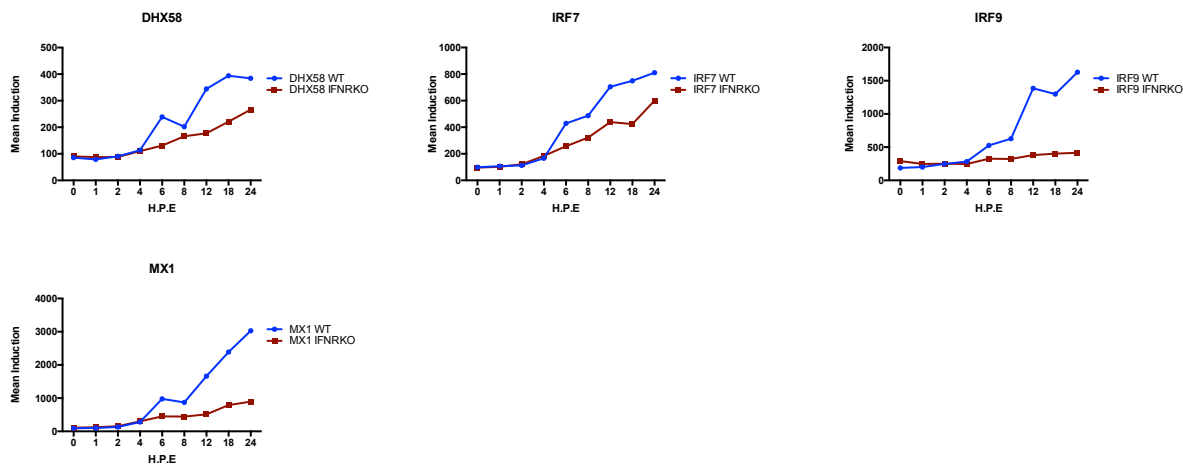
We then examined the profiles of different ISGs in response to RIG-I for both the WT and the IFNA/LR KO cells. As shown from the dynamics of each ISG that was upregulated in response to dsRNA, it can be seen that IRF3 and IRF1 have little dependency on IFN mediated signal transduction, whereas IRF7 was only slightly reduced in its expression over time in the IFNRKO cells, suggesting that that IRF7 is partially regulated by IFN mediated signal transduction. Unsurprisingly, IRF9 expression over time is drastically dependent on IFN mediated signal transduction, and is almost completely non-responsive to dsRNA stimulation in the IFNRKO cells. Astonishingly, the results indicate that many ISGs are not dependent on IFN signalling at all, and that IRF3 mediated expression of ISGs is sufficient. Of the ISGs IRF3, IRF1, IRF7, IRF9, IFIT1, IFIT2, IFIT3, MX1, ISG15, ISG20, DDX58, DHX58, and IFIH1, only MX1, IRF9 and to a certain extent, IRF7 and DHX58, appeared to be in any way effected by knocking out IFN mediated signal transduction (figure 4.3.16 A-B).

**Figure 4.3.16 ISG expression**

**A**



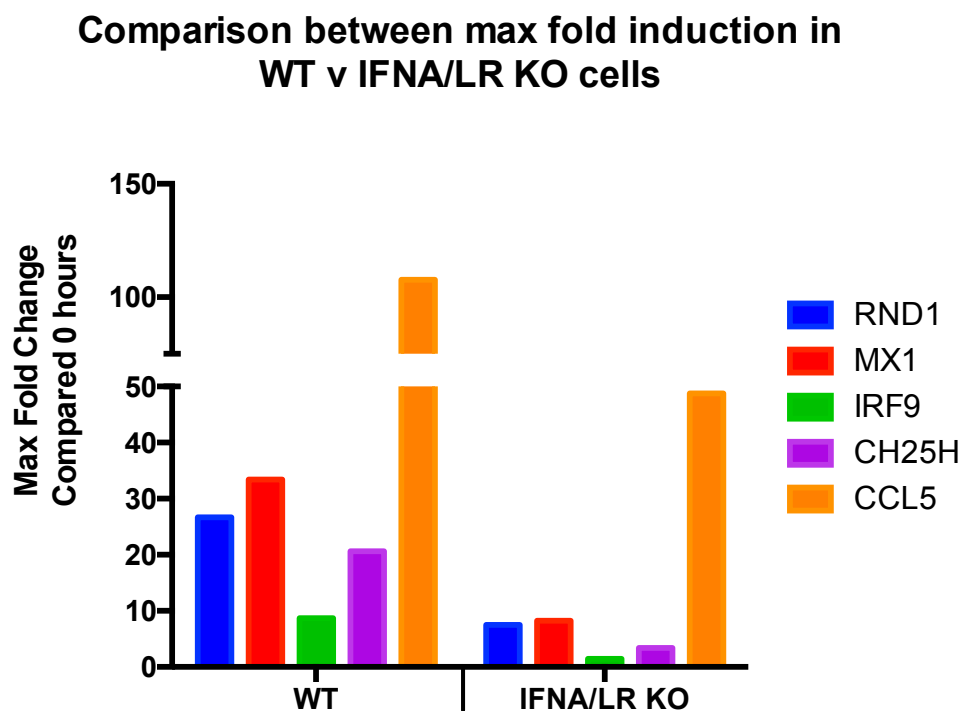
**B**



**Figure 4.3.16:** ISG expression analysis of transcriptome profiling upon electrotransfection of 2 nM 400 bp dsRNA. **A)** subset of ISGs upregulated upon dsRNA treatment in WT vs IFNA/LR KO cells, depicting no major dependence on IFN signalling. **B)** subset of ISG mRNA upregulated upon dsRNA treatment in WT vs IFNA/LR KO cells, depicting a dependence on IFN signalling.

With more in-depth analysis, it was found that only 5 genes were negatively regulated more than 3-fold when IFN signalling was knocked out (figure 4.3.17), RND1, MX1, IRF9, CH25H, CCL5. Interestingly, RND1, which appears to be specific to IFN signalling, has not yet been described as an ISG.

**Figure 4.3.17 IFN dependent ISGs**



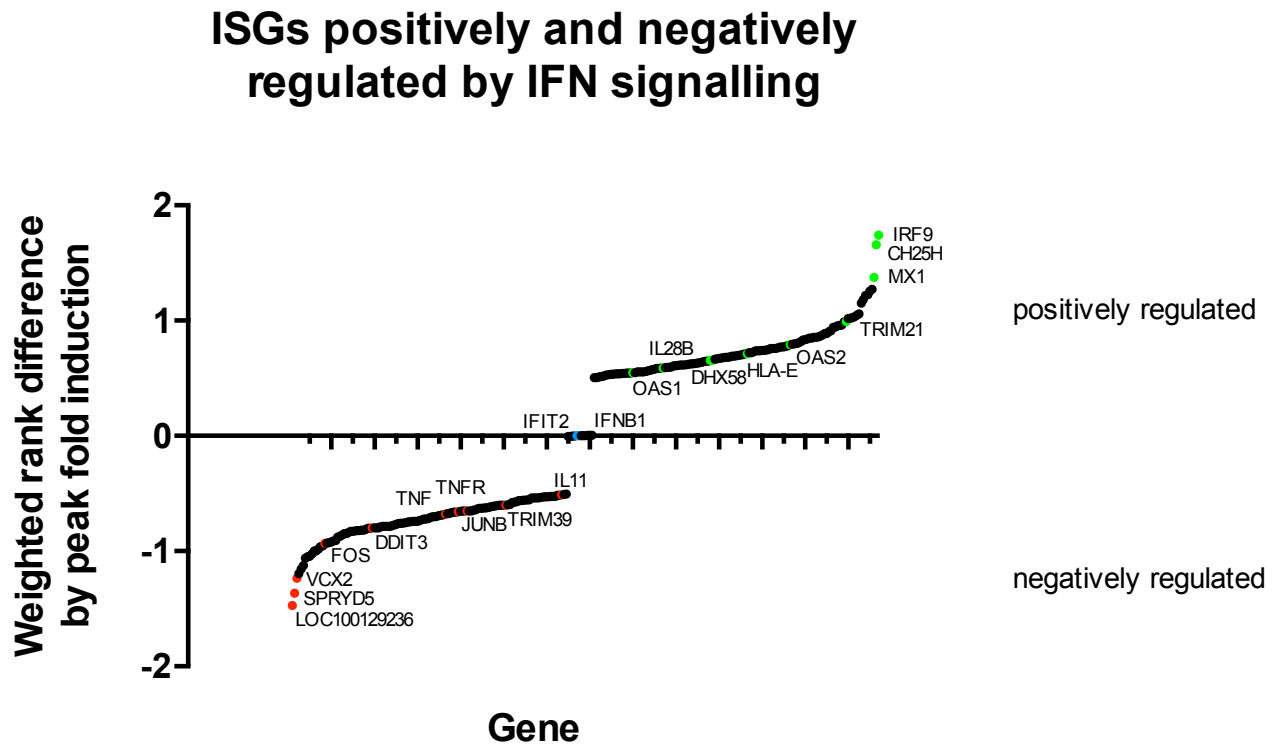
**Figure 4.3.17:** ISG expression analysis of transcriptome profiling upon electrotransfection of 2 nM 400 bp dsRNA, comparing the maximum fold change from the 0 hour value between WT cells and IFNA/LR KO cells with a limiting threshold of 3-fold.

Furthermore, with regard to extending the mathematical modelling and interlinking RIG-I signalling and its regulation by IFN signalling, we analysed the all the genes that up or down regulated depending on whether IFN signalling was present (figure 4.3.18 and table 27). This could be examined by weighting the “Rank” difference of the gene in terms of its fold induction compared to time point 0 hrs between both WT and



IFNA/LR KO cells. For example, IFIT2 is ranked as the one of most induced gene in both cell lines.

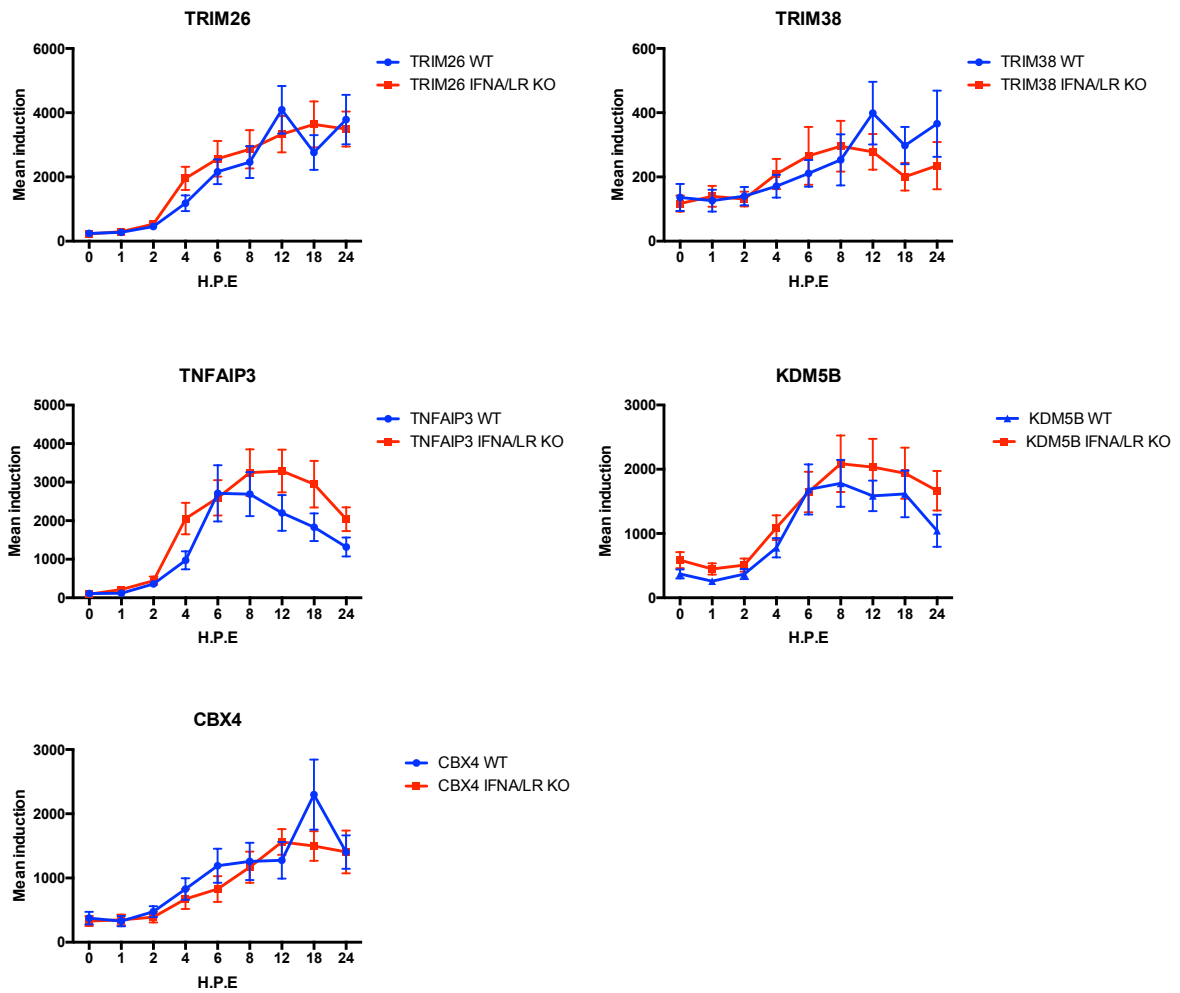
**Figure 4.3.18 IFN regulated ISG expression**



**Figure 4.3.17:** The maximum fold induction for each gene was examined in terms of the time point at which the peak was reached, this was then compared between both experimental replicates and both WT and IFNA/LR KO cells to determine the weighted rank difference in the presence or absence of IFN signalling, if there is a high weighted rank difference, as there is for IRF9, this indicates that the gene is positively regulated by IFN signalling, if it is low, it is negatively regulated by IFN signalling. Genes that are not regulated by IFN signalling have a weighted rank difference approaching 0 (for example IFIT2 and IFNB1).

Furthermore, we cross referenced the transcriptome profiling for the E3 ubiquitin ligase hits that were found to positively or negatively regulate RIG-I signalling, we found that five of our E3 ligase screen hits are in fact ISGs that induced upon RIG-I activation, two of which are not yet described as regulators of RIG-I mediated signal transduction, CBX4 and KDM5B, (figure 4.3.19)

**Figure 4.3.19** Transcriptome of siRNA screen based hits



**Figure 4.3.18:** Transcriptome analysis of the E3 ubiquitin ligase siRNA screen hits that are induced upon dsRNA stimulation of the RIG-I signalling network.

## 5.0 Discussion

To improve our understanding of the RIG-I signalling network we assessed a fully annotated list of E3 ubiquitin ligases to determine novel regulators of IRF3 and NF $\kappa$ B activation. We further characterised the kinetics of activation for canonical signalling proteins within the RIG-I signalling cascade using phospho-specific western blot quantifications of synchronised RIG-I activation. Furthermore, in order to achieve a comprehensive understanding of the transcriptional responses upon RIG-I stimulation, we have performed a time-resolved, full-genomic transcriptome analysis. To discriminate between direct IRF3 mediated transcription and secondary, IFNA/LR signalling mediated ISG transcription, we employed IFNAR/IFNLR double-knockout A549 cells in parallel to wildtype cells. To compliment this, we are carrying out a full proteome analysis in order to generate data on the expression of protein members involved in the regulation of the signalling cascade. Together, this will form the basis of a mathematical model that will act as a strong tool in elucidating the pathogenesis of viral infections that are either cleared by the innate antiviral response, or are successful in establishing an infection that leads to chronicity.

### 5.1 siRNA screen for E3 Ligases regulating RIG-I signalling

The importance of RIG-I mediated signal transduction regulation extends to many aspects of post-translational modifications. Phosphorylation had been the focus of characterising the dynamics of RIG-I signalling, however the importance of ubiquitination is not to be underestimated. Building on the work carried out by Li *et al.*, 2008.,[192] an E3-ligase screen was carried out using a state of the art read-out system based off of stable expression of fluorescently tagged IRF3 and NF $\kappa$ B (RelA) and transient knock down of target E3-ligase enzymes by siRNAs out lined in section . Despite being unsuccessful in our endeavours to generate a multi-spectral cell line encompassing the most important aspects of RIG-I, we were able to produce a top-quality cell line capable of yielding valuable data (Figure 4.1.3). Using a simple translocation determination approach (nuclear signal/no nuclear signal) we could

facilitate the discrimination between E3 ligases that are specific to either IRF3 activation or NF $\kappa$ B activation with respect to RIG-I signalling against a virus infection [120, 139, 192]. Furthermore, the screening approach (figure 4.1.4 A) was optimised in such a way that under normal conditions (non-targeting siRNA's) only ~70% activation efficiency could be achieved. This allows for the prospect of determining E3 ligases that positively or negatively regulate either IRF3 activation, or NF $\kappa$ B activation, or both. With the help from the groups of Dr. Erfle and Dr. Rohr from the Bioquant institute in Heidelberg, Germany, microscopy based imaging and processing yielded statistically significant hits when taking into account all siRNAs or individually significant hits relative to a single siRNA for both IRF3 and NF $\kappa$ B (figure 4.1.4 B). The chosen candidates for further validation are summarised in table 26, section 4.1.

Unfortunately, further validation could not be completed in time for publication of this thesis, however it is planned to carry out a second round of screening to validate the candidate hits using a high throughput luciferase based read-out. Each triplicate siRNAs will be tested in quadruplicate using cells that contain promoter genes specific to either IRF3 or NF $\kappa$ B that express firefly luciferase. These cells will be stimulated with 400 bp dsRNA, and based off of the luminescence signal strength for each candidate siRNA, we will determine whether the hits are valid or not. This will pave the way for future projects characterising the regulation of RIG-I signalling by the validated target E3 ligases.

Despite more work being required, we have identified interesting candidates regarding RIG-I regulation, and furthermore, with our transcriptome profiling, we are able to determine whether these candidates are in fact ISGs. We identified CBX4, KDM5B, TNFAIP3, TRIM26, and TRIM38, as ISGs induced upon dsRNA stimulated RIG-I. while TRIM26 and TRIM38 are known as regulators of innate immune responses (according GO analysis). CBX4 and KD5MB are yet to be characterised as factors involved in antiviral signalling, although KD5MB is described as a therapeutic target in HBV infections [199], and is known to regulate AP-2 [200] transcription factor activity, which in itself has not been implicated in innate antiviral responses. TNFAIP3 (also known as A20) is an interesting protein, as its homology analysis indicates it can act as an E3 ubiquitination enzyme and a deubiquitination enzyme, and has been described to affect TRAF2 and TRAF6, known pathway members of RIG-I signalling

[136, 190, 201]. Indeed, according to our screen, it acts as a negative regulator on RIG-I signalling, and, according to our transcriptome data, is an ISG that is itself slightly negatively regulated by IFN signalling (figure 4.3.19). Those that are not ISGs but are still of great interest include factors that are not yet reported to be involved in RIG-I signalling, for example PIAS1 and PIAS2, the different RNF proteins, and the different TRIM proteins, to name a few (table 26). These are novel findings which may contribute to our knowledge of RIG-I signalling regulation.

## **5.2 Measuring PPIs**

### *5.2.1 PCA*

Due to advancing technology, studying individual PPIs is becoming more and more common. Thus, using such technologies to examine the dynamics of signalling events within the RIG-I signalling pathway, or indeed any signalling pathway, was an exciting prospect. We initially wanted to develop a tool that could be used in to quantify the kinetics of interactions between proteins involved in the transduction of RIG-I signalling. To this end, several technologies were available for such an application. One option was to use fluorescence resonance energy transfer (FRET), which uses the excitation and emission of one fluorescent protein, who's emission compliments the activation of another fluorescent protein. Thus, protein interaction partners tagged with complimentary fluorescent proteins could be used to examine their proximity to one another based on the activation of one of the fluorescent proteins [202]. The extent of the interaction could thus be quantified by measuring the intensity of the specific fluorescent signal.

Another mechanism of using fluorescence to measure the interactions of proteins is bioluminescence resonance energy transfer (BRET), which applies the same principal as FRET, but rather than using fluorescence to activate the probe, bioluminescence is used instead. Typically, Renilla luciferase bioluminescence is used to activate a fluorescent protein such as YFP, which will be dependent on the addition of the substrate for Renilla luciferase, coelenterazine [203, 204]. Both of these

technologies have limiting factors, such as forming stable interactions and the overall size of the modification [205, 206]. An alternative technology, termed Protein Complementation Assay (PCA) served as an alternative for examining its potential as a method for measuring the dynamics of a signalling pathway [197]. By following the protocol outlined in the nature methods paper published in 2011 [196], we attempted to reproduce the technology and apply it to generating quantitative data in the context of RIG-I signalling dynamics. Firstly, a benchmark test was carried out in order to determine the extent of the differences of the application of PCA between the published data and our own data (figure 4.2.3). For the most part, the signal sensitivity was good in comparison to the published data, however for particular protein interaction partners, which are known to interact (for example IRAK2 and TRAF6), there was only background noise, despite the published data providing a strong positive signal for the interaction.

### *5.2.2 PCA suitability*

Given that other interactions were yielded a robust positive signal when tested, it was examined whether optimising the protocol may solve the lack of signal for positive interaction partners. Several parameters regarding PCA were tested; lysis method, different cell clones, substrate concentration, incubation timing, measuring windows, and substrate derivatives. However, the only parameter that had any impact on the sensitivity of the assay was increasing the input concentration of each DNA plasmid expressing the construct of interest. Using the optimised protocol, a panel of PPIs were tested for the extent of their positive interaction signal (figure 4.2.4 A). Unfortunately, 50% of the PPIs tested did not produce a positive interaction signal, suggesting a fundamental flaw in the use of PCA to measure PPIs. Therefore individual controls were analysed in detail (figure 4.2.4 B). The results depicted a single fragment of Gaussia linked to a protein of interest (MAVS) was generating a strong positive signal in terms of absolute light units measured. This suggested that MAVS, when linked to GLuc-N2 and transfected with the negative control Empty-GLuc-N1, was able to form PPIs with the free untagged portion of gaussia luciferase, and given the strong differences in absolute light units, this was not a negligible interaction, but a strong

binding of the untagged gaussia luciferase portion. This suggests that, somehow, GLuc-N1 is being localised to the membranes of mitochondria, where MAVS is expressed along with GLuc-N2. It was speculated that this may be in part due to increased hydrophobicity of the untagged GLuc-N1, since it is split, and only this specific half of gaussia luciferase produces the strong luminescence as seen in the MAVS:MAVS interaction. A more hydrophobic tertiary structure may form from this peptide and thus may arbitrarily localise to membranes within the cell.

Furthermore, When analysing MAVS:MAVS and MAVS:TRAF3 interactions in detail, it was seen that the sensitivity of the positive interaction signal was highly dependent on a specific point in time after input of the substrate, such that the measuring window may be drastically different between different protein interaction partners, and would thus have to be optimised for each individual PPI. For example, MAVS:MAVS interactions were most sensitively detected 14s after substrate addition, while MAVS:TRAF3 interactions were most sensitive detected ~2s after substrate addition (figure 4.2.5 A and B), making it difficult to make robust measurements of several interaction partners. Furthermore, it was unknown how efficient the expression of each plasmid was between experiments, requiring the need for measuring expression each protein of interest, as differential expression of proteins within the cell for a PPI may alter the signal acquired for the PPI. In addition to this drawback, a general problem with any transfection based method, such as PCA, is the artificial overexpression of the proteins of interest. It has been shown in many cases that expression levels of signalling proteins substantially influence the kinetics of signal transduction [207, 208]. For example, we know very well, that expression of MAVS or any of the downstream kinases lead to IRF3 activation even in the absence of an upstream stimulus (not shown). Therefore, the PCA system would represent artificial conditions and may very well not authentically represent the natural situation. Due to these drawbacks, we finally decided to halt our PCA efforts for measuring PPI dynamics in RIG-I signalling. However, the method still represents a potential tool for analysing *specific* PPIs. For example, it may be used as an artificial representation of an interaction (overexpression of proteins of interest) that may support or complement existing data for an unconfirmed PPI (e.g. co-immunoprecipitation of a protein).

## 5.3 RIG-I signalling

### 5.3.1 Quantitatively measuring RIG-I signalling

For the above outlined reasons, we decided to switch to an experimental system solely relying on the endogenous proteins levels. We opted to use quantitative western blotting using phospho-specific antibodies in order to measure the activation state of various signalling proteins within the RIG-I pathway. Phospho-specific western blots have been used in several studies to measure the activation of specific intermediate steps within a molecular network over time, including the RIG-I signalling network [77, 190]. Several intermediate steps of RIG-I signal transduction require the phosphorylation of proteins, including TBK1, I $\kappa$ K $\epsilon$ , I $\kappa$ K $\beta$ , I $\kappa$ B $\alpha$ , IRF3, and RelA (NF $\kappa$ B), which were chosen as targets for the phospho-specific western blots.

Other tools at our disposal was the dual-fluorescent cell line used to track the localisation and hence activation of IRF3 and NF $\kappa$ B. As shown in figure 4.2.1, these provided excellent tools to monitor time dependent downstream activation at a single cell level. However, also these cells rely on the over expression of tagged variants of IRF3 and NF $\kappa$ B and are therefore not necessarily faithful to the physiological situation. Quantitative time-resolved western blotting for phosphorylated proteins of interest was thus chosen as the basis for characterising the dynamics of RIG-I mediated signal transduction.

### 5.3.2 A question of stochasticity

In the grouped cell context, it has been suggested that intracellular molecular networks have a degree of variability between cells [209], and that signalling dynamics may be stochastic in nature, resulting in large cell-to-cell variations in gene expression activation. In the context of this study, the question of stochasticity is of particular importance regarding IFN expression, which has been described on several occasions to be a highly stochastic event [210-212]. Thus, our aim was to determine the stochasticity of RIG-I mediated signal transduction; is RIG-I activation stochastic? Are



there cell-cell variations in the kinetics of RIG-I signalling, and thus are there stochastic dynamics within the RIG-I signalling network between cells?

To provide answers for these questions, we reverted to a tool that was first described in 1982, the electrical transference of nucleic acid from a solution to inside cells, termed “electroporation” due to the biophysical effect it has on the membranes of cells (increasing the permeabilisation of cell membranes) [213]. It has since been used a core technique to deliver DNA and RNA into plant and animal cells [214-217]. The advantage of electro-transfection of dsRNA rather than liposome-transfection is that all cells are pulsed with the electrical current at the exact same time, whereas liposome-transfection relies spontaneous contact with cells adherent to a surface, requiring endocytosis in order for cytoplasmic delivery of the dsRNA to take place. This means that electrically pulsed cells will be delivered with dsRNA at a specific moment in time – a marked difference compared to liposome-transfection, where uptake of dsRNA-covered liposomes is a slow and asynchronous endocytic process. In fact, when we compared the two different modes of dsRNA delivery, we could demonstrate the effect of the staggered RIG-I activation in the liposome-transfected cells, which showed a substantially delayed and less strong activation of IRF3. In contrast, in electro-transfected cells IRF3 appeared to activated be much more rapidly and much stronger overall (figure 4.3.1).

To further confirm the advantages of electroporation over liposome-transfection, we investigated IRF3 activation dynamics on a single cell level, using our cell lines expressing eGFP-tagged IRF3. We could track the nuclear localisation of the transcription factor, and hence the activation of the antiviral response, over time and in single cells. The liposome-transfected samples were activated in the expected staggered fashion, with the first cells getting activated at later times and the percentage of activated cells increasing significantly slower and over a longer period of time. Intriguingly, the electro-transfected samples activated virtually simultaneously and at much earlier time points, removing cell-to-cell variability almost entirely. All cells that became activated, were activated within ~6 min of each other (figure 4.3.2). The electro-transfection of adherent cells expressing eGFP-IRF3 demonstrated that, if cells receive dsRNA at the same moment in time, the activation window for IRF3 to translocate is ~15-20 min. This is in contradiction to liposome-transfection, where cells

become activated over-time for hours, where the percentage of cells activated only increases marginally between the 15 min intervals of measuring.

This is in contradiction to liposome-transfection, where cells become activated over-time for hours, where the percentage of cells activated only increases marginally between the 15 min intervals of measuring. This supports the notion that electro-transfection of dsRNA results in a synchronised delivery system, and thus, synchronised activation of RIG-I. This is a marked advantage over liposome-transfection, as it is generally accepted that RNA and DNA is translocated via endosomal uptake, cytosolic release and in the case of DNA, nuclear entry [218-220]. This is a highly stochastic mechanism and is largely dominated by rare processes within the cell. For dsRNA, the limiting steps of release into the cytosol revolve around the endosomal uptake and lysis, and release from the lipoplexes [221]. In conclusion, the dynamics of RIG-I recognition of dsRNA in the case of liposome transfection is stochastic, but not due to signalling, rather it is due to the randomly endocytosed dsRNA by cells over time, and that this stochasticity is negated by the use of electro-transfection, which synchronises the uptake of dsRNA and ultimately synchronises the activation of RIG-I signalling between all the cells.

### *5.3.3 Characterisation of RIG-I signalling dynamics – progress and limitations*

#### *5.3.3.1 Progress*

While much is known about the RIG-I signalling cascade in terms of activation, PPIs, mechanisms, and downstream responses [123, 124, 222], it was postulated by Rand *et al* to be a stochastic “all or nothing” event, which differed from cell-cell [223]. Rand *et al* claimed that single cell intrinsic stochasticity is a prevalent feature of antiviral signalling and IFN $\beta$  expression, and that this stochasticity is subverted by the paracrine signalling events induced by IFN signalling. We generated data that directly contradicts that claim (see figures 4.3.2 and 4.3.3). Given that RIG-I signalling appears to be a pre-programmed response that does not differ in terms of kinetics from cell-cell, we sought to characterise the dynamics of RIG-I signalling kinetics in A549 cells, which are immune competent cells.

As described previously, quantitative-Western Blotting was used to successfully determine the activation kinetics of individual steps within the RIG-I signalling cascade. Using this tool, we analysed the kinetics of activation of TBK1, I $\kappa$ K $\epsilon$ , I $\kappa$ K $\beta$ , I $\kappa$ B $\alpha$ , IRF3, and NF $\kappa$ B (figure 4.3.3) under synchronised response conditions, which generated temporal activation profiles for each protein of interest.

Using the mean of four independent experimental replicates, quantitative activation dynamics were produced. As shown in figures 4.3.2 and 4.3.3, the speed of activation relative to the published data of the signalling pathway was quite striking, where some published data depict a peak in phosphorylation of TBK1 over 12 hours, whereas our data demonstrates the peak of activation can be reached as early as 40 min upon detection of dsRNA by RIG-I. It is known that the kinase enzymes responsible for transcription activation require phosphorylation in order to mediate their effector function [108-111], [137-139], TBK1, I $\kappa$ K $\epsilon$ , and I $\kappa$ K $\beta$ , appear to have very similar activation dynamics, with very early increase in phospho-levels after 5-10 min, and similar peak time of ~35-40 min. This is congruent with published data for TNF $\alpha$  signalling and NF $\kappa$ B activation, where Nelson *et al.*, 2001., described the kinetics of I $\kappa$ B $\alpha$  degradation and p65 translocation over time in response to 10ng/mL TNF $\alpha$  (also synchronised), depicting similar activation kinetics as we show [224]. In fact, the data published by Nelson *et al.* for I $\kappa$ B $\alpha$ / NF $\kappa$ B activation is almost identical to ours, thus supporting our kinetic data. Further, when comparing our data on pIRF3 to published data, very little is known about the kinetic potential of IRF3 activation. For example, it has been shown under viral infection assays that IRF3 is activated as early as 60 min [225], however our data provides evidence that this can and does occur much faster, as early as ~15 min.

For the signalling dynamics, we can see that IRF3 activation directly follows kinase activation, and that NF $\kappa$ B activation is directly proportional to the degradation of I $\kappa$ B $\alpha$ , which is directly followed by I $\kappa$ K $\beta$  activation. All of these events are in agreement with described sub-steps of the canonical signalling steps (described in detail in section 1.3.1). We now have a detailed kinetic characterisation of these sub-steps in the context of RIG-I signalling, which provides novel insight. For example, an interesting difference was found in terms of the kinetics of IRF3 and NF $\kappa$ B activation. The difference between the canonical pathway dynamics for IRF3 and NF $\kappa$ B lies in

the sustainment of activation, or lack thereof. IRF3 activation peaks at a similar time to NF $\kappa$ B, but the IRF3 activation peak profile is sustained for up to 4 hours – and phosphorylated IRF3 is detected for up to 6 hours (data not shown). NF $\kappa$ B on the other hand, once its peak is reached it is rapidly deactivated, reaching background levels after 4 hours. The fact that total protein levels of RelA did not change over this time course indicated that RelA is dephosphorylated rather degraded, returning to its inactive state (supported by data published by Nelson *et al* [224]), whereas IRF3 dephosphorylation might not take place or at a much slower rate. Data published by Long *et al.*, 2014., demonstrates that IRF3 deactivation occurs due to dephosphorylation by PP2A and RACK1, rather than degradation [226], suggesting that the deactivation of IRF3 and NF $\kappa$ B are differentially regulated, resulting in different deactivation kinetics. This requires further research to elucidate the origin of these differential dynamics. It is interesting to note here that expression of the gene NFKBIA, which encodes for the inhibitor I $\kappa$ B $\alpha$ , is one of the fastest and strongest expressed genes in response to synchronised RIG-I activation, ranking already 10<sup>th</sup> highest expressed gene at 0 hours, increasing 4-fold after only 2 hours, at which point it ranks as the 2<sup>nd</sup> highest expressed gene for up to 8 hours. To put this into perspective, the signal for NFKB1 gene expression is ~13-fold less than NFKBIA 2 hours post electroporation (appendix figure 8.1). Thus, it is possible that when including the major known positive and negative feedback regulators, based off our transcriptome data, into the mathematical model - we could describe the origin on the differential regulation of IRF3/NF $\kappa$ B post RIG-I activation.

Moreover, it has been described for a certain signalling pathways (MAPK and NF $\kappa$ B) that oscillations occur during their activation, such they oscillate between active and inactive. For example, it has been shown that in the MAPK signalling cascade in yeast sustains oscillations of the signalling network in absence of negative feedback regulators [227]. Furthermore, it has been suggested that positive feedback regulators are the origin of oscillations in activatory signals, and that NF $\kappa$ B benefits from positive feedback regulators by increasing its maximal nuclear translocation and prolonging its transcriptional activity [228]. With our fine-tuned temporal dynamics analysis, we show that oscillations in NF $\kappa$ B signalling by RIG-I stimulation does not occur, at least not under the same time dependency that has been described previously for NF $\kappa$ B

activation in BCR signalling, where a peak is shown within the first 60 min, but a second, less strong peak is shown after 120 min, which is not occurring under our experimental conditions [228]. However, it is important to note that different cell lines were used, where protein abundance may vary greatly and thus be may be one reason for the alternative kinetics.

To complement our data-heavy transcriptome profiling, which will be analysed in much greater detail, we are currently producing a proteome analysis, which will provide an even greater insight into the fate of the mRNAs that we have temporally characterised, and we will be able to determine the abundance of ISG proteins over time. Furthermore, with the proteome analysis completed, we will be able to determine the abundance of the canonical proteins within the RIG-I signalling network, as of right now we have only focused on the phosphorylation levels relative to steady state. This data will also be of great importance to the mathematical modelling, as we will be able to determine the abundance of known and putative feedback regulators. In addition, the E3 ubiquitin ligases found to affect RIG-I signalling to a substantial level may be validated as novel regulators of the RIG-I signalling network, with the proteome analysis, in conjunction with the transcriptome analysis, we could elucidate if they might serve as negative or positive feedback regulators, and whether they are induced upon RIG-I or IFN stimulation.

Further, Weber *et al.*, 2013., concluded that RIG-I binding to the 5'3P dsRNA of viral nucleocapsids enables RIG-I to initiate antiviral signalling at the earliest possible time point of infection, however under their infection assays they were only able to detect RIG-I oligomerisation after 2 hours of treatment with the virus [229]. It would be interesting to determine the kinetics of RIG-I oligomerisation under our synchronised approach, rather than measuring the average of RIG-I activation in cells that are infected as well as cells that are uninfected.

### 5.3.3.2 Limitations

The limitations of our data set include a lack of detailed information regarding specific steps in the signalling network. For example, due to technical limitations, our data on RIG-I signalling begins rather downstream of RIG-I activation - at the kinases. The

most important factors that are yet to be measured are RIG-I itself, and MAVS. Several attempts were made to develop a system, based on published data, that could measure RIG-I activation. One such method was based on phospho-specific Western Blots of RIG-I. As described in section 1.3.1.3, one of the activation markers for RIG-I is dephosphorylation at Serine 8 [75, 76]. An antibody specific to S8 was developed in-house in the group of Adolfo García-Sastre, which became commercially available, however, in our hands we could not get the antibody to provide a reliable phosphorylation signal, even in the positive control samples. One difference between the published data by Nistal-Villan *et al* on phospho-specific Western Blots of RIG-I [76] and our data, was that Nistal-Villan *et al* used purified (from bacteria and IFN treated A549 cells) RIG-I, which was used in much higher concentrations, whereas our sample detecting RIG-I were whole cell lysates.

Another form of detecting RIG-I activation was published in 2014 which involved the use of limited tryptic digestion [230], a tool that took advantage of the conformational rearrangements of RIG-I upon activation. Despite in some instances being able to detect the described pattern of cleavage products, the results were usually ambiguous and hard to reproduce (appendix figure 8.2).

We investigated yet another tool for its potential to measure RIG-I activation, which is known as fluorescence polarisation or fluorescence anisotropy, a tool based on the biophysical properties of a fluorescently labelled protein in a bound or unbound state [231]. To briefly explain, if a fluorescently tagged protein is unbound, it will have higher mobility (Brownian motion, tumbling), which can be detected based on the polarised excitation light. Once bound, the effective molecular weight of the protein of interest will increase, which directly affects its mobility. This can be measured using detectors of polarised emitted light. Given the oligomerisation potential of RIG-I, this would be an excellent tool to measure the rate of oligomerisation in real time. However, I was unsuccessful in measuring the polarisation using our Mithras2 LB 943 Multimode reader.

Finally, we tried using formaldehyde based cross-linking [232] in order to detect oligomerisation of RIG-I and MAVS in regular SDS-gel electrophoresis. This was more successful, reproducibly demonstrating time dependent oligomerisation of both RIG-I and MAVS in Sendai virus infection experiments (appendix figure 8.3). However, more

work will be necessary to fine tune this technique to our electroporation based RIG-I activation, in which we expect RIG-I to be activated within a few minutes, based on our observations of the kinases.

We have also demonstrated under a liposome-transfection approach that concentration and length of dsRNA used to stimulate cells has a noticeable effect on the number of cells activated and the speed at which they are activated (figure 4.2.1). Preliminary data (not shown) indicated that when comparing 400 bp dsRNA to 100 bp dsRNA, similar activation rates using liposome-transfection could be achieved if the concentration of the 100 bp sample set was increased 4-fold, such that four 100 bp strands will equal one 400 bp. Taken together, it is possible there is a degree of length dependency on the kinetics of activation, which requires further investigation.

#### *5.3.4 Analysing downstream signalling dynamics*

As stated previously, a comprehensive overview of RIG-I signalling dynamics was sought, thus RNA was analysed in order to determine mRNA production dynamics for particular ISGs by qPCR (IFIT1, IFN $\beta$ , and IFN $\lambda$ ). Interestingly, our results indicated that transcription of these genes was detected as early as 1 hour after delivery of dsRNA, and mRNA production peaked at 6 hours, where it began to decrease again. As described previously (figure 4.3.7) the mRNA expression dynamics of IFIT1 and the two IFNs are very similar for the first 9 hours, however it is at this point that the dynamics diverge. IFIT1, rather than continuing to decrease after 9 hours as IFN $\beta$  and IFN $\lambda$  do, begins to increase in its expression for up to 48 hours, while IFN $\beta$  and IFN $\lambda$  continue decreasing and return to background levels after 24 hours. Interestingly, when comparing the transcriptome data with the data obtained from qPCR, there were differences seen in the dynamics of IFN $\lambda$ . In qPCR, IFN $\lambda$  was measured as returning to background levels after 24 hours post RIG-I stimulation, however according to the transcriptome data, none of the 3 IFNs were reduced to background levels, indicating that different dynamics can be seen depending of the sensitivity of the assay used, more experiments are required with stringent controls in order to determine if the qPCR assay is less sensitive than the transcriptome assay. If the depletion of IFN

mRNA after 24 hours holds true, this suggests a regulatory switch from IRF3 mediated transcription to IFN signalling mediated transcription (ISGF3) IFIT1 production [152].

We compared our qPCR data to our transcriptome data, and on a technical level, both in qPCR and the transcriptome analysis, the fold change in ISGs differed between replicates, while the dynamics did not. This was more evident in the qPCR data than the transcriptome data however, and thus may be an artefact of the assay. Another possibility is that A549 cells themselves may have been sensitised for expression based on growing conditions, which has been suggested to effect gene expression [233]. More stringently controlled experiments are necessary to define the origin of the variation.

Regarding the transcriptome data, we were able to define ISG production based on the phase of their kinetics (early, intermediate, late), we found that of the early kinetics for ISGs, Jun and Fos RNAs were detected. Jun and Fos form a transcription factor known as AP-1 (figure 4.3.14), which has been implicated in many processes including viral infection, apoptosis, stress, etc. [234, 235]. We are further going to test if Jun/Fos factors act as rapid ISGs in response to virus detection by RIG-I, which would be a novel finding, or if they are simply strongly induced due to stress of the cell.

An important aspect of the transcriptome data is the ability to compare IRF3 dependent ISG transcription and ISGF3 dependent transcription. Surprisingly, when individual ISG dynamics were analysed, comparing WT to IFNA/LR KO cells, only very few genes appeared to be effected in terms of knocking out IFN signalling – suggesting that IFN signalling is largely unnecessary to reach an antiviral state, and that IRF3 activation is the all that is required factor in terms of ISG production and antiviral activity (figure 4.3.16). Of the classical ISGs, only MX1 and IRF9 gene expression appeared to be dominated by IFN signalling, as their expression was significantly higher when IFN signalling was present. Only a few other genes were shown to be dependent on IFN signalling, RND1 was an interesting hit, as it is yet to be described as an ISG. Other genes that were strongly dependent on IFN signalling included CH25H and CCL5 (figure 4.3.17). Moreover, we were able to determine the genes that were differentially expressed when IFN signalling was knocked out, which can be found in figure 4.3.18 and appendix table 27.



Further analysis with knock down/knock out studies will determine whether RND1 is an important feedback regulator of RIG-I signalling. Interestingly, IRF7 and DHX59 appeared to be only partially negatively regulated by knocking out IFN signalling, suggesting a dual role for IRF3 and IFN signalling mediated transcription in this respect. Another noteworthy difference was the expression of IL29 and IL28B (IFN  $\lambda$ 1 and IFN  $\lambda$ 3), which was either upregulated (IL29) when IFN signalling was knocked out or downregulated (IL28B). It is likely that feedback regulators are induced upon type I or type III IFNR activation, which then positively/negatively impact the production of type III IFNs.

For the most part however, the ISGs IFIT1/2/3, ISG15, ISG20, IFIH1, DDX58, IRF1, IRF3, IFNB1, and IL29A, were unaffected or only very weakly affected by knocking out IFN signalling. This is somewhat against the dogma of innate antiviral immunity, which is that IFN signalling is required to reach an antiviral state within the cell. The striking aspect of the transcriptome analysis, which has so far been unknown, is that IRF3 can induce nearly all the ISGs that the STAT1/STAT2/IRF9 can.

### *5.3.5 Interferon signalling*

With our development of insights into RIG-I signalling and ISG expression, the next stage in our campaign to characterise RIG-I mediated antiviral signalling was to examine protein production and IFN signal transduction. While much is known about IFN signalling [152, 156, 236], little progress has been made on the temporal interplay between RIG-I signalling and IFN signalling. We sought to address the kinetics of translation of mRNA and the initiation of IFN mediated signal transduction, leading to ISGF3 activation. We first looked at IFIT1 protein expression as a proxy for translation of ISGs upon recognition of dsRNA (figure 4.3.8). Using Western Blotting, IFIT1 protein was quantified in its expression over the course of 48 hours under the same electroporation protocols as used in all previous experiments. Unexpectedly, IFIT1 protein was only detected as early 6 hours, despite mRNA expression being detected as early as 1 hour. This is in contrast to RIG-I - encoded by the gene DDX58, RIG-I protein increases as early as 4 hours post electroporation (data not shown). Since its gene expression kinetics are relatively similar to IFIT1 in the earlier time points (0-6

hrs), this indicates differential ISG translation dynamics, although this may be due to the sensitivity of the tools at hand, which further highlight the importance of the proteome data that is being generated, which will greatly complement our signalling dynamics data.

Secreted IFN $\beta$  was measured in supernatants by ELISA over time. It must be noted that due to a very unreliable lot of ELISA plates, the data is of mediocre quality and also only representative of a single experiment. By this assay, IFN $\beta$  protein could be detected in the supernatant of A549 cells only from 8 hours after electroporation on, which was surprisingly late given the rapid dynamics of other ISGs such as IFIT1 and RIG-I. To corroborate this data, supernatants were also subjected to a bio-assay highly sensitive to interferons and antiviral cytokines. The bio-assay was based on LucUbiNeo-ET cells, which stably replicate subgenomic HCV luciferase-reporter genomes that can be measured readily by luminometry (figure 4.3.9) [198, 237]. Thus, the supernatant containing IFN ( $\beta/\lambda$ ) will negatively affect the production of luciferase in the LucUbiNeo-ET cells [58]. The supernatant of cells 4 hours post electrotransfection completely abolished luciferase expression, indicating the presence of significant levels of antiviral cytokines, most likely IFN $\beta$  or IFN $\lambda$ , or both. Without further experimental work, it is unclear whether the ELISA data for IFN $\beta$  is truly reflective of its expression dynamics, thus indicating that the early perturbation of the HCV replicon after 4 hours is solely due to IFN $\lambda$  or whether the ELISA is not sensitive enough to detect IFN $\beta$  at such an early time point – this is the most likely reason, as there was a very strong background in the ELISA. Indeed, published data indicates that IFN mRNA can be rapidly produced as early as 1-2 hours [225], and protein can be detected as early as 4 hours [77].

As described in section 1.4, one of the read-outs for active IFN signalling is the phosphorylation of the STAT proteins, namely STAT1 and STAT2 [152, 236]. In order to quantify effective IFN signalling over time, we measured the phosphorylation of STAT1. Interestingly, STAT1 phosphorylation was highly dynamic, exhibiting various peaks and falls of various strengths (figure 4.3.10). The first strong activation of STAT1 was observed already between 2 and 4 hours, which was well in line with the finding of 4h supernatants to contain substantial amounts of IFN. This activation was diminished at around 6 hours, possibly indicating the kicking-in of negative feedback

regulators such as SOCS, PIAS or USP18. In fact, according to our transcriptome data analysis, USP18 is upregulated 2.57-fold after 6 hours. SOCS1 is not upregulated after induction of RIG-I signalling, and neither is PIAS1-4, however, SOCS3 is induced as at 4 hours post induction is 3.79-fold increased. Moreover, the signal for PIAS1 expression and PIAS4 expression is relatively high at 0 hours, despite not being induced (~5-fold higher than PIAS2/3).

Even with this very early STAT1 phosphorylation, the activation at 2-4 hours, and deactivation at 6 hours, it is somewhat surprising to see an activation of STAT1 after ~20 min, which suggests that pSTAT1 activation at this time may be due to some factor other than IFN. In fact, it has been described previously that I $\kappa$ K $\epsilon$  plays a role in STAT phosphorylation [238].

We were also able to show that very early IFN release was not the origin of this activation of STAT at 20 min post electroporation using indirect bioassays. As depicted in figure 4.3.11, the supernatant from the negative controls were unable to induce any IFN signalling, suggesting that IFN is not the cause of the early STAT activation. Interestingly, there was a specific signal in both WT and IFNA/LR KO cells from supernatant of dsRNA stimulated cells for IFIT1 mRNA indicating that the supernatant (harvested 30 min after electro-transfection) was specifically able to induce a signalling pathway that leads to the expression of IFIT1. dsRNA may still be present in the supernatant, as the cells are not washed after electroporation, thus, it is possible that remaining dsRNA is taken up into the cell at a later time where it is detected by RIG-I. Further, this phenomenon appears to be highly specific to dsRNA electroporation conditions, which is a compelling point regarding a dsRNA mediated post electroporation-activation artefact of the experimental design.

Nonetheless, the pSTAT1 was measured and quantified using the same technique applied to the RIG-I signalling dynamics, thus completing the antiviral signalling events within cells that detect dsRNA: RIG-I mediated signal transduction, transcription factor activation, ISG expression, ISG protein production, IFN signalling, and IRF3/ISGF3 dependent transcription of ISGs. A depiction of the flow of these events using a synchronised system shows the individual sub-steps as they happen over time (figure 4.3.12); our system removes any stochasticity that may arise due to random time dependent endocytosis events, synchronises RIG-I activation,

synchronises signalling responses leading to transcription factor activation, and allows us to measure mRNA and protein production in a highly discriminatory manner (such as comparing early induced ISGs versus late induced ISGs). With our experimental approach, we have followed each “checkpoint” regarding the progression to an antiviral state within the cells in a time dependent quantitative manner.

## 5.4 Modelling

The consistent signalling profiles of our target proteins during RIG-I mediated signal transduction across approximately  $1.2 \times 10^7$  cells per experiment suggests a pre-programmed linear response system that does not deviate in terms of kinetics or dynamics, and that RIG-I mediated signal transduction is not stochastic. This linear, non-deviating dynamics profile for RIG-I signalling may be dependent certain limiting factors, such as cell cycle, abundance of proteins, or availability of substrate within the cell, which will be discussed later. The implications of these results indicate that, given the specific conditions of A549 cells, the RIG-I signalling pathway and thus antiviral innate immunity has a degree of predictability.

These activation profiles for RIG-I signalling provide an excellent opportunity for mathematical modelling. In the past, many cellular regulatory networks have been described using sets of ordinary differential equations (ODE's) [227, 239-242]. Modelling of cellular networks endeavours to describe a molecular network in as much detail as necessary without being over complicated, such that simulations are feasible. While Boolean network models allow for the investigation of much larger networks due to the simple reduction of the values to a binary 'on or off' phenotype [243], ODEs can be used to describe more complex processes, however are much more limited in terms of the scale of the system they can describe [244]. For RIG-I signalling, as shown in the scheme in figure 4.3.5 A, ODEs to build a biochemical model, which describe the reaction rate for the change of one species to another, for example  $S_1$  will be TBK1, and  $S_2$  will be phospho-TBK1, where  $R_1$  will describe the rate of change from  $S_1 \Rightarrow S_2$ . Given that our data suggests the signalling dynamics are not stochastic, deterministic reaction kinetics were used in the model, where reaction rates are proportional to the product of concentrations of the reactant molecules involved. ODEs

used to describe the rate of change of species within the RIG-I signalling cascade were determined by Darius Schweinoch in the group of Lars Kaderali, University of Greifswald. In order for ODEs to best describe change of species within the RIG-network, different rate constants were tested to determine if the model could closely simulate the experimental results (parameter fitting). The combination of parameters used that best describes the experimental data can be seen in figure 4.3.6.

For the few E3 ubiquitin ligases that we found to be transcriptionally induced upon RIG-I stimulation, in addition to the proteomic data intertwined with the transcriptome data, the next steps would be to knock down/out specific regulators of RIG-I signalling network and then assess the strength and duration of the antiviral signal. This could then further be included in the model to enrich it with even more feedback loops, which will eventually make it very robust and enhance its predictive power. With such a powerful model, it will become possible to *in silico* simulate the arms-race between an infecting virus and the host antiviral response – who would win? Will the invading virus establish a successful infection, or will the antiviral response overwhelm the virus first? Putting these two antagonistic processes together in a meaningful model will finally permit examination of the crucial determinants that ultimately decide if a virus can successfully infect a host or if it is likely to be well-controlled by the immune response. Particularly interesting will be the studying of persistent viruses, such as HCV or certain strains of LCMV, that are known to induce innate and adaptive antiviral immunity, but evolved mechanisms to undermine the innate antiviral responses such that they can coexist (virus and immune response). Understanding this will bridge the gap in our knowledge on how to break persistence through therapeutic means.

## 6.0 References

1. Kawamoto, H. and N. Minato, *Myeloid cells*. Int J Biochem Cell Biol, 2004. **36**(8): p. 1374-9.
2. Roy, C.R., *Immunology: professional secrets*. Nature, 2003. **425**(6956): p. 351-2.
3. Joffre, O.P., et al., *Cross-presentation by dendritic cells*. Nat Rev Immunol, 2012. **12**(8): p. 557-69.
4. Mildner, A. and S. Jung, *Development and function of dendritic cell subsets*. Immunity, 2014. **40**(5): p. 642-56.
5. Burnet, F.M., *A modification of Jerne's theory of antibody production using the concept of clonal selection*. Aust. J. Sci, 1957. **20**: p. 67-69.
6. Jung, S., *In Vivo Depletion of CD11c Dendritic Cells Abrogates Priming of CD8 T Cells by Exogenous Cell-Associated Antigens*. Immunity, 2002. **17**: p. 211-220.
7. Kovacsovics-Bankowski, M. and K.L. Rock, *A phagosome-to-cytosol pathway for exogenous antigens presented on MHC class I molecules*. Science, 1995. **267**(5195): p. 243-6.
8. Katsura, Y., *Redefinition of lymphoid progenitors*. Nat Rev Immunol, 2002. **2**(2): p. 127-32.
9. Maillard, I., T. Fang, and W.S. Pear, *Regulation of lymphoid development, differentiation, and function by the Notch pathway*. Annu Rev Immunol, 2005. **23**: p. 945-74.
10. Galy, A., et al., *Human T, B, natural killer, and dendritic cells arise from a common bone marrow progenitor cell subset*. Immunity, 1995. **3**(4): p. 459-73.
11. Blom, B. and H. Spits, *Development of human lymphoid cells*. Annu Rev Immunol, 2006. **24**: p. 287-320.
12. Zook, E.C. and B.L. Kee, *Development of innate lymphoid cells*. Nat Immunol, 2016. **17**(7): p. 775-82.
13. Zhang, J.A., et al., *Dynamic transformations of genome-wide epigenetic marking and transcriptional control establish T cell identity*. Cell, 2012. **149**(2): p. 467-82.
14. Yui, M.A. and E.V. Rothenberg, *Developmental gene networks: a triathlon on the course to T cell identity*. Nat Rev Immunol, 2014. **14**(8): p. 529-45.
15. Mingueneau, M., et al., *The transcriptional landscape of alphabeta T cell differentiation*. Nat Immunol, 2013. **14**(6): p. 619-32.
16. Russ, B.E., et al., *T cell immunity as a tool for studying epigenetic regulation of cellular differentiation*. Front Genet, 2013. **4**: p. 218.
17. Pennock, N.D., et al., *T cell responses: naive to memory and everything in between*. Adv Physiol Educ, 2013. **37**(4): p. 273-83.
18. Jain, A. and C. Pasare, *Innate Control of Adaptive Immunity: Beyond the Three-Signal Paradigm*. J Immunol, 2017. **198**(10): p. 3791-3800.
19. Lanzavecchia, A., *Pillars article: Antigen-specific interaction between T and B cells*. 1985. J Immunol, 2007. **179**(11): p. 7206-8.
20. Treanor, B., *B-cell receptor: from resting state to activate*. Immunology, 2012. **136**(1): p. 21-7.

21. Harwood, N.E. and F.D. Batista, *New insights into the early molecular events underlying B cell activation*. *Immunity*, 2008. **28**(5): p. 609-19.
22. DeFranco, A.L., *The complexity of signaling pathways activated by the BCR*. *Curr Opin Immunol*, 1997. **9**(3): p. 296-308.
23. Martin, P. and J. Moscat, *Th1/Th2 Differentiation and B Cell Function by the Atypical PKCs and Their Regulators*. *Front Immunol*, 2012. **3**: p. 241.
24. Ricci, S., et al., *OL-EDA-ID Syndrome: a Novel Hypomorphic NEMO Mutation Associated with a Severe Clinical Presentation and Transient HLH*. *J Clin Immunol*, 2017. **37**(1): p. 7-11.
25. Notarangelo, L.D., et al., *Primary immunodeficiencies: 2009 update*. *J Allergy Clin Immunol*, 2009. **124**(6): p. 1161-78.
26. Lim, H.K., et al., *TLR3 deficiency in herpes simplex encephalitis: high allelic heterogeneity and recurrence risk*. *Neurology*, 2014. **83**(21): p. 1888-97.
27. Alexopoulou, L., et al., *Recognition of double-stranded RNA and activation of NF-kappaB by Toll-like receptor 3*. *Nature*, 2001. **413**(6857): p. 732-8.
28. Seth, R.B., L. Sun, and Z.J. Chen, *Antiviral innate immunity pathways*. *Cell Res*, 2006. **16**(2): p. 141-7.
29. Jensen, S. and A.R. Thomsen, *Sensing of RNA viruses: a review of innate immune receptors involved in recognizing RNA virus invasion*. *J Virol*, 2012. **86**(6): p. 2900-10.
30. O'Neill, L.A., D. Golenbock, and A.G. Bowie, *The history of Toll-like receptors - redefining innate immunity*. *Nat Rev Immunol*, 2013. **13**(6): p. 453-60.
31. Bowie, A.G. and L. Unterholzner, *Viral evasion and subversion of pattern-recognition receptor signalling*. *Nat Rev Immunol*, 2008. **8**(12): p. 911-22.
32. Akira, S., S. Uematsu, and O. Takeuchi, *Pathogen recognition and innate immunity*. *Cell*, 2006. **124**(4): p. 783-801.
33. Rallabhandi, P., et al., *Respiratory syncytial virus fusion protein-induced toll-like receptor 4 (TLR4) signaling is inhibited by the TLR4 antagonists Rhodobacter sphaeroides lipopolysaccharide and eritoran (E5564) and requires direct interaction with MD-2*. *MBio*, 2012. **3**(4).
34. Rawling, D.C. and A.M. Pyle, *Parts, assembly and operation of the RIG-I family of motors*. *Curr Opin Struct Biol*, 2014. **25**: p. 25-33.
35. Luo, D., et al., *Visualizing the determinants of viral RNA recognition by innate immune sensor RIG-I*. *Structure*, 2012. **20**(11): p. 1983-8.
36. Yoneyama, M., et al., *The RNA helicase RIG-I has an essential function in double-stranded RNA-induced innate antiviral responses*. *Nat Immunol*, 2004. **5**(7): p. 730-7.
37. Civril, F., et al., *The RIG-I ATPase domain structure reveals insights into ATP-dependent antiviral signalling*. *EMBO Rep*, 2011. **12**(11): p. 1127-34.
38. Cui, S., et al., *The C-terminal regulatory domain is the RNA 5'-triphosphate sensor of RIG-I*. *Mol Cell*, 2008. **29**(2): p. 169-79.
39. Myong, S., et al., *Cytosolic viral sensor RIG-I is a 5'-triphosphate-dependent translocase on double-stranded RNA*. *Science*, 2009. **323**(5917): p. 1070-4.
40. Yoneyama, M. and T. Fujita, *RNA recognition and signal transduction by RIG-I-like receptors*. *Immunol Rev*, 2009. **227**(1): p. 54-65.
41. Luo, D., et al., *Structural insights into RNA recognition by RIG-I*. *Cell*, 2011. **147**(2): p. 409-22.
42. Wang, Y., et al., *Structural and functional insights into 5'-ppp RNA pattern recognition by the innate immune receptor RIG-I*. *Nat Struct Mol Biol*, 2010. **17**(7): p. 781-7.

43. Ramanathan, A., et al., *The autoinhibitory CARD2-Hel2i Interface of RIG-I governs RNA selection*. Nucleic Acids Res, 2016. **44**(2): p. 896-909.
44. Wu, B., et al., *Structural basis for dsRNA recognition, filament formation, and antiviral signal activation by MDA5*. Cell, 2013. **152**(1-2): p. 276-89.
45. Binder, M., et al., *Molecular mechanism of signal perception and integration by the innate immune sensor retinoic acid-inducible gene-I (RIG-I)*. J Biol Chem, 2011. **286**(31): p. 27278-87.
46. Wu, B., et al., *Molecular imprinting as a signal-activation mechanism of the viral RNA sensor RIG-I*. Mol Cell, 2014. **55**(4): p. 511-23.
47. Zeng, W., et al., *Reconstitution of the RIG-I pathway reveals a signaling role of unanchored polyubiquitin chains in innate immunity*. Cell, 2010. **141**(2): p. 315-30.
48. Jiang, X., et al., *Ubiquitin-induced oligomerization of the RNA sensors RIG-I and MDA5 activates antiviral innate immune response*. Immunity, 2012. **36**(6): p. 959-73.
49. Kowalinski, E., et al., *Structural basis for the activation of innate immune pattern-recognition receptor RIG-I by viral RNA*. Cell, 2011. **147**(2): p. 423-35.
50. Rawling, D.C., et al., *The RIG-I ATPase core has evolved a functional requirement for allosteric stabilization by the Pincer domain*. Nucleic Acids Res, 2014. **42**(18): p. 11601-11.
51. Venkataraman, T., et al., *Loss of DExD/H box RNA helicase LGP2 manifests disparate antiviral responses*. J Immunol, 2007. **178**(10): p. 6444-55.
52. Satoh, T., et al., *LGP2 is a positive regulator of RIG-I- and MDA5-mediated antiviral responses*. Proc Natl Acad Sci U S A, 2010. **107**(4): p. 1512-7.
53. Saito, T., et al., *Regulation of innate antiviral defenses through a shared repressor domain in RIG-I and LGP2*. Proc Natl Acad Sci U S A, 2007. **104**(2): p. 582-7.
54. Pippig, D.A., et al., *The regulatory domain of the RIG-I family ATPase LGP2 senses double-stranded RNA*. Nucleic Acids Res, 2009. **37**(6): p. 2014-25.
55. Li, X., et al., *The RIG-I-like receptor LGP2 recognizes the termini of double-stranded RNA*. J Biol Chem, 2009. **284**(20): p. 13881-91.
56. Bruns, A.M., et al., *The innate immune sensor LGP2 activates antiviral signaling by regulating MDA5-RNA interaction and filament assembly*. Mol Cell, 2014. **55**(5): p. 771-81.
57. Fu, J., et al., *MDA5 is SUMOylated by PIAS2beta in the upregulation of type I interferon signaling*. Mol Immunol, 2011. **48**(4): p. 415-22.
58. Chiang, J.J., M.E. Davis, and M.U. Gack, *Regulation of RIG-I-like receptor signaling by host and viral proteins*. Cytokine Growth Factor Rev, 2014. **25**(5): p. 491-505.
59. Hornung, V., et al., *5'-Triphosphate RNA is the ligand for RIG-I*. Science, 2006. **314**(5801): p. 994-7.
60. Pichlmair, A., et al., *RIG-I-mediated antiviral responses to single-stranded RNA bearing 5'-phosphates*. Science, 2006. **314**(5801): p. 997-1001.
61. Schlee, M., et al., *Recognition of 5' triphosphate by RIG-I helicase requires short blunt double-stranded RNA as contained in panhandle of negative-strand virus*. Immunity, 2009. **31**(1): p. 25-34.
62. Rehwinkel, J., et al., *RIG-I detects viral genomic RNA during negative-strand RNA virus infection*. Cell, 2010. **140**(3): p. 397-408.
63. Chiang, C., et al., *Sequence-Specific Modifications Enhance the Broad-Spectrum Antiviral Response Activated by RIG-I Agonists*. J Virol, 2015. **89**(15): p. 8011-25.



64. Goubau, D., et al., *Antiviral immunity via RIG-I-mediated recognition of RNA bearing 5'-diphosphates*. *Nature*, 2014. **514**(7522): p. 372-5.
65. Spengler, J.R., et al., *RIG-I Mediates an Antiviral Response to Crimean-Congo Hemorrhagic Fever Virus*. *J Virol*, 2015. **89**(20): p. 10219-29.
66. Hou, F., et al., *MAVS forms functional prion-like aggregates to activate and propagate antiviral innate immune response*. *Cell*, 2011. **146**(3): p. 448-61.
67. Nan, Y., G. Nan, and Y.J. Zhang, *Interferon induction by RNA viruses and antagonism by viral pathogens*. *Viruses*, 2014. **6**(12): p. 4999-5027.
68. Fitzgerald, K.A., et al., *IKKepsilon and TBK1 are essential components of the IRF3 signaling pathway*. *Nat Immunol*, 2003. **4**(5): p. 491-6.
69. Hacker, H. and M. Karin, *Regulation and function of IKK and IKK-related kinases*. *Sci STKE*, 2006. **2006**(357): p. re13.
70. Schlee, M. and G. Hartmann, *The chase for the RIG-I ligand--recent advances*. *Mol Ther*, 2010. **18**(7): p. 1254-62.
71. Oshiumi, H., et al., *Riplet/RNF135, a RING finger protein, ubiquitinates RIG-I to promote interferon-beta induction during the early phase of viral infection*. *J Biol Chem*, 2009. **284**(2): p. 807-17.
72. Gack, M.U., et al., *TRIM25 RING-finger E3 ubiquitin ligase is essential for RIG-I-mediated antiviral activity*. *Nature*, 2007. **446**(7138): p. 916-920.
73. Oshiumi, H., et al., *A distinct role of Riplet-mediated K63-Linked polyubiquitination of the RIG-I repressor domain in human antiviral innate immune responses*. *PLoS Pathog*, 2013. **9**(8): p. e1003533.
74. Oshiumi, H., et al., *The ubiquitin ligase Riplet is essential for RIG-I-dependent innate immune responses to RNA virus infection*. *Cell Host Microbe*, 2010. **8**(6): p. 496-509.
75. Wies, E., et al., *Dephosphorylation of the RNA sensors RIG-I and MDA5 by the phosphatase PP1 is essential for innate immune signaling*. *Immunity*, 2013. **38**(3): p. 437-49.
76. Nistal-Villan, E., et al., *Negative role of RIG-I serine 8 phosphorylation in the regulation of interferon-beta production*. *J Biol Chem*, 2010. **285**(26): p. 20252-61.
77. Willemsen, J., et al., *Phosphorylation-Dependent Feedback Inhibition of RIG-I by DAPK1 Identified by Kinome-wide siRNA Screening*. *Mol Cell*, 2017. **65**(3): p. 403-415.e8.
78. Seth, R.B., et al., *Identification and characterization of MAVS, a mitochondrial antiviral signaling protein that activates NF-kappaB and IRF 3*. *Cell*, 2005. **122**(5): p. 669-82.
79. Xu, L.G., et al., *VISA is an adapter protein required for virus-triggered IFN-beta signaling*. *Mol Cell*, 2005. **19**(6): p. 727-40.
80. Sun, Q., et al., *The specific and essential role of MAVS in antiviral innate immune responses*. *Immunity*, 2006. **24**(5): p. 633-42.
81. Kumar, H., et al., *Essential role of IPS-1 in innate immune responses against RNA viruses*. *J Exp Med*, 2006. **203**(7): p. 1795-803.
82. Lin, R., et al., *Dissociation of a MAVS/IPS-1/VISA/Cardif-IKKepsilon molecular complex from the mitochondrial outer membrane by hepatitis C virus NS3-4A proteolytic cleavage*. *J Virol*, 2006. **80**(12): p. 6072-83.
83. Xu, H., et al., *Structural basis for the prion-like MAVS filaments in antiviral innate immunity*. *Elife*, 2014. **3**: p. e01489.
84. Liu, S., et al., *MAVS recruits multiple ubiquitin E3 ligases to activate antiviral signaling cascades*. *Elife*, 2013. **2**: p. e00785.

85. Saha, S.K., et al., *Regulation of antiviral responses by a direct and specific interaction between TRAF3 and Cardif*. *Embo j*, 2006. **25**(14): p. 3257-63.
86. Chiba, Y., et al., *Retinoic acid-inducible gene-I-like receptor (RLR)-mediated antiviral innate immune responses in the lower respiratory tract: Roles of TRAF3 and TRAF5*. *Biochem Biophys Res Commun*, 2015. **467**(2): p. 191-6.
87. Paz, S., et al., *A functional C-terminal TRAF3-binding site in MAVS participates in positive and negative regulation of the IFN antiviral response*. *Cell Res*, 2011. **21**(6): p. 895-910.
88. Tang, E.D. and C.Y. Wang, *TRAF5 is a downstream target of MAVS in antiviral innate immune signaling*. *PLoS One*, 2010. **5**(2): p. e9172.
89. Mikkelsen, S.S., et al., *RIG-I-mediated activation of p38 MAPK is essential for viral induction of interferon and activation of dendritic cells: dependence on TRAF2 and TAK1*. *J Biol Chem*, 2009. **284**(16): p. 10774-82.
90. Hsu, H., et al., *TRADD-TRAF2 and TRADD-FADD interactions define two distinct TNF receptor 1 signal transduction pathways*. *Cell*, 1996. **84**(2): p. 299-308.
91. Balachandran, S., E. Thomas, and G.N. Barber, *A FADD-dependent innate immune mechanism in mammalian cells*. *Nature*, 2004. **432**(7015): p. 401-5.
92. Ea, C.K., et al., *Activation of IKK by TNF $\alpha$  requires site-specific ubiquitination of RIP1 and polyubiquitin binding by NEMO*. *Mol Cell*, 2006. **22**(2): p. 245-57.
93. Michallet, M.C., et al., *TRADD protein is an essential component of the RIG-like helicase antiviral pathway*. *Immunity*, 2008. **28**(5): p. 651-61.
94. Mao, A.P., et al., *Virus-triggered ubiquitination of TRAF3/6 by cIAP1/2 is essential for induction of interferon-beta (IFN-beta) and cellular antiviral response*. *J Biol Chem*, 2010. **285**(13): p. 9470-6.
95. McWhirter, S.M., et al., *IFN-regulatory factor 3-dependent gene expression is defective in Tbk1-deficient mouse embryonic fibroblasts*. *Proc Natl Acad Sci U S A*, 2004. **101**(1): p. 233-8.
96. Perry, A.K., et al., *Differential requirement for TANK-binding kinase-1 in type I interferon responses to toll-like receptor activation and viral infection*. *J Exp Med*, 2004. **199**(12): p. 1651-8.
97. Sharma, S., et al., *Triggering the interferon antiviral response through an IKK-related pathway*. *Science*, 2003. **300**(5622): p. 1148-51.
98. Miyahira, A.K., et al., *TANK-binding kinase-1 plays an important role during in vitro and in vivo type I IFN responses to DNA virus infections*. *J Immunol*, 2009. **182**(4): p. 2248-57.
99. Hemmi, H., et al., *The roles of two I $\kappa$ B kinase-related kinases in lipopolysaccharide and double stranded RNA signaling and viral infection*. *J Exp Med*, 2004. **199**(12): p. 1641-50.
100. Sasai, M., et al., *NAK-associated protein 1 participates in both the TLR3 and the cytoplasmic pathways in type I IFN induction*. *J Immunol*, 2006. **177**(12): p. 8676-83.
101. Ryzhakov, G. and F. Randow, *SINTBAD, a novel component of innate antiviral immunity, shares a TBK1-binding domain with NAP1 and TANK*. *Embo j*, 2007. **26**(13): p. 3180-90.
102. Guo, B. and G. Cheng, *Modulation of the interferon antiviral response by the TBK1/IKKi adaptor protein TANK*. *J Biol Chem*, 2007. **282**(16): p. 11817-26.
103. Goncalves, A., et al., *Functional dissection of the TBK1 molecular network*. *PLoS One*, 2011. **6**(9): p. e23971.

104. Kawagoe, T., et al., *TANK is a negative regulator of Toll-like receptor signaling and is critical for the prevention of autoimmune nephritis*. *Nat Immunol*, 2009. **10**(9): p. 965-72.
105. Soulat, D., et al., *The DEAD-box helicase DDX3X is a critical component of the TANK-binding kinase 1-dependent innate immune response*. *Embo j*, 2008. **27**(15): p. 2135-46.
106. Gu, L., et al., *Human DEAD box helicase 3 couples I $\kappa$ B kinase epsilon to interferon regulatory factor 3 activation*. *Mol Cell Biol*, 2013. **33**(10): p. 2004-15.
107. Gu, L., et al., *DDX3 directly regulates TRAF3 ubiquitination and acts as a scaffold to coordinate assembly of signalling complexes downstream from MAVS*. *Biochem J*, 2017. **474**(4): p. 571-587.
108. Kishore, N., et al., *IKK-i and TBK-1 are enzymatically distinct from the homologous enzyme IKK-2: comparative analysis of recombinant human IKK-i, TBK-1, and IKK-2*. *J Biol Chem*, 2002. **277**(16): p. 13840-7.
109. Chau, T.L., et al., *Are the IKKs and IKK-related kinases TBK1 and IKK-epsilon similarly activated?* *Trends Biochem Sci*, 2008. **33**(4): p. 171-80.
110. Marion, J.D., et al., *Mechanism of endogenous regulation of the type I interferon response by suppressor of I $\kappa$ B kinase epsilon (SIKE), a novel substrate of TANK-binding kinase 1 (TBK1)*. *J Biol Chem*, 2013. **288**(25): p. 18612-23.
111. Muvaffak, A., et al., *Evaluating TBK1 as a therapeutic target in cancers with activated IRF3*. *Mol Cancer Res*, 2014. **12**(7): p. 1055-66.
112. Li, S., et al., *Mapping a dynamic innate immunity protein interaction network regulating type I interferon production*. *Immunity*, 2011. **35**(3): p. 426-40.
113. Clark, K., et al., *Novel cross-talk within the IKK family controls innate immunity*. *Biochem J*, 2011. **434**(1): p. 93-104.
114. Wang, L., S. Li, and M.E. Dorf, *NEMO binds ubiquitinated TANK-binding kinase 1 (TBK1) to regulate innate immune responses to RNA viruses*. *PLoS One*, 2012. **7**(9): p. e43756.
115. Ma, X., et al., *Molecular basis of Tank-binding kinase 1 activation by transautophosphorylation*. *Proc Natl Acad Sci U S A*, 2012. **109**(24): p. 9378-83.
116. Mori, M., et al., *Identification of Ser-386 of interferon regulatory factor 3 as critical target for inducible phosphorylation that determines activation*. *J Biol Chem*, 2004. **279**(11): p. 9698-702.
117. Weaver, B.K., K.P. Kumar, and N.C. Reich, *Interferon regulatory factor 3 and CREB-binding protein/p300 are subunits of double-stranded RNA-activated transcription factor DRAF1*. *Mol Cell Biol*, 1998. **18**(3): p. 1359-68.
118. Yang, H., et al., *Transcriptional activity of interferon regulatory factor (IRF)-3 depends on multiple protein-protein interactions*. *Eur J Biochem*, 2002. **269**(24): p. 6142-51.
119. Lin, R., et al., *Virus-dependent phosphorylation of the IRF-3 transcription factor regulates nuclear translocation, transactivation potential, and proteasome-mediated degradation*. *Mol Cell Biol*, 1998. **18**(5): p. 2986-96.
120. Reich, N.C., *Nuclear/cytoplasmic localization of IRFs in response to viral infection or interferon stimulation*. *J Interferon Cytokine Res*, 2002. **22**(1): p. 103-9.
121. Lu, R., et al., *Regulation of the promoter activity of interferon regulatory factor-7 gene. Activation by interferon and silencing by hypermethylation*. *J Biol Chem*, 2000. **275**(41): p. 31805-12.
122. Ning, S., J.S. Pagano, and G.N. Barber, *IRF7: activation, regulation, modification and function*. *Genes Immun*, 2011. **12**(6): p. 399-414.

123. Chan, Y.K. and M.U. Gack, *Viral evasion of intracellular DNA and RNA sensing*. Nat Rev Microbiol, 2016. **14**(6): p. 360-73.
124. Chan, Y.K. and M.U. Gack, *RIG-I-like receptor regulation in virus infection and immunity*. Curr Opin Virol, 2015. **12**: p. 7-14.
125. Honda, K. and T. Taniguchi, *IRFs: master regulators of signalling by Toll-like receptors and cytosolic pattern-recognition receptors*. Nat Rev Immunol, 2006. **6**(9): p. 644-58.
126. Honda, K., et al., *IRF-7 is the master regulator of type-I interferon-dependent immune responses*. Nature, 2005. **434**(7034): p. 772-7.
127. Huxford, T. and G. Ghosh, *A structural guide to proteins of the NF-kappaB signaling module*. Cold Spring Harb Perspect Biol, 2009. **1**(3): p. a000075.
128. Hoffmann, A., G. Natoli, and G. Ghosh, *Transcriptional regulation via the NF-kappaB signaling module*. Oncogene, 2006. **25**(51): p. 6706-16.
129. Bouwmeester, T., et al., *A physical and functional map of the human TNF-alpha/NF-kappa B signal transduction pathway*. Nat Cell Biol, 2004. **6**(2): p. 97-105.
130. Basak, S., et al., *A fourth IkappaB protein within the NF-kappaB signaling module*. Cell, 2007. **128**(2): p. 369-81.
131. Michel, F., et al., *Crystal structure of the ankyrin repeat domain of Bcl-3: a unique member of the IkappaB protein family*. Embo j, 2001. **20**(22): p. 6180-90.
132. Trinh, D.V., et al., *The nuclear I kappaB protein I kappaB zeta specifically binds NF-kappaB p50 homodimers and forms a ternary complex on kappaB DNA*. J Mol Biol, 2008. **379**(1): p. 122-35.
133. Yamamoto, M., et al., *Regulation of Toll/IL-1-receptor-mediated gene expression by the inducible nuclear protein IkappaBzeta*. Nature, 2004. **430**(6996): p. 218-22.
134. Malek, S., et al., *IkappaBbeta, but not IkappaBalpha, functions as a classical cytoplasmic inhibitor of NF-kappaB dimers by masking both NF-kappaB nuclear localization sequences in resting cells*. J Biol Chem, 2001. **276**(48): p. 45225-35.
135. Malek, S., et al., *X-ray crystal structure of an IkappaBbeta x NF-kappaB p65 homodimer complex*. J Biol Chem, 2003. **278**(25): p. 23094-100.
136. Sun, L., et al., *The TRAF6 ubiquitin ligase and TAK1 kinase mediate IKK activation by BCL10 and MALT1 in T lymphocytes*. Mol Cell, 2004. **14**(3): p. 289-301.
137. Delhase, M., et al., *Positive and negative regulation of IkappaB kinase activity through IKKbeta subunit phosphorylation*. Science, 1999. **284**(5412): p. 309-13.
138. Mercurio, F., et al., *IkappaB kinase (IKK)-associated protein 1, a common component of the heterogeneous IKK complex*. Mol Cell Biol, 1999. **19**(2): p. 1526-38.
139. Karin, M., *How NF-kappaB is activated: the role of the IkappaB kinase (IKK) complex*. Oncogene, 1999. **18**(49): p. 6867-74.
140. Yamaoka, S., et al., *Complementation cloning of NEMO, a component of the IkappaB kinase complex essential for NF-kappaB activation*. Cell, 1998. **93**(7): p. 1231-40.
141. Rothwarf, D.M., et al., *IKK-gamma is an essential regulatory subunit of the IkappaB kinase complex*. Nature, 1998. **395**(6699): p. 297-300.
142. Li, Y., et al., *Identification of a cell protein (FIP-3) as a modulator of NF-kappaB activity and as a target of an adenovirus inhibitor of tumor necrosis factor alpha-induced apoptosis*. Proc Natl Acad Sci U S A, 1999. **96**(3): p. 1042-7.
143. Ghosh, S., M.J. May, and E.B. Kopp, *NF-kappa B and Rel proteins: evolutionarily conserved mediators of immune responses*. Annu Rev Immunol, 1998. **16**: p. 225-60.
144. Karin, M. and Y. Ben-Neriah, *Phosphorylation meets ubiquitination: the control of NF-[kappa]B activity*. Annu Rev Immunol, 2000. **18**: p. 621-63.

145. Pando, M.P. and I.M. Verma, *Signal-dependent and -independent degradation of free and NF-kappa B-bound IkappaBalpha*. J Biol Chem, 2000. **275**(28): p. 21278-86.
146. Zhao, T., et al., *The NEMO adaptor bridges the nuclear factor-kappaB and interferon regulatory factor signaling pathways*. Nat Immunol, 2007. **8**(6): p. 592-600.
147. Belgnaoui, S.M., et al., *Linear ubiquitination of NEMO negatively regulates the interferon antiviral response through disruption of the MAVS-TRAF3 complex*. Cell Host Microbe, 2012. **12**(2): p. 211-22.
148. Gibbert, K., et al., *IFN-alpha subtypes: distinct biological activities in anti-viral therapy*. Br J Pharmacol, 2013. **168**(5): p. 1048-58.
149. Donnelly, R.P. and S.V. Kotenko, *Interferon-lambda: a new addition to an old family*. J Interferon Cytokine Res, 2010. **30**(8): p. 555-64.
150. Hansson, M., et al., *Hematopoietic secretory granules as vehicles for the local delivery of cytokines and soluble cytokine receptors at sites of inflammation*. Eur Cytokine Netw, 2004. **15**(3): p. 167-76.
151. Duitman, E.H., et al., *How a cytokine is chaperoned through the secretory pathway by complexing with its own receptor: lessons from interleukin-15 (IL-15)/IL-15 receptor alpha*. Mol Cell Biol, 2008. **28**(15): p. 4851-61.
152. de Weerd, N.A., S.A. Samarajiwa, and P.J. Hertzog, *Type I interferon receptors: biochemistry and biological functions*. J Biol Chem, 2007. **282**(28): p. 20053-7.
153. Pattyn, E., et al., *Dimerization of the interferon type I receptor IFNAR2-2 is sufficient for induction of interferon effector genes but not for full antiviral activity*. J Biol Chem, 1999. **274**(49): p. 34838-45.
154. Mennechet, F.J. and G. Uze, *Interferon-lambda-treated dendritic cells specifically induce proliferation of FOXP3-expressing suppressor T cells*. Blood, 2006. **107**(11): p. 4417-23.
155. Bustamante, J., et al., *Novel primary immunodeficiencies revealed by the investigation of paediatric infectious diseases*. Curr Opin Immunol, 2008. **20**(1): p. 39-48.
156. Stark, G.R., et al., *How cells respond to interferons*. Annu Rev Biochem, 1998. **67**: p. 227-64.
157. Ortmann, R.A., et al., *Janus kinases and signal transducers and activators of transcription: their roles in cytokine signaling, development and immunoregulation*. Arthritis Res, 2000. **2**(1): p. 16-32.
158. O'Shea, J.J., et al., *Advances in the understanding of cytokine signal transduction: the role of Jaks and STATs in immunoregulation and the pathogenesis of immunodeficiency*. J Clin Immunol, 1997. **17**(6): p. 431-47.
159. Zhang, J., et al., *Distinct expression of interferon-induced protein with tetratricopeptide repeats (IFIT) 1/2/3 and other antiviral genes between subsets of dendritic cells induced by dengue virus 2 infection*. Immunology, 2016. **148**(4): p. 363-76.
160. Schoggins, J.W. and C.M. Rice, *Interferon-stimulated genes and their antiviral effector functions*. Curr Opin Virol, 2011. **1**(6): p. 519-25.
161. Baum, A. and A. Garcia-Sastre, *Induction of type I interferon by RNA viruses: cellular receptors and their substrates*. Amino Acids, 2010. **38**(5): p. 1283-99.
162. Ye, J. and T. Maniatis, *Negative regulation of interferon-beta gene expression during acute and persistent virus infections*. PLoS One, 2011. **6**(6): p. e20681.
163. McNab, F., et al., *Type I interferons in infectious disease*. Nat Rev Immunol, 2015. **15**(2): p. 87-103.

164. Pervolaraki, K., et al., *Type I and Type III Interferons Display Different Dependency on Mitogen-Activated Protein Kinases to Mount an Antiviral State in the Human Gut*. Front Immunol, 2017. **8**: p. 459.
165. Shuai, K. and B. Liu, *Regulation of JAK-STAT signalling in the immune system*. Nat Rev Immunol, 2003. **3**(11): p. 900-11.
166. Hoffmann, A., et al., *The I $\kappa$ B-NF- $\kappa$ B signaling module: temporal control and selective gene activation*. Science, 2002. **298**(5596): p. 1241-5.
167. Hershko, A. and A. Ciechanover, *The ubiquitin system*. Annu Rev Biochem, 1998. **67**: p. 425-79.
168. Goldknopf, I.L., et al., *Presence of protein A24 in rat liver nucleosomes*. Proc Natl Acad Sci U S A, 1977. **74**(12): p. 5492-5.
169. Goldstein, G., et al., *Isolation of a polypeptide that has lymphocyte-differentiating properties and is probably represented universally in living cells*. Proc Natl Acad Sci U S A, 1975. **72**(1): p. 11-5.
170. Baker, R.T. and P.G. Board, *The human ubiquitin gene family: structure of a gene and pseudogenes from the Ub B subfamily*. Nucleic Acids Res, 1987. **15**(2): p. 443-63.
171. Breslow, E., et al., *Role of methionine-1 in ubiquitin conformation and activity*. Biochem Biophys Res Commun, 1986. **138**(1): p. 437-44.
172. Swatek, K.N. and D. Komander, *Ubiquitin modifications*. Cell Res, 2016. **26**(4): p. 399-422.
173. Komander, D. and M. Rape, *The ubiquitin code*. Annu Rev Biochem, 2012. **81**: p. 203-29.
174. Pickart, C.M., *Mechanisms underlying ubiquitination*. Annu Rev Biochem, 2001. **70**: p. 503-33.
175. Schulman, B.A. and J.W. Harper, *Ubiquitin-like protein activation by E1 enzymes: the apex for downstream signalling pathways*. Nat Rev Mol Cell Biol, 2009. **10**(5): p. 319-31.
176. Ye, Y. and M. Rape, *Building ubiquitin chains: E2 enzymes at work*. Nat Rev Mol Cell Biol, 2009. **10**(11): p. 755-64.
177. Deshaies, R.J. and C.A. Joazeiro, *RING domain E3 ubiquitin ligases*. Annu Rev Biochem, 2009. **78**: p. 399-434.
178. Kimura, Y. and K. Tanaka, *Regulatory mechanisms involved in the control of ubiquitin homeostasis*. J Biochem, 2010. **147**(6): p. 793-8.
179. Komander, D., M.J. Clague, and S. Urbe, *Breaking the chains: structure and function of the deubiquitinases*. Nat Rev Mol Cell Biol, 2009. **10**(8): p. 550-63.
180. Pickart, C.M. and M.J. Eddins, *Ubiquitin: structures, functions, mechanisms*. Biochim Biophys Acta, 2004. **1695**(1-3): p. 55-72.
181. Wilkinson, K.D., *The discovery of ubiquitin-dependent proteolysis*. Proc Natl Acad Sci U S A, 2005. **102**(43): p. 15280-2.
182. Ikeda, F., N. Crosetto, and I. Dikic, *What determines the specificity and outcomes of ubiquitin signaling?* Cell, 2010. **143**(5): p. 677-81.
183. Chattopadhyay, S., et al., *Ubiquitination of the Transcription Factor IRF-3 Activates RIPA, the Apoptotic Pathway that Protects Mice from Viral Pathogenesis*. Immunity, 2016. **44**(5): p. 1151-61.
184. Emmerich, C.H., et al., *Lys63/Met1-hybrid ubiquitin chains are commonly formed during the activation of innate immune signalling*. Biochem Biophys Res Commun, 2016. **474**(3): p. 452-61.

185. Nguyen, N.T., et al., *Ubiquitin-like modifier FAT10 attenuates RIG-I mediated antiviral signaling by segregating activated RIG-I from its signaling platform*. Sci Rep, 2016. **6**: p. 23377.
186. Bhoj, V.G. and Z.J. Chen, *Ubiquitylation in innate and adaptive immunity*. Nature, 2009. **458**(7237): p. 430-7.
187. Nakhaei, P., et al., *The E3 ubiquitin ligase Triad3A negatively regulates the RIG-I/MAVS signaling pathway by targeting TRAF3 for degradation*. PLoS Pathog, 2009. **5**(11): p. e1000650.
188. Zeng, W., et al., *Key role of Ubc5 and lysine-63 polyubiquitination in viral activation of IRF3*. Mol Cell, 2009. **36**(2): p. 315-25.
189. Arimoto, K., et al., *Negative regulation of the RIG-I signaling by the ubiquitin ligase RNF125*. Proc Natl Acad Sci U S A, 2007. **104**(18): p. 7500-5.
190. Panda, S., J.A. Nilsson, and N.O. Gekara, *Deubiquitinase MYSM1 Regulates Innate Immunity through Inactivation of TRAF3 and TRAF6 Complexes*. Immunity, 2015. **43**(4): p. 647-59.
191. Maelfait, J. and R. Beyaert, *Emerging role of ubiquitination in antiviral RIG-I signaling*. Microbiol Mol Biol Rev, 2012. **76**(1): p. 33-45.
192. Wei Li, a.H.B., Axel Ulbrich, Akio Matsudo, Vektreshwar A. Reddy, Anthony Orth, Sumit K. Chandra, Serge Batalov, Claudio A. P. Joazeiro, *Genome-Wide and Functional Annotation of Human E3 Ubiquitin Ligases Identifies MULAN, a Mitochondrial E3 that Regulates the Organelle's Dynamics and Signaling*. PLoS One, 2008. **1487**(1).
193. Li, W., et al., *Genome-wide and functional annotation of human E3 ubiquitin ligases identifies MULAN, a mitochondrial E3 that regulates the organelle's dynamics and signaling*. PLoS One, 2008. **3**(1): p. e1487.
194. Matula, P., et al., *Single-cell-based image analysis of high-throughput cell array screens for quantification of viral infection*. Cytometry A, 2009. **75**(4): p. 309-18.
195. Wang, S., et al., *RNF123 has an E3 ligase-independent function in RIG-I-like receptor-mediated antiviral signaling*. EMBO Rep, 2016. **17**(8): p. 1155-68.
196. Cassonnet, P., et al., *Benchmarking a luciferase complementation assay for detecting protein complexes*. Nat Methods, 2011. **8**(12): p. 990-2.
197. Remy, I. and S.W. Michnick, *A highly sensitive protein-protein interaction assay based on Gaussia luciferase*. Nat Methods, 2006. **3**(12): p. 977-9.
198. Lohmann, V., et al., *Replication of subgenomic hepatitis C virus RNAs in a hepatoma cell line*. Science, 1999. **285**(5424): p. 110-3.
199. Wang, X., et al., *Hepatitis B virus X protein induces hepatic stem cell-like features in hepatocellular carcinoma by activating KDM5B*. World J Gastroenterol, 2017. **23**(18): p. 3252-3261.
200. Wong, P.P., et al., *Histone demethylase KDM5B collaborates with TFAP2C and Myc to repress the cell cycle inhibitor p21(cip) (CDKN1A)*. Mol Cell Biol, 2012. **32**(9): p. 1633-44.
201. Li, S., L. Wang, and M.E. Dorf, *PKC phosphorylation of TRAF2 mediates IKKalpha/beta recruitment and K63-linked polyubiquitination*. Mol Cell, 2009. **33**(1): p. 30-42.
202. Broussard, J.A., et al., *Fluorescence resonance energy transfer microscopy as demonstrated by measuring the activation of the serine/threonine kinase Akt*. Nat Protoc, 2013. **8**(2): p. 265-81.
203. Stoddart, L.A., et al., *Application of BRET to monitor ligand binding to GPCRs*. Nat Methods, 2015. **12**(7): p. 661-663.

204. Pflieger, K.D. and K.A. Eidne, *Illuminating insights into protein-protein interactions using bioluminescence resonance energy transfer (BRET)*. Nat Methods, 2006. **3**(3): p. 165-74.
205. Song, Y., V. Madahar, and J. Liao, *Development of FRET assay into quantitative and high-throughput screening technology platforms for protein-protein interactions*. Ann Biomed Eng, 2011. **39**(4): p. 1224-34.
206. Couturier, C. and B. Deprez, *Setting Up a Bioluminescence Resonance Energy Transfer High throughput Screening Assay to Search for Protein/Protein Interaction Inhibitors in Mammalian Cells*. Front Endocrinol (Lausanne), 2012. **3**: p. 100.
207. Breiman, A., et al., *Inhibition of RIG-I-dependent signaling to the interferon pathway during hepatitis C virus expression and restoration of signaling by IKKepsilon*. J Virol, 2005. **79**(7): p. 3969-78.
208. Budzynska, P.M., et al., *IRF4 Deficiency Leads to Altered BCR Signalling Revealed by Enhanced PI3K Pathway, Decreased SHIP Expression and Defected Cytoskeletal Responses*. Scand J Immunol, 2015. **82**(5): p. 418-28.
209. Snijder, B. and L. Pelkmans, *Origins of regulated cell-to-cell variability*. Nat Rev Mol Cell Biol, 2011. **12**(2): p. 119-25.
210. Elowitz, M.B., et al., *Stochastic gene expression in a single cell*. Science, 2002. **297**(5584): p. 1183-6.
211. Paixao, T., et al., *Quantitative insights into stochastic monoallelic expression of cytokine genes*. Immunol Cell Biol, 2007. **85**(4): p. 315-22.
212. Zhao, M., et al., *Stochastic expression of the interferon-beta gene*. PLoS Biol, 2012. **10**(1): p. e1001249.
213. Neumann, E., et al., *Gene transfer into mouse lymphoma cells by electroporation in high electric fields*. Embo j, 1982. **1**(7): p. 841-5.
214. Andre, F. and L.M. Mir, *DNA electrotransfer: its principles and an updated review of its therapeutic applications*. Gene Ther, 2004. **11 Suppl 1**: p. S33-42.
215. Fromm, M., L.P. Taylor, and V. Walbot, *Expression of genes transferred into monocot and dicot plant cells by electroporation*. Proc Natl Acad Sci U S A, 1985. **82**(17): p. 5824-8.
216. Chu, G., H. Hayakawa, and P. Berg, *Electroporation for the efficient transfection of mammalian cells with DNA*. Nucleic Acids Res, 1987. **15**(3): p. 1311-26.
217. Chang, D.C., *Cell poration and cell fusion using an oscillating electric field*. Biophys J, 1989. **56**(4): p. 641-52.
218. Kamiya, H., H. Akita, and H. Harashima, *Pharmacokinetic and pharmacodynamic considerations in gene therapy*. Drug Discov Today, 2003. **8**(21): p. 990-6.
219. Dinh, A.T., et al., *Understanding intracellular transport processes pertinent to synthetic gene delivery via stochastic simulations and sensitivity analyses*. Biophys J, 2007. **92**(3): p. 831-46.
220. Varga, C.M., K. Hong, and D.A. Lauffenburger, *Quantitative analysis of synthetic gene delivery vector design properties*. Mol Ther, 2001. **4**(5): p. 438-46.
221. Leonhardt, C., et al., *Single-cell mRNA transfection studies: delivery, kinetics and statistics by numbers*. Nanomedicine, 2014. **10**(4): p. 679-88.
222. Chan, Y.K. and M.U. Gack, *RIG-I works double duty*. Cell Host Microbe, 2015. **17**(3): p. 285-7.
223. Rand, U., et al., *Multi-layered stochasticity and paracrine signal propagation shape the type-I interferon response*. Mol Syst Biol, 2012. **8**: p. 584.



224. Nelson, G., et al., *Multi-parameter analysis of the kinetics of NF-kappaB signalling and transcription in single living cells*. J Cell Sci, 2002. **115**(Pt 6): p. 1137-48.
225. Makela, S.M., et al., *RIG-I Signaling Is Essential for Influenza B Virus-Induced Rapid Interferon Gene Expression*. J Virol, 2015. **89**(23): p. 12014-25.
226. Long, L., et al., *Recruitment of phosphatase PP2A by RACK1 adaptor protein deactivates transcription factor IRF3 and limits type I interferon signaling*. Immunity, 2014. **40**(4): p. 515-29.
227. Wang, X., et al., *Bistability, stochasticity, and oscillations in the mitogen-activated protein kinase cascade*. Biophys J, 2006. **90**(6): p. 1961-78.
228. Inoue, K., et al., *Oscillation dynamics underlie functional switching of NF-kappaB for B-cell activation*. NPJ Syst Biol Appl, 2016. **2**: p. 16024.
229. Weber, M., et al., *Incoming RNA virus nucleocapsids containing a 5'-triphosphorylated genome activate RIG-I and antiviral signaling*. Cell Host Microbe, 2013. **13**(3): p. 336-46.
230. Weber, M. and F. Weber, *Monitoring activation of the antiviral pattern recognition receptors RIG-I and PKR by limited protease digestion and native PAGE*. J Vis Exp, 2014(89): p. e51415.
231. Rossi, A.M. and C.W. Taylor, *Analysis of protein-ligand interactions by fluorescence polarization*. Nat Protoc, 2011. **6**(3): p. 365-87.
232. Hoffman, E.A., et al., *Formaldehyde crosslinking: a tool for the study of chromatin complexes*. J Biol Chem, 2015. **290**(44): p. 26404-11.
233. McFarland, K.L., et al., *Culture medium and cell density impact gene expression in normal skin and abnormal scar-derived fibroblasts*. J Burn Care Res, 2011. **32**(4): p. 498-508.
234. Karin, M., Z. Liu, and E. Zandi, *AP-1 function and regulation*. Curr Opin Cell Biol, 1997. **9**(2): p. 240-6.
235. Zhong, B., P. Tien, and H.B. Shu, *Innate immune responses: crosstalk of signaling and regulation of gene transcription*. Virology, 2006. **352**(1): p. 14-21.
236. Levy, D.E., I.J. Marie, and J.E. Durbin, *Induction and function of type I and III interferon in response to viral infection*. Curr Opin Virol, 2011. **1**(6): p. 476-86.
237. Bradford, S. and J.A. Cowan, *Catalytic metallodrugs targeting HCV IRES RNA*. Chem Commun (Camb), 2012. **48**(25): p. 3118-20.
238. Tenoever, B.R., et al., *Multiple functions of the IKK-related kinase IKKepsilon in interferon-mediated antiviral immunity*. Science, 2007. **315**(5816): p. 1274-8.
239. Kofahl, B. and E. Klipp, *Modelling the dynamics of the yeast pheromone pathway*. Yeast, 2004. **21**(10): p. 831-50.
240. Kuhn, C., et al., *Exploring the impact of osmoadaptation on glycolysis using time-varying response-coefficients*. Genome Inform, 2008. **20**: p. 77-90.
241. Klipp, E., et al., *Integrative model of the response of yeast to osmotic shock*. Nat Biotechnol, 2005. **23**(8): p. 975-82.
242. Yildirim, N., et al., *Mathematical modeling of RGS and G-protein regulation in yeast*. Methods Enzymol, 2004. **389**: p. 383-98.
243. Albert, R. and H.G. Othmer, *The topology of the regulatory interactions predicts the expression pattern of the segment polarity genes in Drosophila melanogaster*. J Theor Biol, 2003. **223**(1): p. 1-18.
244. Mori, T., et al., *Stochastic simulation of Boolean rxncon models: towards quantitative analysis of large signaling networks*. BMC Syst Biol, 2015. **9**: p. 45.



# 7.0 Presentations and Publications

## 7.1 Poster/oral presentations

- I. *Heidelberg Young Scientist Conference, DKFZ, oral presentation, 2015*
  - “Antiviral response mediated by RIG-I” Jamie Frankish, Marco Binder.
  
- II. *Intrinsic and Innate Immunity to Pathogens, Novara congress centre, poster presentation, 2016.*
  - “Dynamics and Regulation of the RIG-I Signalling Network” Jamie Frankish, Darius Schweinoch, Lars Kaderali, Marco Binder.
  
- III. *Annual Meeting for the Society of Virology, Marburg University, poster presentation, 2017.*
  - “Dynamics and Regulation of the RIG-I Signalling Network” Jamie Frankish, Darius Schweinoch, Lars Kaderali, Marco Binder.
  - **Awarded best poster presentation.**

## 7.2 Publications

- I. HBV bypasses the innate immune system and does not protect HCV against the antiviral activity of interferon – **in review as of 21.08.17**

### Authors:

Pascal Mutz<sup>1,2,&</sup>, Philippe Metz<sup>1,7</sup>, Florian Lempp<sup>1</sup>, Silke Bender<sup>1,2,8</sup>, Bingqian Qu<sup>1</sup>, Katrin Schöneweis<sup>1</sup>, Stefan Seitz<sup>1</sup>, Agnese Restuccia<sup>1,2,9</sup>, Jamie Frankish<sup>2</sup>, Benjamin Schusser<sup>3</sup>, Ronald Koschny<sup>4</sup>, Georgios Polychronidis<sup>5</sup>, Peter Schemmer<sup>5</sup>, Katrin Hoffmann<sup>5</sup>, Thomas Baumert<sup>6</sup>, M. Binder<sup>1,2</sup>, Stephan Urban<sup>1</sup> and Ralf Bartenschlager<sup>1,2</sup>

# 8.0 Appendix

Table 27. Gene regulated by IFN signalling

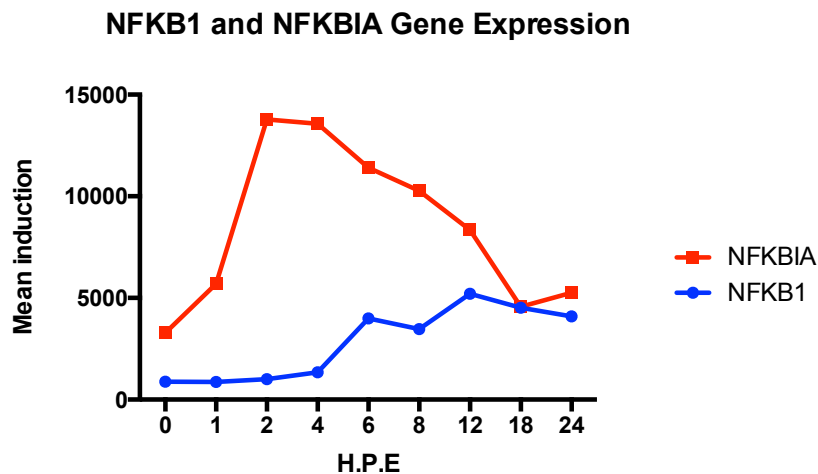
Gene	WRD	Gene	WRD	Gene	WRD
LOC100129236	-1.472603	PTGS2	-0.784	SNORA61	-0.625
SPRYD5	-1.365622	LOC647334	-0.7817509	LOC100134364	-0.6218097
VCX2	-1.236284	SGK	-0.7745098	FBXO33	-0.6135458
PHLDA2	-1.194748	DNAJB6	-0.7698864	SLC5A8	-0.6118501
STC2	-1.15528	RAGE	-0.7628083	LOC440093	-0.6072131
SERPINE1	-1.124682	TUBB4Q	-0.7593308	SNORA57	-0.6057386
VCX-C	-1.061728	RAXL1	-0.7578806	LOC644884	-0.6026201
LOC649346	-1.04878	LOC100132394	-0.7561837	USP38	-0.6022393
HPS5	-1.045764	LOC340970	-0.7522013	ANKRD57	-0.6021922
ZNF280C	-1.025	HSPA5	-0.7457098	TRIM39	-0.6001406
VCX	-1	FAM90A2P	-0.7438017	PTGR2	-0.5982028
ADM	-1	EHD1	-0.7431907	C3orf19	-0.595211
FLJ10374	-0.9813849	C1orf128	-0.7430556	PNO1	-0.5790408
CTGF	-0.9613259	SAV1	-0.7411487	LOC653506	-0.5737399
ATF4	-0.9565218	LOC158160	-0.7348018	ID2	-0.5719626
FOS	-0.9333333	LOC100133760	-0.7299864	CLCF1	-0.5613079
SGK1	-0.9333333	NR1H4	-0.7225258	RRAGC	-0.5610561
RNU4ATAC	-0.9240349	LOC791120	-0.7206267	PIM1	-0.5575916
MYLIP	-0.9218329	RGS20	-0.7185355	HIST2H2AA4	-0.5572917
NCRNA00152	-0.9107011	CCRN4L	-0.7080745	TAF4B	-0.5557587
HN1	-0.9074244	LOC389765	-0.7024055	RRAD	-0.5535055
EOMES	-0.8777555	TSPYL2	-0.7017301	EGR3	-0.5394191
CYR61	-0.8712871	LOC650832	-0.6986899	ZNF274	-0.5388789
KLHL15	-0.862069	DNAJB4	-0.6917293	MED26	-0.5387454
RNY4	-0.8498074	LRP5L	-0.6875	HOXD1	-0.5369979
EFNB2	-0.8471178	PIM2	-0.6851735	CRISPLD2	-0.5341464
MKKS	-0.8393136	TNF	-0.6785714	CSRNP2	-0.5323383
LOC342933	-0.8298755	ELF3	-0.6749117	ZNF787	-0.529563
HIST2H2AA3	-0.8286189	MTMR14	-0.6702341	C18orf19	-0.5283019
LOC100133984	-0.8245955	SLC9A1	-0.6649485	LOC100130445	-0.5270936
SOCS1	-0.8216833	LPIN1	-0.6618576	RASL11B	-0.5241845
RND3	-0.8206039	NKX3-1	-0.6611741	CASP3	-0.52349
SMG5	-0.8193384	TNFRSF12A	-0.6569536	SNHG1	-0.5233645
FOXD1	-0.8187919	KLF2	-0.656	LOC100133012	-0.5165239
HES6	-0.8130406	C10orf67	-0.6532663	VPS37B	-0.5160121
ANKRD1	-0.8015979	HIST1H4H	-0.652439	IL11	-0.5118979

<b>LOC100129882</b>	-0.8002672	<b>JUNB</b>	-0.6521739	<b>ZFP36</b>	-0.5074627
<b>DDIT3</b>	-0.8	<b>FAM90A1</b>	-0.6514286	<b>NEFM</b>	-0.5065711
<b>IER5</b>	-0.8	<b>SNORD104</b>	-0.6507592	<b>AHSA2</b>	-0.00464756
<b>TOB1</b>	-0.7979966	<b>SNORD12C</b>	-0.6462436	<b>TBC1D8</b>	-0.004175365
<b>RGS2</b>	-0.7972028	<b>CABYR</b>	-0.6414415	<b>SGMS2</b>	-0.002059732
<b>NR4A1</b>	-0.7876289	<b>CD83</b>	-0.6322581	<b>AMHR2</b>	-0.00180018
<b>ARGLU1</b>	-0.786141	<b>LOC644250</b>	-0.6293873	<b>IFIT2</b>	0
<b>TBPL1</b>	-0.7858082	<b>DNAJB1</b>	-0.6271732	<b>IFNB1</b>	0
<b>VCX3A</b>	-0.7857143	<b>C9orf156</b>	-0.6265233	<b>OASL</b>	0
<b>TIPARP</b>	0	<b>POU2F1</b>	0.6142778	<b>RFX1</b>	0.7610009
<b>RIC8B</b>	0.003139717	<b>KDM6B</b>	0.6143791	<b>NAT15</b>	0.7698413
<b>PER2</b>	0.003976143	<b>LOC728640</b>	0.6147186	<b>LOC728014</b>	0.7702265
<b>SNX11</b>	0.00436205	<b>LOC728153</b>	0.6168675	<b>PLEKHH3</b>	0.771633
<b>BCMO1</b>	0.005665722	<b>SOCS3</b>	0.6221693	<b>STC1</b>	0.779002
<b>SLC38A2</b>	0.5045372	<b>ZBTB20</b>	0.6238015	<b>C10orf10</b>	0.7816994
<b>LOC728888</b>	0.5066667	<b>LOC646626</b>	0.6255924	<b>OAS2</b>	0.7906274
<b>TXNL4B</b>	0.508612	<b>ITGA5</b>	0.6296296	<b>CFB</b>	0.7958115
<b>OTUD1</b>	0.5138889	<b>FZD4</b>	0.6314678	<b>IL29</b>	0.8
<b>LOC90586</b>	0.5156398	<b>IFI16</b>	0.6341463	<b>DMWD</b>	0.8002586
<b>BTG1</b>	0.5240893	<b>SP110</b>	0.6385405	<b>SESN2</b>	0.8098522
<b>INTS6</b>	0.5267576	<b>TIGA1</b>	0.6442812	<b>DCP1A</b>	0.818638
<b>TMEM156</b>	0.5300113	<b>SETX</b>	0.6473029	<b>MBD6</b>	0.8324325
<b>ALB</b>	0.5357873	<b>RP5-1022P6.2</b>	0.6480938	<b>NR0B1</b>	0.834375
<b>PRKD2</b>	0.5362079	<b>CRTC2</b>	0.6537998	<b>ELF1</b>	0.8431373
<b>RN7SK</b>	0.5384616	<b>DHX58</b>	0.656	<b>RGAG1</b>	0.8485264
<b>MTF2</b>	0.5384616	<b>BEX2</b>	0.6652221	<b>ATXN7L3</b>	0.8492429
<b>OGFR</b>	0.5397816	<b>CCL5</b>	0.6666667	<b>NKD2</b>	0.8549906
<b>PUM1</b>	0.5415713	<b>RIPK4</b>	0.6718147	<b>YY1AP1</b>	0.8552486
<b>ULBP2</b>	0.5420561	<b>GABARAPL1</b>	0.6734694	<b>CBLL1</b>	0.8594164
<b>NFE2L2</b>	0.5437263	<b>ASAP1</b>	0.677686	<b>BCL2L13</b>	0.8647115
<b>SIRT2</b>	0.54385	<b>ZNF410</b>	0.6803219	<b>COL7A1</b>	0.8738676
<b>BCAR1</b>	0.5456608	<b>SHOC2</b>	0.6817102	<b>ISL2</b>	0.8873239
<b>OAS1</b>	0.5476923	<b>TGIF2</b>	0.6845238	<b>ZFP36L2</b>	0.8896552
<b>DDIT4</b>	0.5485232	<b>HERC6</b>	0.6915888	<b>OAS3</b>	0.9048086
<b>MUC5AC</b>	0.5538462	<b>NPPI</b>	0.692422	<b>PLSCR1</b>	0.9128631
<b>ZNF503</b>	0.5554425	<b>NDRG1</b>	0.6961483	<b>PLEKHA4</b>	0.9411765
<b>VAMP2</b>	0.5561358	<b>NCALD</b>	0.6985962	<b>STAT2</b>	0.9444033
<b>XBP1</b>	0.5563093	<b>LOC401317</b>	0.7011494	<b>CXCL1</b>	0.955414
<b>FBRS</b>	0.557377	<b>EHD4</b>	0.7059713	<b>ARID5B</b>	0.9571328
<b>SNHG8</b>	0.5654281	<b>PRIC285</b>	0.7114094	<b>STK40</b>	0.9627851
<b>LMO4</b>	0.5672371	<b>HLA-E</b>	0.7117009	<b>FAM46A</b>	0.989733

AKAP13	0.5762712	TICAM1	0.7208672	TRIM21	0.9929078
TAP1	0.5785536	WHAMM	0.7216495	ARID3B	1.016897
DEDD2	0.5842531	PVRL2	0.7293128	IRX5	1.021475
WARS	0.5854859	LOC100131713	0.7366864	EIF4A2	1.026263
LOC100132247	0.5869565	CNOT2	0.7372073	ULBP1	1.034749
IL28B	0.5882353	PHACTR4	0.7377279	LOC387763	1.047619
EFHD1	0.5920537	LOC286512	0.7405356	ERF	1.05864
GATAD2B	0.5957447	GAS2L3	0.7431124	SOD2	1.150301
NFIL3	0.5964912	B4GALT5	0.7465438	PTPRH	1.181818
LOC730316	0.5975976	SNPH	0.7468672	RND1	1.219512
TNFAIP2	0.6074767	LOC440353	0.7569721	PARP9	1.22449
SP2	0.609319	SDCBP	0.7571338	SAMD9	1.256281
C5orf41	0.6122977	MARCH7	0.7586207	PARP12	1.273044
				MX1	1.376147
				CH25H	1.659341
				IRF9	1.740741

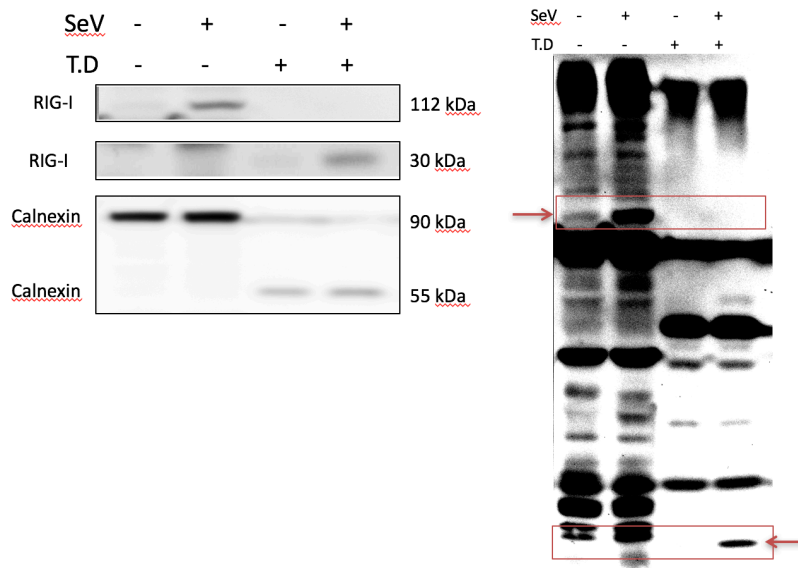
**Table 27.** Table of genes positively or negatively regulated by IFN signalling defined by their difference in peak induction rank difference from transcriptomic expression profiling (weighted rank difference) in WT vs. IFNA/LR KO cells.

**Figure 8.1 NFKB signalling gene expression comparison**



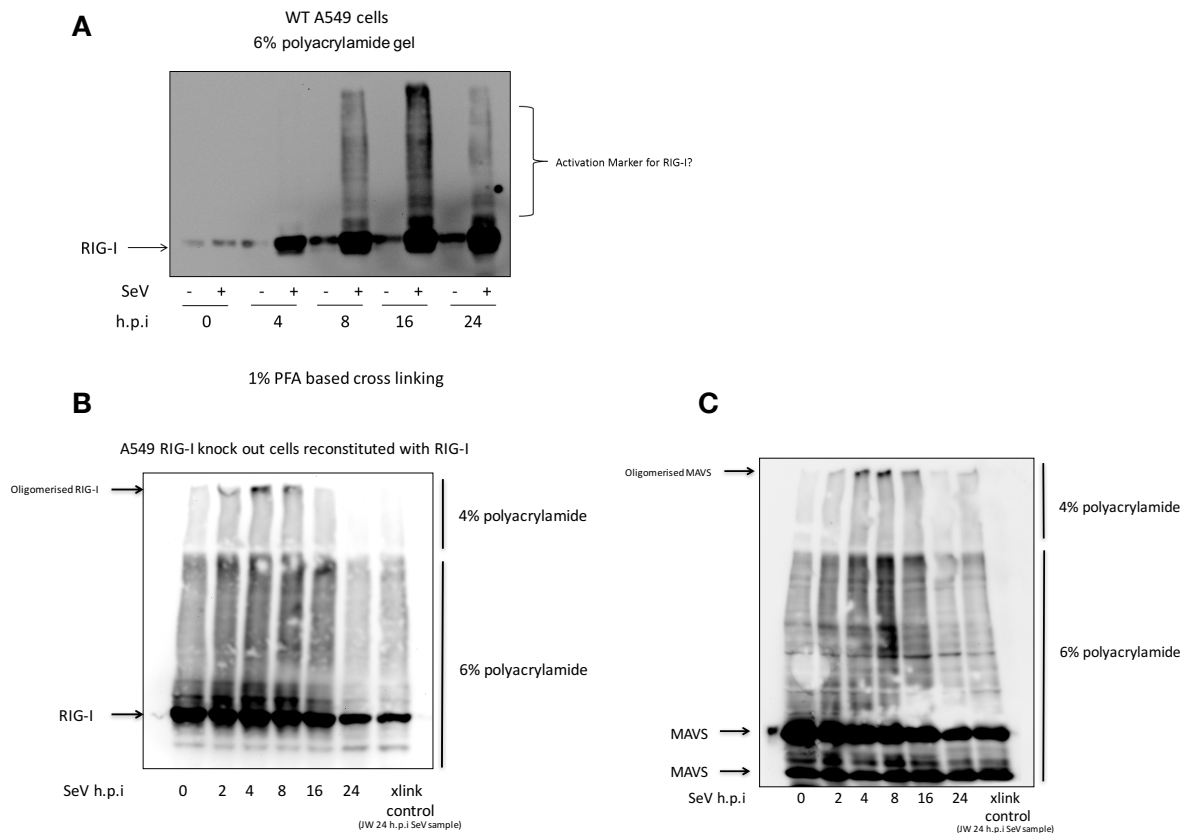
**Figure 8.1:** Transcriptome data for NFKBIA and NFKB1 in wild-type A549 cells.

**Figure 8.2 Partial tryptic digestion of RIG-I**



**Figure 8.2:** Partial tryptic digestion assay of activated RIG-I by Sendai Virus (MOI 5x).

**Figure 8.3 Cross-linking of RIG-I and MAVS**



**Figure 8.3:** PFA based cross-linking assay. **A)** Sendai virus infected cells treated with 1% PFA to cross link oligomerised RIG-I was detected on 6% SDS-PAGE gel. **B)** and **C)** Using RIG-I KO cells reconstituted with RIG-I, oligomerisation was detected by gel electrophoresis for RIG-I and MAVS.



